PERMFORMANCE CHARACTERIZTION AND MODELING OF A PASSIVE DIRECT METHANOL FUEL CELL (DMFC) OVER A RANGE OF OPERATING TEMPERATURES AND RELATIVE HUMIDITIES

David Glenn Woolard

Thesis Submitted to the Faculty of the Virginia Polytechnic Institute and State University
in Partial Fulfillment of the Requirements for the Degree of:

Master of Science
In
Mechanical Engineering

Committee Members:

Michael W. Ellis, Chair

Doug Nelson

Michael von Spakovsky

June 4, 2010

Blacksburg, Virginia, USA

Keywords: direct methanol fuel cell, fuel cell, DMFC, air breathing

PERMFORMANCE CHARACTERIZTION AND MODELING OF A PASSIVE DIRECT METHANOL FUEL CELL (DMFC) OVER A RANGE OF OPERATING TEMPERATURES AND RELATIVE HUMIDITIES

David Glenn Woolard

ABSTRACT

As the world begins to focus more and more on new and more effective means of energy production, fuel cells become increasingly more popular. While different fuel cells are already found in industry today, the direct methanol fuel cell (DMFC) is becoming an increasingly more probable means for portable power production. In such applications a passive air breathing direct methanol fuel cell would be ideal. However, successful use of the passive DMFC in such applications requires that the fuel cell be capable of operating at various temperatures and relative humidities. A passive air breathing direct methanol fuel cell was developed and manufactured for this study. This work studied the effects of varying relative humidity and temperature over a probable range of operating conditions for small scale portable power applications on the performance of the fuel cell, both in relation to power production and fuel consumption. Potentiostatic, electrochemical impedance spectroscopy, and polarization tests were performed in order to characterize the performance of the fuel cell. Additionally, a one dimensional steady state isothermal mass transport model was developed to provide insight to the behavior of the fuel cell. The experimental data and model results show that increasing the fuel cell temperature and decreasing the ambient relative humidity increases the current production capabilities of the fuel cell. Further, the experimental data suggests that the major problem hindering current production in passive air breathing direct methanol fuel cells is flooding of the cathode diffusion layer.

ACKNOWLEDGMENTS

This work was made possible by the support, time, and commitment of a number of individuals. I would like to thank my advisor and committee chairperson, Dr. Michael Ellis, for all of his advice, encouragement, guidance, and patience through this long journey. I would like to thank Jonas Gunter and Luna Innovations for their fiscal support to this and other projects. I want to express my appreciation to my other committee members, Dr. Michael von Spakovsky and Dr. Doug Nelson for their support in completing my thesis. Finally, I would like to thank my family and friends for all of their undying love and encouragement along the way.

TABLE OF CONTENTS

LIST OF FIGURES

LIST OF TABLES

NOMENCLATURE

ENGLISH

a_w = water vapor activity
b = GDL tortuosity parameter
c_{CH_3OH} = molar concentration of methanol [mol/m^3]
$c^0_{CH_3OH}$ = reference molar concentration of methanol [mol/m^3]
c_{H_2O} = molar concentration of water [mol/m^3]
D_{i-j} = binary diffusion coefficient of species i in species j [m^2/s]
D_{CH_3OH-N} = diffusion coefficient of methanol in Nafion® [m^2/s]
D_{H_2O-N} = diffusion coefficient of water in Nafion® [m^2/s]
d_M = membrane thickness [m]
D_{ij} = *ij* component of the multicomponent Fick diffusivity
EW = equivalent weight of Nafion® [g/mol]
F = Faraday's constant (96,497 C/mol)
i = current density [mA/cm^2]
j = volumetric current density [mA/cm^3]
j_0 = volumetric exchange current density [mA/cm^3]
k_ϕ = electro-kinetic permeability of membrane [m^2]
k_p = hydraulic permeability of membrane [m^2]
M = molecular weight [g/mol]
m_i = mass flux of species i [kg/m^2-s]
n_d = electro-osmotic drag coefficient
n_i = molar flux of species i [mol/m^2-s]
P = local pressure [Pa]
P_{cr} = critical pressure [Pa]
P_{cap} = capillary pressure [Pa]
P_{sat} = saturation pressure [Pa]
P_v = vapor pressure [Pa]
P_0 = atmospheric pressure [Pa]
R = universal gas constant (8.314 J/mol-K)
ASR = area specific resistance (ohms-cm^2)
r_c = pore radius [m]
T = temperature [K]
T_{cr} = critical temperature [K]
v = molar average velocity [m/s]
v* = mass average velocity [m/s]

x = position [m]
X_i = mol fraction of species i

GREEK

α = transfer coefficient
β = current/concentration proportionality coefficient
ε = GDL porosity
η_a = anode overpotential
θ_c = contact angle
Θ = relative humidity of the environment
λ = water content
μ = viscosity [kg/m-s]
ρ = density [kg/ m^3]
σ = surface tension [N/m]
ω_i = mass fraction of species i

SUBSCRIPTS

a = anode
c = cathode
CH_3OH = methanol
d = dry Nafion®
env = environment
g = gas
ga = gauge
l = liquid
H_2O = water
N_2 = nitrogen
O_2 = oxygen

SUPERSCRIPTS

B = boundary
D = domain
eff = effective

1. INTRODUCTION

As energy costs continue to rise and concern over global warming and the health of the environment increases, so does the interest in renewable and sustainable energy production. Domestic political focus on alternative energy has recently increased, as has federal funding for research and development in the field. Industry is now more interested than ever in creating new and effective ways to produce renewable and sustainable energy. Areas of focus include wind turbines and hydro-electric power plants for large scale power production, and solar panels and fuel cells for portable and residential power production. Fuel cells have become increasingly popular for small scale portable applications and they may one day replace batteries for use in many electronic devices. Fuel cells are devices which harness electrical energy from an electrochemical reaction. One of the most popular fuel cells today is the proton exchange membrane fuel cell (PEMFC) which draws power from a hydrogen-oxygen reaction producing only water as a byproduct. The hydrogen source can be compressed hydrogen, or it can be produced from a secondary source such as methanol or fossil fuels. Another fuel cell that is becoming increasingly popular is the direct methanol fuel cell (DMFC) which draws power from a methanol-oxygen reaction.

Both of these kinds of fuel cells are already being used in the market today, and research is currently being conducted to find new ways to apply fuel cells. Most of the major automobile companies including but not limited to Audi, BMW, Daimler, Ford Motor Company, GM, Honda, Nissan, and Toyota are in the process of producing fuel cell cars for daily and commercial use. The city of Burbank California has began to use a hybrid fuel cell bus for public transportation. Fuel cells are also a very viable alternative to replace batteries in forklifts. This is because fuel cells do not self heat as much as batteries which have been known to explode during operation and because fuel cells can be refilled instead of having to be exchanged during forklift operation like batteries. Research is also attempting to use fuel cells for small scale stationary and portable electronics. The Smart Fuel Cell company is currently manufacturing methanol fuel cell power generators that they advertise for use with mobile homes, boats, military applications, and more [1]. Both Fujitsu and Casio Corp. have manufactured fuel cells

that can replace batteries in laptops, and the Casio fuel cell is capable of running a laptop for up to 20 hours [2]. The military is also interested in using fuel cells for portable power in devices such as micro air vehicles (MAV), power generators, communications devices, and other unmanned vehicles [3].

The goal of this thesis is to characterize and model the performance of a passive air breathing direct methanol fuel cell (DMFC) operating over a spectrum of relative humidities and temperatures that are relevant to the operation of micro air vehicles (MAV). There is currently a large amount of performance data available describing the operation of proton exchange membrane fuel cells (PMFC) and direct methanol fuel cells (DMFC). However, most of the reported experimental data for DMFCs was taken at relatively high anode and or cathode humidities, a condition which is often associated with cathode flooding. However, it is not uncommon for MAVs to fly at high altitudes characterized by low relative humidities, or in dry warm environments. Operation under these conditions increases the rate of evaporation of water from the cathode and may prevent or significantly reduce flooding. Further, these conditions may affect water loss and methanol usage. This research specifically focuses on the performance of passive DMFCs operating at low relative humidities, an operating range in which there is currently a lack of performance data reported in literature. The performance of the fuel cells is determined by performing polarization, lifetime, and electrochemical impedance tests. A one dimensional model of the mass transport processes acting on the passive DMFC under these varying conditions is described and used to explain the experimental data. The model is used to determine the rate of methanol consumption and crossover, the rate of water consumption and crossover, the concentration profile of methanol in the anode diffusion layer and in the membrane, the concentration profile of water in the membrane, and the concentration profile of oxygen in the gas diffusion layer.

The first chapter of this thesis provides a summary of fuel cell applications and an overview of how a direct methanol fuel cell operates. The second chapter provides a review of literature published on proton exchange membrane fuel cells and direct methanol fuel cells, providing summaries of both experimental studies and numerical model results. The third chapter describes the analytical model and associated parameters that were developed to describe the fuel cell performance. The fourth chapter

gives a description of the instruments and procedures used during testing and an overview of the experimental design. The fifth chapter provides an overview and analysis of the experimental results, and discusses these results in the context of the analytical model results which describe the transport processes that occurred in the fuel cell testing. The sixth chapter provides conclusions and a discussion of future work.

1.1. Direct Methanol Fuel Cell Basics

Direct methanol fuel cells (DMFC) produce electricity through an electrochemical reaction of methanol with oxygen. Equation 1.1 below shows the overall reaction in which one mole of methanol reacts with 3/2 moles of oxygen to produce one mole of carbon dioxide and 2 moles of water. Equations 1.2 and 1.3 show the half reactions that occur at the anode and cathode respectively.

$$CH_3OH + \frac{3}{2}O_2 \rightarrow CO_2 + 2H_2O \tag{1.1}$$

$$CH_3OH + H_2O \leftrightarrow CO_2 + 6H^+ + 6e^- \tag{1.2}$$

$$\frac{3}{2}O_2 + 6H^+ + 6e^- \leftrightarrow 3H_2O) \tag{1.3}$$

Figure 1 depicts a DMFC during normal operation. A basic DMFC consists of a membrane electrode assembly surrounded by two current collectors or bipolar plates (depicted in black).

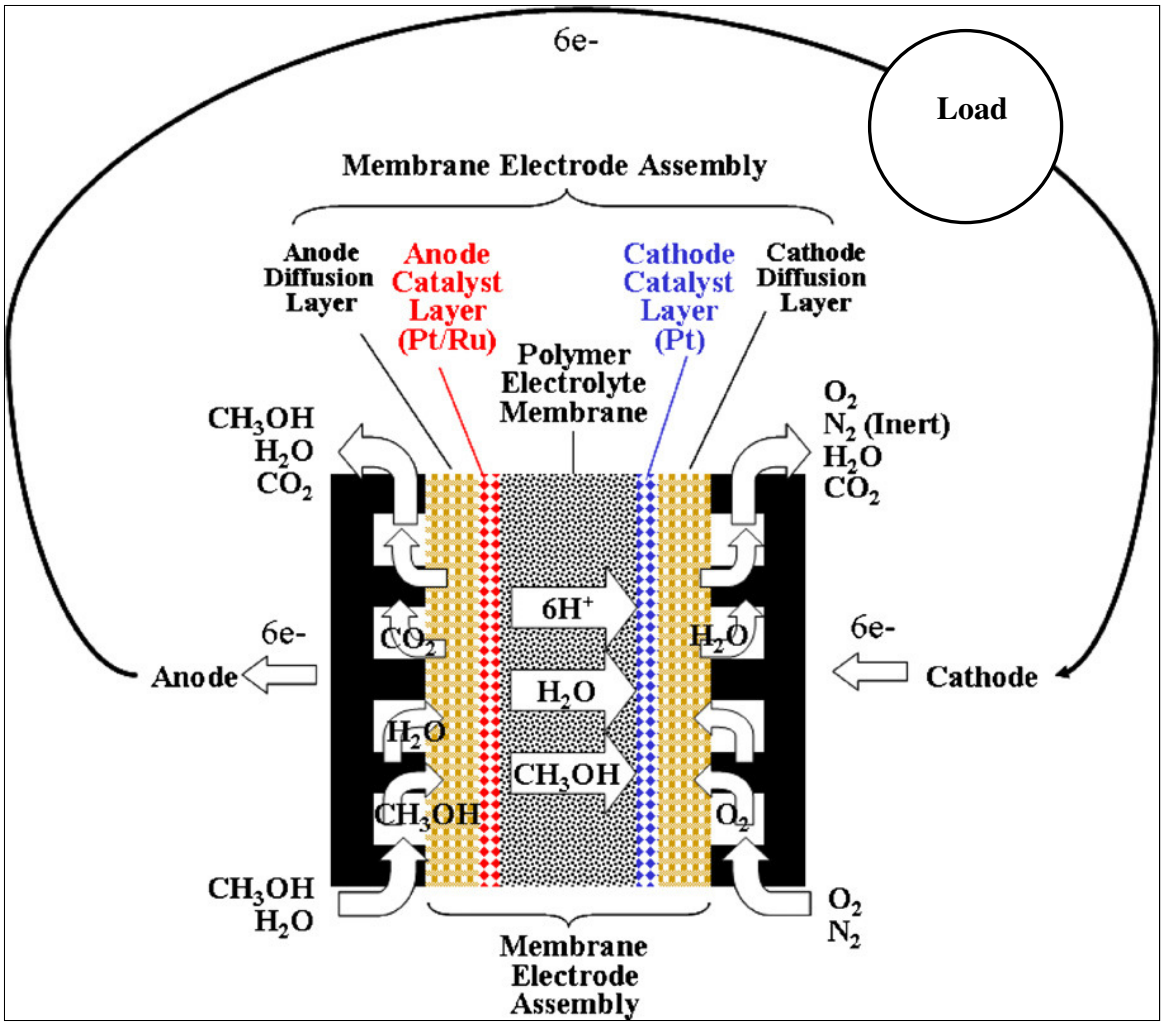

Figure 1. Operating schematic of a direct methanol fuel cell (DMFC) [4].

The membrane electrode assembly (MEA) separates the methanol on the anode side and the oxygen on the cathode side. The MEA consists anode and cathode catalyst layers and a polymer electrolyte membrane. The MEA and its components will be discussed in more detail later in this chapter. A solution of methanol and water is fed through a flow channel (part of the bipolar plate) on the anode side at which point it permeates through the diffusion layer to the anode catalyst layer. The methanol and water react according to the half reaction shown in equation 1.2 within anode the catalyst layer. The electrons produced by the reaction flow back through the conductive anode diffusion layer, through the load, and to the cathode current collector. The protons produced by the anode half reaction permeate through the polymer electrolyte membrane to the cathode catalyst layer, while the carbon dioxide dissolves into the methanol-water solution and is

eventually removed. At the cathode, oxygen from the air stream in the flow channel permeates through the cathode diffusion layer to the cathode catalyst layer where it reacts with the electrons and protons from the anode half reaction, producing water. The water then must permeate through the cathode diffusion layer to the flow channel where it is removed.

1.2. DMFC Components

A basic direct methanol fuel cell is made up of the membrane electrode assembly and surrounding current collectors. The typical seven layer membrane electrode assembly (MEA) consists of anode and cathode diffusion layers, anode and cathode microporous layers (not present in five layer MEAs), anode and cathode catalyst layers, and a polymer electrolyte membrane (PEM). These are each discussed in more detail in the following sections.

Current Collectors

Current collectors serve two major purposes in DMFC operation. The first is to direct the flow of the methanol-water fuel or oxygen from the source, along flow channels within the plates, to the diffusion layer of the fuel cell. The second is to conduct current produced by the catalyst layers to the electronic device where useful work is performed. Current collectors are typically made of rigid conductive material such as stainless steel or graphite. The rigid material allows the current collectors to uniformly compress the MEA to insure minimal electrical contact losses between the diffusion layers and plates. Flow channels are machined into the current collectors. There are many different flow channel configurations each designed to achieve a different goal. The design of the flow channel can affect many aspects of fuel cell performance such as reducing mass transport losses, reducing electrical contact losses, or improving water removal from the cathode.

Current collectors are commonly used in active DMFCs, or fuel cells that require the use of external devices to aid in the operation of the fuel cell. These devices can

incorporate heat management systems such as heaters, or devices such as pumps that push the methanol, water, or oxygen through the flow channels. All such devices must consume some of the power produced by the fuel cell to operate, resulting in parasitic power losses. They also increase the size and cost of the overall fuel cell system. Passive fuel cells however do not require the use of external power consuming devices which reduces parasitic losses and keeps the system size small. Passive fuel cells typically use perforated or porous current collectors, as opposed to the bulkier current collectors with machined flow fields, to conduct the current away from the diffusion layers. Current collectors are typically made of highly conductive metals such as 316 stainless steel and are often gold or nickel plated to increase electrical conductivity and to prevent corrosion or contamination of the MEA. Current collectors also have many different configurations and are designed to optimize the flow of fuel through their pores to the diffusion layer while reducing electrical contact losses and ensuring structural integrity.

a)  *b*) 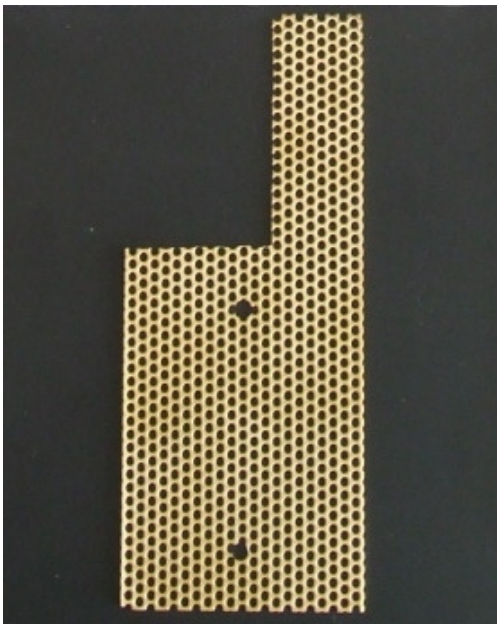

Figure 2. Comparison between (a) a current collector with machined flow field and (b) a perforated current collector.

Diffusion Layers

The bipolar plates or current collectors come into direct contact with the diffusion layers, or gas diffusion layers (GDL). The diffusion layers are responsible for diffusing the fuel from the flow channels or pores across the entire surface of the catalyst layer, while still providing a conductive media through which electrical current can flow. Diffusion layers are typically made of specially processed carbon cloth or carbon paper which are permeable to both liquid and gas, and are also electrically conductive. Many different types of diffusion layers are available today which are designed to for many different applications. Different additives such as Teflon™ (PTFE) or carbon black are often added to the diffusion layer to improve different aspects of their operation. For instance, increasing Teflon content increases the hydrophobic nature of the GDL which helps it to repel water which is desirable to reduce flooding on the cathode of DMFCs. BASF produces a popular type of GDL known as ELAT™ which is used commercially for low temperature DMFCs.

Microporous Layers

The microporous layer (MPL) is found in seven-layer (not present in five-layer) MEAs. The microporous layer is a thin layer located between the diffusion layer and the catalyst layer that serves to improve electrical conductivity between the two layers while managing water or methanol mass transport. A MPL is typically made up of a combination of carbon black and a fluoropolymer such as Teflon®. The electrically conductive carbon black serves to reduce the contact losses between the diffusion layer and the catalyst layer. The fluoropolymer is added because its hydrophobic nature aids the MPL in forming a water barrier between the diffusion layer and the catalyst layer which aids the PEM in retaining water and also helps prevent flooding of the cathode.

Catalyst Layers

The anode and cathode catalyst layers are regions of the fuel cell where the chemical reactions occur. There has been a large research effort to create effective and affordable catalysts for the fuel cells. Catalyst layers in PEMFCs typically consist of

platinum supported on carbon black particles. However, in DMFCs, ruthenium particles are also used to catalyze the anode methanol oxidation reaction. Catalyst layers are typically made by applying a catalyst ink, which is a suspension of the supported catalyst particles in a mixture of the ionomer (e.g. Nafion®) and a dispersant, to a polymer electrolyte membrane. The ink is cured through a heating process. The specifics of the catalyst ink compositions and curing processes are a topic of ongoing research and are often proprietary and patented. The catalyst layer is a very expensive part of the membrane electrode assembly because of the high platinum content within the layer. Efforts have been made to employ nickel based catalyst inks as apposed to platinum based inks in order to cut costs, but the nickel based inks simply are not as effective at catalyzing the fuel cell oxidation-reduction reactions. Factors other than composition that affect the catalyst layer effectiveness are particle size, catalyst layer thickness, and porosity.

Polymer Electrolyte Membrane

The catalyst layers are applied directly to a polymer electrolyte membrane (PEM). The PEM is ionically conductive material that is permeable to protons, impermeable to electrons, durable enough to withstand the fuel cell oxidation-reduction reaction, and capable of separating the anode and cathode reactants. The most popular PEM material in use today is Nafion®, a product of DuPont chemical company. Nafion® is an ionomer that has a polymer backbone similar to that of PTFE with sulfonic acid side chains when in the acid form. The ability of Nafion® to conduct ions is strongly related to its level of hydration. Water is essential to the ion transport process in Nafion®, which makes water management within a fuel cell very important. One drawback of Nafion® for use in DMFCs is that it is also somewhat permeable to methanol. The phenomenon of methanol permeating from the anode to the cathode of a fuel cell through the PEM membrane is known as methanol crossover. While increasing the thickness of the Nafion® membrane has been shown to reduce the rate of methanol crossover, it also increases the cost of the membrane. Another factor that affects the performance of the membrane is the equivalent weight (EW) of the Nafion®. The equivalent weight is the number of grams of

dry Nafion per mole of sulfonic acid groups when the material is in the acid form. For more information on Nafion® see the review paper by Mauritz et al. [5].

1.3. Technical Challenges for DMFC Systems

While direct methanol fuel cells are becoming increasingly popular as a possible portable power option, their power production and fuel utilization capabilities are still less than desirable. Current roadblocks to improved power production include ineffective and costly catalysts, production of carbon dioxide at the anode, methanol and water crossover, and cathode flooding. While drastic improvement of catalyst activity may not be feasible in the near future, effective and promising methods of reducing methanol and water crossover and cathode flooding are currently being developed.

Methanol and water crossover occurs because the Nafion® membrane is permeable to both. The first problem that crossover presents is that the methanol and water that travel from the anode to the cathode are no longer capable of undergoing an oxidation-reduction reaction that produces electrical current to perform usable work. Also, methanol that reaches the cathode then undergoes an oxidation reaction which lowers the electrical potential of the cathode while blocking a reaction site, consuming oxygen, and producing water. Water that reaches the cathode may then contribute to flooding and may eventually be lost to the atmosphere. New membranes that exhibit lower permeability to water and methanol while retaining high ionic conductivity are under development. However, Nafion® remains the benchmark material and most alternatives represent compromises in some aspect of performance. Therefore, other methods of controlling or prohibiting methanol and water crossover are being actively explored. A very popular method of combating crossover is the employment of hydrophobic MPLs and GDLs. Promising research has shown that it is even possible to induce back diffusion of water from the cathode to the anode by use of multiple hydrophobic layers [6].

1.4. Thesis Objectives

Before direct methanol fuel cells can be used commercially in the area of small scale portable power production, their performance must be evaluated over a full range of possible operating conditions. Furthermore, in order to improve the overall performance and fuel utilization of a DMFC, the mass transport of methanol and water within the fuel cell must be fully understood. In this work a commercially produced DMFC MEA was purchased from BASF for use in experimental characterization of the fuel cell performance. The Multiphysics computer program COMSOL was also utilized to create a mass transport model for methanol and water within the DMFC. The research objectives of this work are as follows:

- Characterize the performance of a passive DMFC over the entire operating range of a small scale electronic device (in this case a micro aerial vehicle) by performing an array of potentiostatic, polarization, and electrochemical impedance spectroscopy tests.
- Measure rates of methanol and water consumption by a passive DMFC over the full range of environmental conditions.
- Create a one dimensional steady state mass transport model of a passive DMFC and compare its results to experimental results.
- Explain the effects of relative humidity and temperature on the power production, methanol use, and water use of a DMFC.

2. LITERATURE REVIEW

This chapter provides an overview of proton exchange membrane fuel cell (PEMFC) and direct methanol fuel cell (DMFC) experimental humidity studies, PEMFC and DMFC mass transport models, and the need for new low humidity DMFC performance studies.

2.1. Introduction

Many factors affect the performance of a proton exchange membrane fuel cell, and one such factor that is currently of major concern is water transport within the cell. One of the most popular proton exchange membranes today is Nafion®, a copolymer invented by DuPont that is permeable to protons. It has been shown [5,7,8] that the ionic conductivity of Nafion® changes drastically due to its level of hydration. The level of hydration is interrelated with water transport through the membrane since water is introduce to the membrane by transport from the anode or cathode and since the transport mechanisms are influenced by the level of hydration.

Water molecules move across the membrane from the anode to the cathode in conjunction with protons in a phenomenon known as electro-osmotic drag. If a water concentration gradient exists, water will also diffuse through the membrane in a direction opposite to the gradient, either toward the anode or cathode. And if a pressure gradient exists, water will also move through the membrane in a direction opposite the pressure gradient due to hydraulic permeation. The study of water transport is very important because the flow of water affects the Nafion® hydration and thus the Nafion® conductivity. However, the benefit of a fully hydrated Nafion® membrane can be offset by the occurrence of flooding on the cathode. Flooding occurs when liquid water fills catalytic sites on the cathode and or pores in the gas diffusion layer thus preventing oxygen from reaching the reaction sites [9,10]. Therefore, properly hydrating the membrane while prohibiting flooding is a very important task and is required to produce efficient and powerful fuel cells.

During the overall reaction of a DMFC, methanol and oxygen react to produce water and carbon dioxide (Equation 1.1). This overall reaction can be divided into two electrochemical half reactions, the first occurring at the anode catalyst layer where methanol and water react to produce carbon dioxide, protons, and electrons (Equation 1.2), and the second occurring at the cathode catalyst layer where oxygen reacts with the protons and electrons to produce water (Equation 1.3). Water transport in DMFCs is very import because it not only hydrates the Nafion® membrane, but it also serves as a reactant for the anode half reaction. Because liquid water is in contact with the anode surface of the Nafion® membrane, flooding of the cathode is a much more likely occurrence than membrane dry-out. However, water is still lost to the environment due to evaporation at the cathode.

Methanol transport in DMFCs is also of great importance. While some methanol is consumed at the anode catalyst layer, additional methanol is lost due to methanol crossover, a process in which methanol permeates from the anode through the Nafion® membrane to the cathode. The primary driving forces of methanol crossover are diffusion and electro-osmotic drag [11]. Methanol that reaches the cathode catalyst layer is oxidized which lowers the cathode potential. This also blocks reaction sites and consumes methanol, reducing fuel efficiency, power production, and energy density. Because increased rates of water crossover are related to increased rates of methanol crossover, it is important to understand and manage both water transport and methanol transport in a DMFC.

2.2. PEMFC Humidity Studies

One important factor that controls the hydration of the membrane and water transport within a fuel cell is the cathode humidity. Fuel cells that operate in dry environments tend to experience less flooding on the cathode due to higher rates of evaporation of water. However, if the cathode environment is not humid enough, the cell may never experience flooding but rather may experience drying which can reduce the ionic conductivity of the Nafion®. Ju et al. [12] studied the effects of cathode humidity on a proton exchange membrane fuel cell (PEMFC), specifically under low humidity

conditions. These tests were performed with forced convective air on the cathode using a novel ribbed flow channel. This flow channel incorporated air ports to sample the humidity of the gas throughout the flow channel, and also allowed separate localized current measurements to be taken at incremental locations across the cell. Tests were performed with anode and cathode humidities ranging from 0% to 100% relative humidity (RH). The author found that fuel cells experienced poor performance under low humidity conditions at the beginning of the flow channel due to water evaporation from the cell resulting in poor hydration. The cell performance reached a peak further down the flow channel as the gas stream became more hydrated and the rate of evaporation decreased. The performance then dropped near the end of the flow channel as oxygen depletion in the cathode gas stream became an issue. However, when both the cathode and anode gases were 100% humidified, the cell performed well upstream but began to experience decreases in performance downstream, which the author attributes to flooding. The author also concludes that the current density was affected mostly by the level of hydration of the membrane upstream while downstream the oxygen transport was the dominant factor.

Forced convection on the anode or cathode is a popular means of providing fuel and hydration to the fuel cell membrane. The use of pumps, humidifiers, sensors, and other such instruments are often used to manage the water content and water transport in fuel cells. However, these active methods make a fuel cell system more complex and introduce parasitic power losses. In the application of fuel cells to portable devices, the fuel cells are typically small and cannot afford to experience parasitic power losses. In these cases, a passive alternative for achieving water management is preferred. Once such passive route is to use a free breathing cathode that is exposed to ambient air as opposed to forced air in order to reduce parasitic power losses. However, fuel cells with a free breathing cathode suffer from a lack of cathode humidification control because they cannot rely on a constant flow of air to remove excess water or hydrate the cell, which can result in poor power production relative to that of forced convection fuel cells.

The work of Fabian et al. [13] studied the role of ambient conditions of the performance of an air breathing PEMFC. They created a fuel cell housing that consisted of a hydrogen feed chamber through which conditioned hydrogen was supplied to the

fuel cell anode and a cathode current collector that allowed the air from the surrounding environment to flow to the cathode catalyst layer while maintaining housing rigidity. Figure 3 shows an exploded view of the fuel cell housing they used.

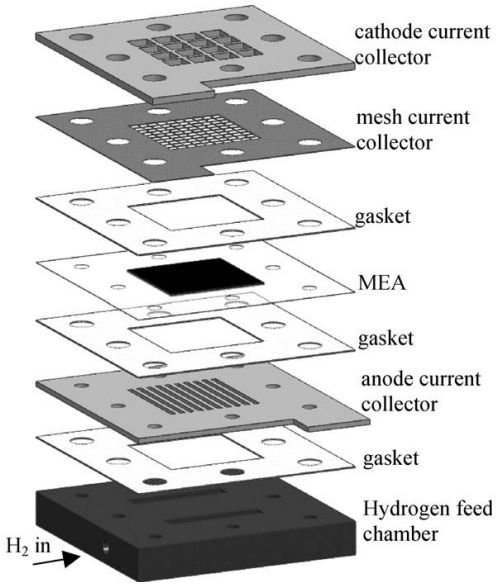

Figure 3. Exploded view of the air-breathing fuel cell stack described by Fabian et al. [13].

The PEMFC was placed in an environmental chamber to control the temperature and the relative humidity of the cathode air, and tests were conducted at air temperatures ranging from 10ºC to 40ºC and at relative humidities ranging from 20% to 80%. They found that the PEMFC operated in three regions: hydration, fully hydrated with flooding, and drying. They also found that once the cathode GDL reached a temperature of 60ºC, the membrane began to dry out regardless of ambient conditions. This was possible because the fuel cell cathode GDL was able to achieve temperatures of approximately 45ºC greater than those of the ambient air due to self-heating. The fuel cell produced a maximum power density of 356 mW/cm^2 at an ambient temperature of 20ºC and an ambient relative humidity of 40%.

Jeong et al. [14] studied the effects of varying the area of the cathode exposed to air, as well as the effects of varying the cathode relative humidity, on fuel cell performance. They tested a PEMFC while varying the open area of the cathode current collector plate. Cathode current collectors with 52%, 64%, 77%, and 92% open area

were tested, and they found that at both a relative humidity of 80% and a relative humidity of 20%, the fuel cell achieved the greatest power density during a polarization test with a cathode open area of 77%. However, during galvanostatic tests (constant current) with low current densities (approximately 40 mA/cm^2) the cell voltage decreased as the open area was increased. This voltage drop was attributed to increased activation and ohmic losses. The activation and ohmic losses were caused by lower ionic conductivity of the membrane phase in the catalyst layer that was due to greater evaporation of water as the open area increased, and by increased in-plane electrical resistance attributed to longer electron pathways through the GDL to reach the current collector. During high current (approximately 240 mA/cm^2) galvanostatic testing, mass transport losses became a factor, and these were reduced by increasing the open area.

When studying the effects of relative humidity on the air breathing PEMFC, Jeong et al. applied dry hydrogen to the anode while controlling the relative humidity of the air that surrounded the cathode over a range from 20% to 100% RH. The figure below shows how the cell voltage varies at two different current densities over the range of relative humidities. The experiments showed that under low current operation, 60 mA/cm^2, the PEMFC performed better when exposed to more humidified air because the cell experienced better hydration. However, under high current operation, 340 mA/cm^2, the fuel cell performed better at lower humidity because, under high humidity, the cathode experienced flooding due water production. Lower relative humidity is preferred under high current operation in order to increase evaporation of water on the cathode and reduce flooding.

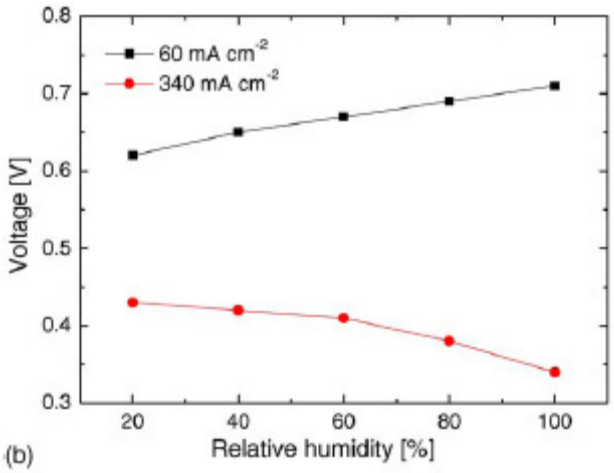

Figure 4: Effect of the relative humidity of the atmosphere on cell performance with cathode open area of 77%. Cell voltage at 60 and 340 mA/cm^2 [14].

2.3. DMFC Humidity Studies

Like PEM fuel cells, the performance of direct methanol fuel cells (DMFCs) is also affected by the humidity of the cathode gas. However, unlike PEM fuel cells which use gaseous hydrogen as fuel source, DMFCs use a methanol in water solution as the fuel source. Therefore, the anode is always 100% hydrated, and under most cathode humidity conditions, the DMFC performance suffers from cathode flooding, not from membrane drying. As a result, most DMFC cathode gas streams require no humidification [15]. However, these fuel cells have additional problems such as water crossover and methanol crossover.

As discussed in Chapter 1, water crossover through the membrane can be caused by electro-osmotic drag, by diffusion, and by hydraulic permeation. Water crossover is of great concern in DMFCs because liquid water is in contact with the membrane at the anode. Thus the membrane is typically in a highly hydrated state which enhances transport process and presents the risk of cathode flooding. Increased water crossover also increases the rate of methanol crossover [15], and its associated effects.

The methanol solution concentration also affects the both the methanol and water transport processes. During DMFC operation H^+ ions, accompanied by water, travel through the membrane from the anode to the cathode, in a manner similar to that of PEM

fuel cells. During ideal DMFC operation there is no methanol crossover. As methanol and water from the anode solution are depleted in the anode reaction, water is also removed from the solution and crosses over to the cathode. For every molecule of methanol consumed by the reaction, 16 water molecules are also lost from the solution, which corresponds to a three molar methanol solution [15]. However, methanol crossover does occur in DMFC operation, and increasing the concentration of methanol in the anode solution also increases the rate of methanol crossover due to diffusion. This methanol crossover blocks flow paths that could be filled with protons, and the methanol that reaches the cathode surface blocks reaction sites, thus reducing power. But increasing the concentration of methanol in the anode solution also improves the reaction kinetics at the anode thus increasing the power production capabilities. A three molar methanol solution is commonly used in DMFCs because it provides the optimal ratio of water to methanol to encourage reaction kinetics while limiting crossover.

Current humidity studies focus primarily on the effects of cathode gas humidity on flooding and water crossover, and how to remedy these problems. Jewett et al. tested passive free breathing DMFCs over a range of low humidity conditions from 15% RH to 45% RH. The author applied various types of gas diffusion electrodes (GDE) to the anode and cathode in order to determine which kind of GDE was most effective at improving performance. A gas diffusion electrode (GDE) consists of a gas diffusion layer (GDL) with a specified catalyst loading. The author obtained a maximum power density of 25 mW/cm^2 by applying a GDE manufactured by E-TEK which had a porosity of approximately 70% and a permeability of $4x10^{-10}$ m^{-2}. The author also increased the number of gas diffusion layers applied to the anode to determine if number of layers affected the water flow within the fuel cell. Adding additional GDLs proved to decrease the water balance coefficients, meaning less water was lost from the methanol solution due to crossover and evaporation. The author attributed this to increased hydraulic water pressure at the cathode that forced water back to the anode [6]. The water retention of the fuel cell was mostly affected by the number of GDLs, and the power density was most affected by the type of GDE used. Application of multiple GDLs provides an effective way to control water flow within a cell and to prevent water loss.

Another DMFC study was performed by Peled et al. [16] in which the author achieved a water neutral condition (no net water loss) in the fuel cells by using a nanoporous proton-conducting membrane (NP-PCM), as opposed to a proton exchange membrane (PEM) such as Nafion®, in combination with a liquid-water barrier layer (LWBL). The NP-PCM is a membrane that is cheaper than Nafion®, less susceptible to methanol crossover, and less sensitive to heavy metal impurities such as ferrous ion poisoning. The methanol fuel in cells using a NP-PCM is in solution with sulfuric acid. The NP-PCM is described in more detail in the work by Peled et al. [17]. The LWBL prevents water from leaving the fuel cell at the cathode due to evaporation, and improves the rate of back diffusion within the membrane. The LWBL is created on the cathode GDL by applying and curing several layers of a paste consisting of PVDF or Teflon and carbon powders such as Black Pearl 2000, XC-72, and Shawingan Black [16]. The tests were conducted with an engraved cathode air channel using dry oxygen as the cathode gas source instead of free breathing air. While testing with the dry cathode gas supply, the author was able to induce more water flow from the cathode to the anode due to back diffusion within the membrane than water flow from the anode to the cathode due to electro-osmotic drag. This method proves to be very effective at preventing water loss due to evaporation. However, the rate of back diffusion only overcame the rate of electro-osmotic drag when cathode gas flow rates were low. Also, because all tests were conducted with dry oxygen and forced cathode gas convection, neither the effects of varying the cathode gas humidity nor the effects of using a free breathing cathode were determined.

Both the effects of cathode side air flow and the effects of methanol concentration and temperature on the performance of a passive air breathing DMFC were studied by C. Y. Chen et al. [18]. Their study was performed on MEA fabricated in-house that was tested in a passive DMFC test fixture utilizing perforated stainless steel current collectors. A two-hour potentiostatic was conducted on the DMFC at 22ºC in which a constant voltage of 0.23V was applied. The results from this test are shown in Figure 5. When the test was performed with stagnant air (air-breathing), the power density declined for the first 40 minutes until reaching a steady state. However, when running the same test while blowing air over the cathode, the power density did not decline. Chen et al.

contributed the decline in power density during the air breathing test to the accumulation of water on the cathode (flooding) which increasingly blocked the oxygen supply until the rate of diffusion of oxygen through the water to the cathode reached a steady state. In the case of the air blown test, the air was able to remove much of the water and prevent a rapid decline in power density. This test shows that in order to keep power production up it is very important to reduce the amount of water that accumulated on the cathode.

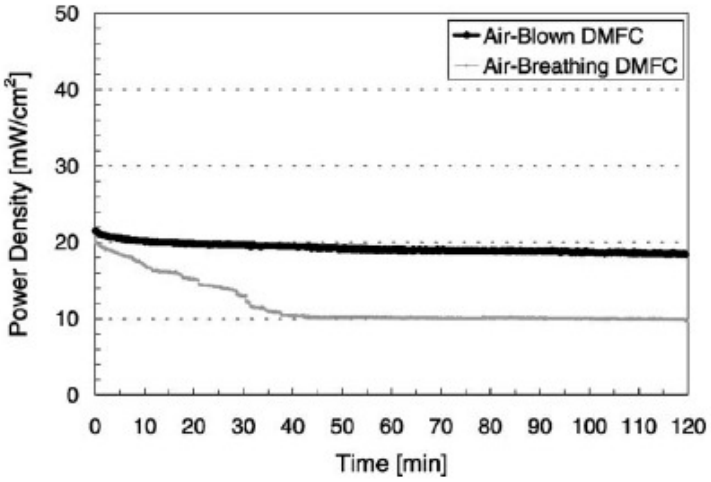

Figure 5. Two-hour potentiostatic test at 0.23V and 22ºC for air-breathing and air-blown DMFCs tested with 3 wt.% methanol [18].

Additional tests were performed by Chen et. al. to study the effects of methanol concentration and temperature on the performance of a passive air breathing DMFC. Polarization curves were obtained at multiple methanol concentrations and temperatures. Figure 6 shows the peak power densities obtained during each of these tests. The peak power density decreased slightly as the methanol concentration increased from three to six weight percent, and then decreased more rapidly as the concentration increased from six to nine weight percent. Chen et al. attributes these declines in peak power density to increased methanol crossover as the concentration increased. Temperature had a stronger effect on the power density. While increasing the temperature from 20ºC to 30ºC only slightly increased the peak power densities, increasing the temperature from 30ºC to 50ºC approximately doubled the peak power densities. Chen et al. concludes that power density increases with temperature despite possible increases in methanol crossover with increasing temperature because the methanol oxidation rates increased with temperature.

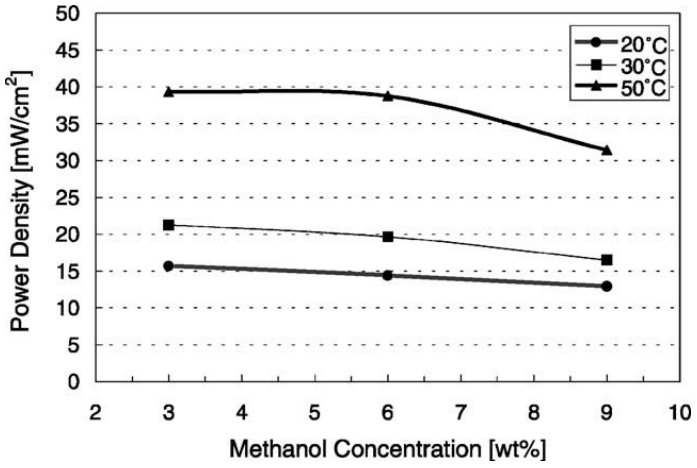

Figure 6. Effect of methanol concentration on power density at various temperatures [18].

2.4. Modeling

A variety of models have been developed to describe the mass transport of water, methanol, and other species through a fuel cell. These are discussed in more detail in the review papers by Wang [11] and Weber et al. [19]. According to the review from Wang, complete models for direct methanol fuel cells must incorporate methanol, water, and heat transfer processes. Specific physiochemical phenomena that occur in DMFC models are species, charge, and momentum transfer, multiple electrochemical reactions, and gas-liquid two phase flows in both the anode and cathode regions [11]. Other important factors that are addressed differently in different models are methanol and water crossover, carbon dioxide accumulation and removal from the anode region, and water accumulation and removal associated with flooding at the cathode region. Fuel cell models range from one dimensional to three dimensional flow models. Simpler models are isothermal and therefore do not incorporate a heat transfer model. More complex nonisothermal models couple both the heat and mass transfer models together, and may also address dynamic changes to the fuel cell.

2.4.1. Anode GDL

Mass transport in the anode GDL consists of three species: methanol, water, and carbon dioxide. The methanol and water solution must travel from the fuel reservoir or flow channel through the GDL to the anode catalyst layer where the oxidation reaction occurs. Carbon dioxide is produced as a byproduct of the methanol oxidation reaction and must be removed from the catalyst layer region. In many models, the production and mass transport of carbon dioxide is ignored because it is a byproduct and not a reactant. The mass transport of methanol and water in the anode GDL is often modeled using a convection and diffusion model. One such model was developed by Scott et al. [20] which states that methanol diffuses through the anode GDL according to Fick's Law. An effective diffusion coefficient was used that adjusts for the porosity and tortuosity of the GDL. The bulk flux found in the convection term for methanol was assumed to be equal to the flux of water through the GDL because the methanol solution was assumed to be dilute. The water transport through the anode GDL was not modeled directly, but the flux was assumed to be caused by three factors: the water consumed in the methanol oxidation reaction, the water transfer through the proton exchange membrane (PEM) due electro-osmotic drag, and the water transfer through the PEM due to diffusion. The production and mass transport of carbon dioxide was neglected. These modes of water transfer through the PEM will be discussed in more detail later in this section.

A separate model developed by Jeng et al. [21] also represents the methanol transport through the anode GDL with convection and diffusion. However, in addition to the transport through the GDL, Jeng et al. also models methanol convection and diffusion through the anode catalyst layer. While the methanol flux equation for the catalyst layer is very similar to the flux equation for the GDL, the divergence of the flux is no longer equal to zero due to methanol consumption by the anode half-reaction. The divergence is instead represented as a function of the current gradient in the catalyst layer, and this current is described by a Tafel expression. In the Jeng paper, the water transport in the catalyst layer is not directly modeled but the water flux equation includes the water consumption by the methanol oxidation reaction and the water flux in the PEM. Again, the production and mass transport of carbon dioxide was neglected.

One model which included carbon dioxide in the both the mass transport analysis and the electrochemistry analysis was developed by Baxter et al. [22]. In this isothermal steady state pseudo two dimensional model of a DMFC anode, the anode catalyst layer is considered to be a porous electrode consisting of a electrically conductive catalyst structure coated with a ionomer bond layer. The methanol solution flows through the pore in the x-direction as it contacts the bond layer. While flowing in the x-direction, the methanol solution diffuses into and across the bond layer in the pseudo y-direction until it reaches the bond layer and catalyst structure interface where the anode reaction takes place. The carbon dioxide that is produced there diffuses back across the bond layer where it enters the methanol solution stream in the pore. Baxter et al. found that the production of carbon dioxide in the DMFC anode causes a loss of anodic performance. The carbon dioxide gas blocks the methanol solution and prevents it from reaching the anode reaction site, the prohibiting the anode reaction and limiting current production. Baxter et al. also found that the production of enough carbon dioxide gas could prevent water from hydrating the bond layer in the anode thus lowering the ionic conductivity of the ionomer and increasing the ohmic losses of the cell. They suggested increasing the methanol feed stream flow rate as a means of removing the carbon dioxide, although this is not possible in passive DMFCs. While Baxter et al. showed that the production and mass transport of carbon dioxide within the DMFC anode is important, this work assumes neglects the effects of carbon dioxide production (as is the case in other one-dimensional models) in order to maintain simplicity of the model.

2.4.2. Proton Exchange Membrane

Mass transport in the Nafion® membrane consists of three species: methanol, water, and protons. Methanol mass flux is generally attributed to convection and diffusion. The major difference between most models is the representation of the convective velocity. The model developed by Sundmacher et al. [23] uses a modified Schlögl velocity based on the original work of R. Schlögl [24]. The modified Schlögl velocity is the velocity of water moving through the PEM and is a function of the proton concentration, the electrostatic gradient, and the pressure gradient within the PEM. In

order to solve for this velocity, Sundmacher et al. applies the Nernst-Planck equation for proton transport through the membrane. This equation also includes an electrostatic gradient term, and the proton flux in the membrane can be calculated from the cell current using Faraday's Law. The drawback to this method is that the mass transport of water is not directly modeled.

A different approach to modeling the methanol transport through the PEM applies a convective velocity that is derived directly from a water mass transport model. Both the model developed by Scott et al. [20] and Jeng et al. [21] use this approach. In both models, because the solution is dilute the methanol flux is assumed to be small compared to the water flux. Therefore, the bulk flux is determined solely from the water flux. In the work of Scott et al., the water flux through the PEM is assumed to be caused solely by electro-osmotic drag as long as the cell current density is above a critical current density. In the work of Jeng et al., the water flux is caused by both electro-osmotic drag and diffusion. A separate model developed by Lu et al. [15] also includes a hydraulic permeation term in the flux equation. Hydraulic permeation is water transport due to a pressure gradient. Lu et al. solves for the pressure difference across the PEM in terms of the anode and cathode external pressures and the capillary pressure of the cathode GDL.

A third approach to modeling the methanol and water transport through the PEM is to apply the Maxwell-Stefan diffusion equations. These are used for multicomponent flow for cases when the dilute solution assumption is not applicable. The model developed by Meyers et al. [25] assumes that the methanol and ion concentrations in the membrane are too high to neglect solute/solute interactions and therefore applies a modification of the approach established by Pollard and Newman [26] for multicomponent solutions which includes the Maxwell-Stefan equations. This approach employs a driving force caused by an electrochemical potential gradient on a given species equal to the sum of frictional forces on that species caused by relative motion with other species. Another more complex model developed by Schultz et al. [27] applies the Maxwell-Stefan equations to mass transport in the PEM as well as in the anode and cathode GDLs and catalyst layers. Schultz et al. also includes the effects of membrane swelling on the mass transport of the mobile species within. As a membrane begins to absorb species, the membrane volume must swell. However, if the membrane

is constrained by rigid objects such as current collectors or flow channels, the membrane is unable to swell and the space available for species to occupy is limited. Schultz et al. address this issue as well by applying a thermodynamic activity model.

2.4.3. Cathode GDL

Mass transport within the cathode GDL consists of three species: water, oxygen, and nitrogen. However, water can exist in the GDL in either the liquid phase or the gas phase. Simple single phase models assume that the water in the GDL exists only in the gaseous phase ignoring phase interactions. More complex models assume that water exists in both the liquid and gas phases and must address liquid water saturation and liquid-gas phase interactions within the GDL. Both the model developed by Meyers et al. [25] and the model developed by Schultz et al. [27] assume that all species in the cathode GDL exist in the gaseous phase and therefore neglect flooding. For these models, the bulk velocity in the cathode GDL is derived from the fact that the nitrogen within the GDL is non-reacting and does not diffuse into the PEM. Therefore, the nitrogen flux must be zero at the PEM, thus leading to the conclusion that the convective and diffusive fluxes of nitrogen must be equal in magnitude and opposite in direction. A two phase model for transport in the cathode GDL was developed by Murgia et al. [28] that addresses the level of liquid saturation within the GDL and the mass exchange between liquid and gaseous water due to evaporation and condensation within the cathode GDL.

2.4.4. Effects of Temperature

The majority of non-isothermal models found in literature are for PEMFCs. One such model developed by O'Hayre et al. [29] and expanded by Paquin et al. [30] is a one-dimensional non-isothermal heat and mass transfer model of an air breathing PEMFC with a dead ended dry hydrogen anode supply. The O'Hayre et al. model applies heat transfer, oxygen mass transfer, and water mass transfer to both the cathode GDL and the cathode convection boundary layer. Heat transfer in the cathode GDL is attributed to

conduction and mass transport in the cathode GDL is attributed to diffusion. In the convection boundary layer, the natural heat convection is represented using the non-dimensional Nusselt number, which is the dimensionless temperature gradient at the convective surface [31]. The Nusselt number is also a correlation between the non-dimensional Grashof number and the non-dimensional Prandtl number, where the Grashof number is the ratio of buoyancy to viscous forces and the Prandtl number is the ratio of the momentum and thermal diffusivities. The free convection mass transfer is represented by the non-dimensional Sherwood number, which is the dimensionless concentration gradient at the convective surface. The relationship between the heat transfer and the mass transfer is represented by the non-dimensional Lewis number. When the Lewis number is close to unity, then there is simultaneous heat and mass transfer and an analogy can be applied that relates the two [30].

O'Hayre et al. found good agreement between their experimental results and model results. They concluded that fuel cell self-heating has a strong effect on water balance and specifically membrane dry-out for passive PEMFCs, and attributed membrane dry-out as the limiting factor in passive air breathing PEMFCs, not oxygen depletion. Further, they found that the natural convection boundary layer is a significant barrier to heat and mass transfer. In order to limit membrane dry-out, O'Hayre et al. stated that the fuel cell heat rejection must be maximized while minimizing flooding on the cathode. While these observations are applicable to passive air breathing PEMFCs, they may not be applicable to passive air breathing DMFCs, which are characteristically well hydrated due to the presence of a liquid methanol fuel source. This may lessen the effects of membrane dry out on cell performance. Also, the presence of liquid methanol solution on the anode side of the fuel cell may also increase the rate of heat conduction away from the fuel cell and help keep the temperature low, which may lead to cathode flooding instead of membrane dry-out.

One of the few available non-isothermal models for a DMFC was developed by Ko et al [4]. This is a dynamic optimization model that expanded the isothermal dynamic lumped parameter DMFC model previously developed by Sundmacher et al. [23]. This was accomplished by the addition of an energy balance enabling the model to predict the influence of temperature on the mass transport and reaction kinetics of the DMFC. Ko et

al. also included a water crossover expression derived from the work of Lu et al. [15]. This model was used to analyze the effects of anode and cathode inlet flow rates, temperatures, and feed concentrations on the fuel cell and flow outlet temperature, the methanol and water crossover rates, and the cell voltage and power density in order to determine optimal operating parameters. Ko et al. concluded that the model could serve as an effective aid in optimizing the operating parameters for DMFCs and that the feed concentration of the methanol has a strong effect on the cell voltage, the rate of methanol and water crossover, and the cell temperature. However, Ko et al. did not discuss the effects of internal temperature gradients on the fuel cell performance.

2.5. Need for a Low Humidity DMFC Study

Passive direct methanol fuel cells serve as promising power sources for several small scale and portable power applications. Passive DMFCs offer the ability to produce power with little to no parasitic losses. However, because passive DMFCs must operate with unconditioned air, the power production capabilities of the passive DMFC is limited by the conditions of the operating environment. These conditions include but are not limited to environmental temperature and relative humidity. In order for the passive DMFC to serve as a practical power source for applications such as unmanned aerial vehicles, portable communications devices, portable power generators, or laptops, the passive DMFC would have to be capable of operating in various climates such as the hot and dry climates typical of deserts or the cool and humid climates typical of many cities in the North America. However, there are currently few studies on direct methanol fuel cells that were conducted in low humidity environments. The studies that have been conducted address the effects of varying some fuel cell parameters on the performance of the fuel cell within low humidity environments, but not the effects of varying relative humidity over a low range on the fuel cell performance. However, the effects of relative humidity itself on the cell performance are often overlooked. Low relative humidity environments are characteristic of high rates of water evaporation, which in the case of PEM fuel cells could lead to dehydration of the membrane and thus decrease the ionic

conductivity. Increased rates of water evaporation would also deplete the water supply at increased rates. The increased rate of water transport through the membrane may also increase the rate of methanol crossover, thus depleting the methanol supply more quickly. Instead of focusing on the effects of relative humidity on the DMFC, most studies focus on flooding and suggest various methods of water management such as the addition of multiple gas diffusion layers or a liquid-water barrier layer to prevent flooding while assuming that the Nafion® membrane of the DMFC is fully hydrated during operation, though this may not be the case under low humidity conditions. Furthermore, the bulk of the humidity studies reported in the literature were not conducted on free breathing fuel cells, which tend to produce less current and therefore are less likely to experience flooding due to lower water production levels on the cathode. I propose to conduct a DMFC study that focuses directly on the effects of a low humidity environment on the performance of a free breathing DMFC fuel cell. The range of operating conditions that will be analyzed will be chosen based on the possible operating conditions that may be experienced by a passive DMFC providing power for an unmanned aerial vehicle. Additionally, I propose to develop a one dimensional iso-thermal model that predicts the rates of methanol and water consumption and the rates of methanol and water crossover in the membrane given the cell operating temperature, the environmental relative humidity, and the cell current density.

3. EXPERIMENTAL PROCEDURES

Experiments were conducted to characterize the performance of direct methanol fuel cells over the entire spectrum of operating conditions for an unmanned aerial vehicle. The specifics of the testing, a description of the membrane electrode assembly used, and information on the equipment used for testing are presented in the following sections.

3.1. Design of Experiment

Both the relative humidity of the cathode and the temperature of the environment must be varied to characterize the performance of the fuel cell over the entire spectrum of operating conditions. The operating conditions for the micro air vehicle of interest are described in the Air Force Solicitation F061-144-0607 (Topic # AF06-144) [32]. The solicitation states that the temperature operating range for the fuel cell is from 20ºF to 120ºF (approximately -10ºC to 50ºC). The solicitation does not state an operating range for the cathode relative humidity, but it would be desirable to operate unmanned aerial vehicles in any relative humidity ranging from 0% to 100%. However, limitations imposed by the test equipment restricted testing to relative humidities between 10% and 90%, and temperatures no lower than room temperature (25°C). The matrix below specifies the combinations of temperatures and relative humidities at which each test was conducted with the respective test number.

Table 1. External conditions for each test. Test names numerated from 22 to 30.

Temperature (ºC)	Cathode Gas Relative Humidity (%)		
	10	50	90
25.0	28	29	30
37.5	25	26	27
50.0	22	23	24

For each given temperature and relative humidity combination, four potentiostatic tests, three electrochemical impedance spectroscopy (EIS) tests, and three polarization tests were performed. First, a potentiostatic test was performed at an operating voltage of 0.2

volts for 30 minutes. This was immediately followed by an EIS test conducted at a current corresponding to a cell voltage of 0.2 volts, with frequencies ranging from 10 kHz to 1 Hz, and with an oscillating current amplitude of 0.01 A. This was immediately followed by a polarization test over a range of voltages from 0.7 V to 0.1 V. These three tests were then repeated at 0.3 volts and 0.1 volts. The diagram shown in Figure 7 summarizes each test conducted, excluding the 12-hour potentiostatic test. The voltages chosen for potentiostatic and EIS tests were chosen because they cover the portion of the power curve containing both the peak power density and high current density. The EIS tests were performed after the potentiostatic tests to ensure the fuel cell reached a steady hydration level and a steady operating temperature. Following the three potentiostatic, EIS, and polarization tests, an additional extended potentiostatic test was conducted to determine the fuel cell methanol and water usage. Prior to running the test, the fuel tank was filled with a known mass of methanol solution with a known methanol concentration. Given the mass of methanol solution in the fuel tank at the beginning of the test, and the methanol concentration at that time, both the mass of methanol and the mass of water in the fuel tank could be calculated. The extended potentiostatic test was then performed at 0.3 volts for 12 hours, and the methanol concentration was monitored during testing. After completion of the test the mass of methanol solution remaining in the fuel tank and the methanol concentration of this solution were measured. Given the mass and the methanol solution concentration, both the mass of methanol and the mass of water in the fuel tank at the end of the test could be calculated. The difference between the mass of methanol in the fuel tank at the beginning and end of the 12-hour test was the methanol usage, and the difference between the mass of water in the fuel tank at the beginning and end of the 12-hour test was the water usage. The accuracy of the procedure for measuring the mass of the methanol and water mixture within the fuel tank before and after the test was measured to within +/- 0.15 grams of methanol/water mixture.

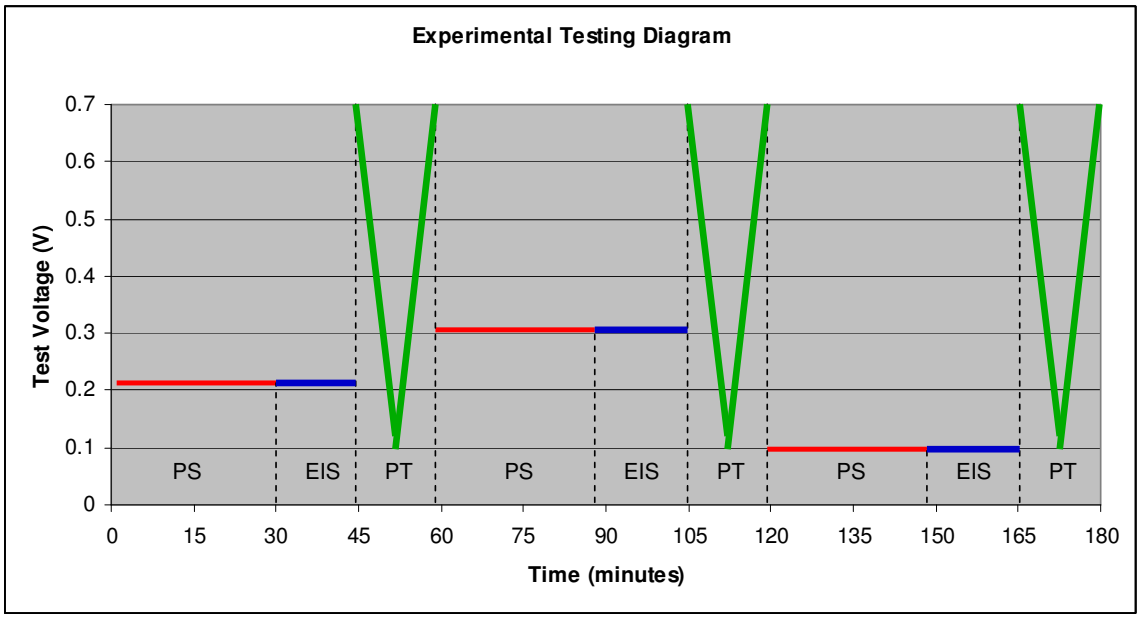

Figure 7. Diagram of tests performed at each operating condition. The cell voltage and the duration of each test are shown, where "PS" stands for potentiostatic test, "EIS" stands for electrochemical impedance spectroscopy test, and "PT" stands for polarization test. The 12-hour potentiostatic test is not shown here.

3.2. MEA Materials and Preparation

The direct methanol fuel cells used for this research incorporated membrane electrode assemblies (MEA) purchased from BASF Fuel Cell, Inc. Specifically, the MEAs purchased were the series 12D-W 5-layer membrane electrode assemblies for general purpose DMFC use (model ES12D-W-5L). The MEAs included woven gas diffusion layers and unattached sealing gaskets. The membrane size was 7cm x 8cm with an active area of 2.24cm x 2.24cm or 5cm^2.

Prior to any testing, each MEA had to be conditioned. The conditioning steps were provided by BASF Fuel Cell, Inc. and are summarized below:

- MEA Humidification. Feed hot water at 80ºC to the anode side and air saturated at 80ºC to the cathode side and maintain the cell at 80ºC for one hour or until an AC impedance of less than 280 milliohm-cm^2 is met.
- Hydrogen Activation. Feed hydrogen to the anode and air to the cathode. Set the hydrogen supply to a dew point of 95ºC and 15 psig. Set the air supply to a dew

point of 80ºC and 15 psig. Set the cell temperature to 80ºC. Run the cell for four hours at 0.6V.

All conditioning was conducted with a 5 cm^2 cell hardware assembly provided by Fuel Cell Technologies, Inc. Following conditioning of the MEA, the anode flow channel was flushed with nitrogen and the MEA was removed from the cell hardware assembly and was inserted into the DMFC test hardware made by Virginia Tech. The methanol fuel tank was filled with 2 molar methanol, the proper electrical connections were made, and the fuel cell assembly was inserted into the environmental chamber and brought to operating conditions. These steps are discussed in more detail in the following sections.

3.3. Test Equipment

Several pieces of equipment were needed to conduct the performance tests on the direct methanol fuel cell. These items are listed below and will be discussed in this section:

3.3.1. Test Stands
3.3.2. DMFC Hardware
3.3.3. Environmental Chamber
3.3.4. Temperature and Relative Humidity Transmitter
3.3.5. NI Data Acquisition
3.3.6. Fuel Supply and Monitoring

3.3.1. Test Stands

The Fuel Cell Technologies (FCT) single fuel cell test station (100 amp, 150 watt model) was used to provide conditioned air to environmental chamber. The test station is capable of delivering a cathode air flow rate up to 26,000 sccm, and an anode hydrogen flow rate of up to 14,000 sccm. The test station was modified by replacing the hydrogen anode supply with a compressed air supply. The anode was then capable of delivering an anode air flow rate of up to 14,000 sccm, providing a combined maximum air flow rate

for the modified test station of 40,000 sccm. The air temperature can be controlled from room temperature to 120ºC, and the relative humidity of the air can be controlled over a range from 0% to 100% relative humidity (RH). Although conditioned air was supplied to the test chamber to control the temperature and relative humidity of the environment, the methanol fuel cell cathode environment is still considered passive and free breathing because the fuel cell cathode was far from the supply gas stream and the air around the fuel cell is stagnant.

Although the single test station has the capabilities to perform polarization and electrochemical impedance spectroscopy tests, a separate FCT dual test station (10/100 amp, 60/150 watt model) was instead used to conduct the tests because it can more accurately measure and control the small current produced by a single methanol cell. Whereas the single test station has a 100 amp, 150 watt load, the dual test station has both a 100 amp, 150 watt load and a 10 amp, 60 watt load. The 10 amp, 60 watt load of the dual test station was used for testing.

3.3.2. DMFC Hardware

The fuel cell housing and methanol fuel tank was made of several polycarbonate sheets. The housing was designed to operate in both horizontal and vertical orientations, although only the vertical orientation was tested here. The fuel cell housing consisted of a methanol storage section, a carbon dioxide purge valve, a fueling port, a thermocouple port, cathode and anode current collectors, silicone gaskets, and a cathode gas port. A diagram of the fuel cell housing is presented in Figure 8.

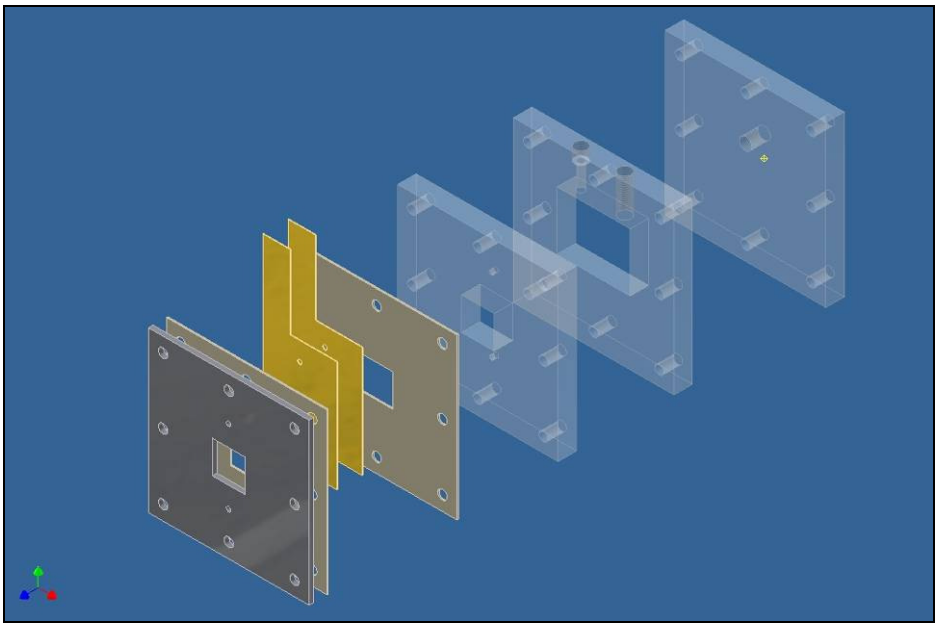

Figure 8. Fuel cell housing (MEA not shown).
The following components are listed in the order depicted from left to right: cathode plate, cathode gasket, cathode current collector, anode current collector, anode gasket, first anode plate, center anode plate, and back plate.

The membrane electrode assembly (MEA), which came from BASF with carbon cloth gas diffusion layers already attached, was sandwiched between 200 µm thick PFA gaskets. These were then sandwiched between two gold coated steel current collectors. Each current collector was made from 26 gauge 0.0178 inch thick perforated 304 stainless steel sheet with 5/64 inch holes on 7/64 inch staggered centers with a 2 µm thick gold coating. The type I grade C gold coating was applied via an electroplating process by Gold Plating Services, Kaysville, UT. The current collectors were bolted between a front polycarbonate cathode plate and a polycarbonate methanol fuel tank. The cathode plate was made from 1/8" aluminum purchased from McMaster Carr (this plate was originally designed as polycarbonate, but the polycarbonate did not provide enough rigidity to produce uniform pressure on the gasket which led to leaking). A 5 cm^2 square hole was cut into the middle of the plate to allow air to reach the fuel cell cathode. The methanol fuel tank was made of three 1/2" thick polycarbonate plates each measuring 11 cm by 11 cm. The first plate had a 5 cm^2 square hole cut into the middle of the plate to allow methanol to reach the fuel cell anode. The center plate had a larger 4 cm by 5 cm rectangular hole cut into the plate to store the majority of the methanol fuel. There were

also two ports cut into the top of the plate. One was a 1/8 inch pipe threaded port where a thermocouple could be inserted for use during horizontal testing or a carbon dioxide purge valve could be inserted for use during vertical orientation testing. The other port was a 1/8 inch pipe threaded port over a 0.2 inch hole that held a septum compressed by a hollow steel plug. This port was used for adding fuel to the tank with a syringe. The polycarbonate back plate for the fuel cell housing measured 11 cm by 11 cm. This plate also had a 1/8 inch pipe threaded port in the middle of the sheet where a thermocouple could be inserted for use during vertical testing or a carbon dioxide purge valve could be inserted for use during horizontal orientation testing. The back plate also had two 1/16" barbed connectors that were attached to fuel lines to sample and test the methanol from the fuel tank while running experiments. The entire assembly was bolted together with eight 2 inch long bolts, each tightened to 50 in-lb torque.

3.3.3. Environmental Chamber

A Thermo Scientific Labline Vacuum Oven (model 3608-5) with 19.8 liter chamber was modified for use as an environmental chamber during testing. The front glass was replaced with a piece of 1/2" polycarbonate that had a one inch diameter hole in the center. Air from the single test station was piped into the oven to control the relative humidity. Test leads and air lines entered the oven via the hole in the polycarbonate sheet. The temperature and relative humidity inside the vacuum oven were monitored with a Vaisala humidity and temperature transmitter. The relative humidity reading was then used by a LabVIEW program to control the ratio of wet to dry air that was sent from the FCT single test station into the vacuum oven, thus controlling the relative humidity inside the oven. The temperature within the methanol fuel tank was measured with a Teflon coated K-type thermocouple, and the temperature at the surface of cathode current collector was measured with a T-type foil thermocouple. The thermocouple data was transmitted with a NI data acquisition unit. An Integrated Sensing Systems, Inc. (ISSYS) FC6 methanol concentration meter was used to monitor the density of the methanol during testing. The methanol was pumped from the fuel tank to the sensor through 1/16" silicone tubing with a Gilson Micropuls 3 peristaltic pump,

and then returned to the fuel tank. The temperature and relative humidity data was logged to a computer with LabVIEW 8.6. Figure 9 shows the environmental chamber with the enclosed DMFC and associated test leads and air lines attached during testing.

Figure 9. Vacuum oven during testing.
DMFC test hardware depicted inside oven. Gilson peristaltic pump depicted on top of oven to the left. Methanol concentration meter depicted on top of oven to the right. Air flow lines wrapped in strip heaters enter oven though hole in front glass.

Figure 10 shows the DMFC within the environmental chamber prior to testing. Also depicted are the anode electrical lead (black), the cathode electrical lead (red), the Vaisala relative humidity sensor (left), and the Vaisala temperature probe (right). The relative humidity sensor and temperature probe are supported by a silicone shelf. An additional thermocouple enters the fuel tank as depicted. The methanol concentration sampling lines that are attached to the bottom of the fuel tank are also depicted.

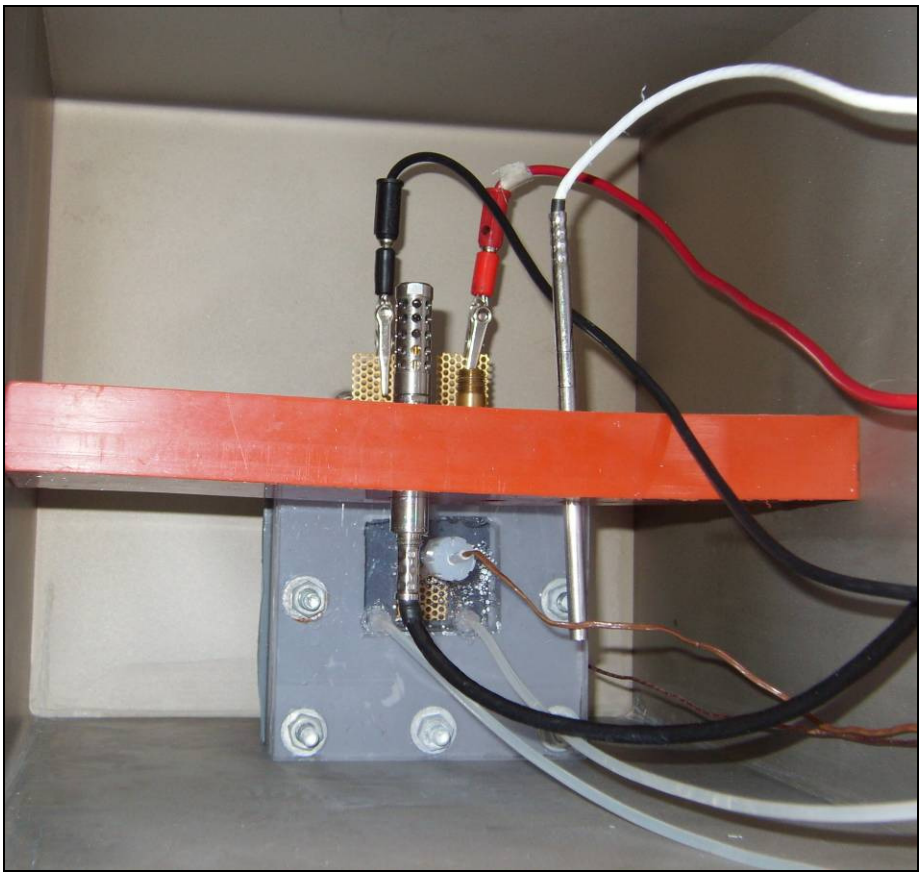

Figure 10. Fuel cell housing and connections inside vacuum oven.

3.3.4. Temperature and Relative Humidity Transmitter

The temperature and relative humidity within the environmental chamber were monitored and recorded during testing using a Vasaila HUMICAP® Humidity and Temperature Transmitter (model HMT337). This humidity and temperature transmitter used a warmed humidity probe to measure the dew point and had a separate temperature probe to measure temperature. The humidity and temperature transmitter connected to the computer via a USB port. The transmitter sent the measured temperature, relative humidity, and dew point to a LabVIEW virtual instrument which recorded the data. The transmitter was calibrated by the manufacturer and the error was reported to be +/- 1.0% for relative humidity and +/- 0.10ºC for temperature.

3.3.5. NI Data Acquisition

The temperatures of the fuel tank and cathode current collector were monitored and recorded during testing using thermocouples attached to a National Instruments (NI) data acquisition unit. This unit consisted of a NI-9211 Thermocouple Input module and a NI-USB 9162 USB carrier. The thermocouple input module was capable of monitoring up to four thermocouples at a time, although only two were used here. The data acquisition unit sent the monitored temperatures to a LabVIEW virtual instrument which recorded the data. The NI-9211 Thermocouple Input module error as reported in the owner's manual was +/- 5.0ºC. However, prior to testing the NI-9211 Thermocouple Input module was calibrated using Labview to agree with the Vaisala HMT337 temperature probe reading to within +/- 1.0ºC. Given the Vaisala HMT337 calibration, the NI-9211 Thermocouple Input module should be accurate to within +/- 2ºC.

3.3.6. Fuel Supply and Monitoring

The methanol solution concentration was monitored by a Integrated Sensing Systems, Inc. (ISSYS) (Integrated Sensing Systems, Inc., 391 Airport Industrial Drive Ypsilanti, MI 48198 USA) FC6 Methanol Concentration Meter. This concentration meter was capable of measuring and outputting the methanol concentration up to 10 times per second. The concentration meter was both powered by and communicated with the computer via a USB connection. The concentration meter output the methanol concentration as a weight percentage in terms of grams of methanol per gram of solution. The accuracy of the FC6 concentration meter as reported by the owner's manual is +/- 0.3 weight percent methanol and +/- 1ºC. A small sample of methanol solution was pumped from the fuel tank to the concentration meter and back to the fuel tank during testing using a Gilson Micropuls 3 peristaltic pump. A PVC reference tube provided by Gilson was attached directly to the pump. This tube was then extended by silicone tubes which connected the pump to the concentration meter and to the fuel tank. A 10 micron filter was also inserted in line between the pump and the concentration meter to filter any

contaminants from the methanol solution before it reached the concentration meter. The filter was an inline filter (model A411) manufactured by IDEX filters.

3.4. Experimental Procedures

This study takes advantage of three different types of tests to characterize the performance of the methanol fuel cells. Polarization tests were used to measure the relationship between voltage and current density and to characterize the polarization losses of the fuel cell. Potentiostatic tests were used to measure the steady state performance of the fuel cells over extended periods of time. EIS tests were used to determine the ohmic losses associated with the fuel cell.

3.4.1. Polarization Curve Measurement

When operating at a low current, the fuel cell experiences activation losses. When operating at a high current, the fuel cell may experience mass transport losses. And, at all currents, the fuel cell experiences ohmic losses. Polarization curves are produced from a set of current measurements collected over a range of voltages. In a stepwise manner, the fuel cell load slowly reduces the voltage of the fuel cell while measuring the current output at each voltage step. The cell voltage should be held at each set point long enough to obtain a stead state current measurement. A typical hydrogen PEM fuel cell polarization curve is shown in the figure below. A hydrogen PEM fuel cell is depicted as opposed to a DMFC in order to include the region of the curve where mass. transport losses are dominant (not present in all DMFC polarization curves).

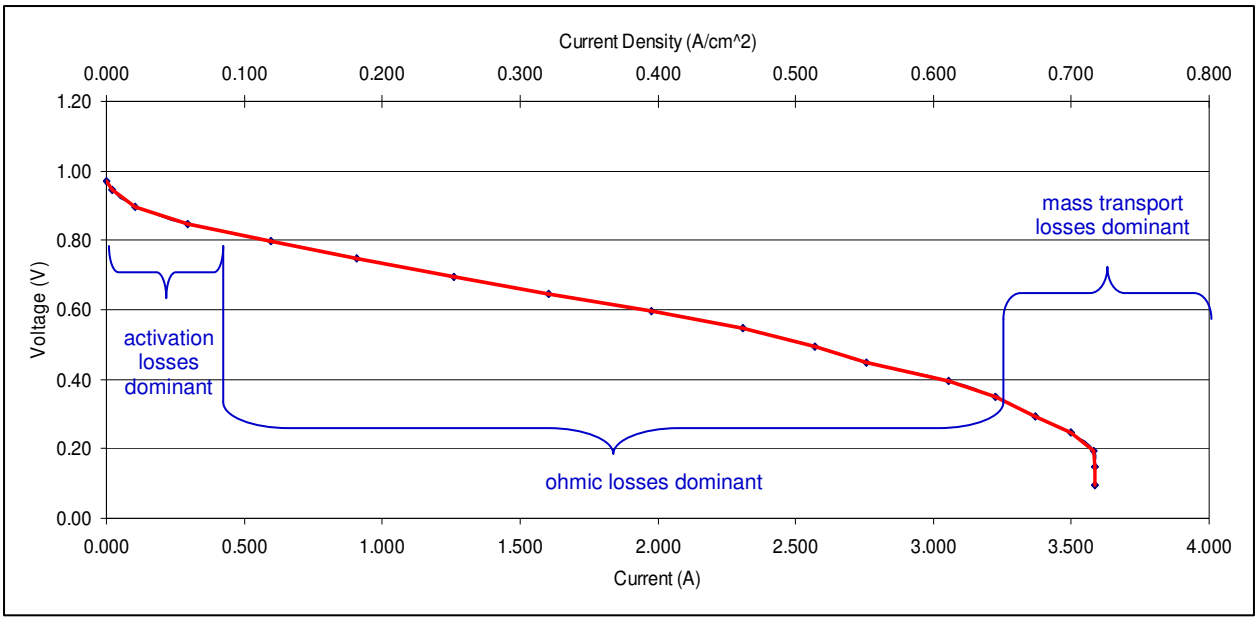

Figure 11. Hydrogen PEM fuel cell polarization curve.

Polarization tests conducted in this research were voltage sweep tests. The starting voltage was 0.7 volts. The voltage increment was 0.02 volts with a 15 second delay between readings. The cell voltage was reduced until the voltage reached 0.10 volts, and then voltage was increased stepwise until it returned to 0.7 volts. During the test, the voltage and current response were measured and recorded at 61 separate points. These tests were performed with the FCT dual test station and associated LabVIEW software.

3.4.2. Long Term Potentiostatic Testing

In a potentiostatic test, a certain voltage potential is set and held while the current response is measured. Potentiostatic tests reveal the long term performance of fuel cells under specific conditions. In this research, potentiostatic tests were performed at various temperatures and relative humidities to determine the steady state response of the methanol fuel cell. As illustrated in Figure 7, potentiostatic tests were performed at 0.3 volts, 0.2 volts, and 0.1 volts. Each test was conducted for 30 minutes. This voltage range was chosen because the 0.3 volt operating condition represents a typical operating voltage for methanol fuel cells. The 0.1 volt operating condition represents a high current

draw condition which has increased water production and crossover rates corresponding to an increased chance of flooding. An additional extended potentiostatic test was performed at 0.3 volts for a duration of 12 hours at each operating condition. These tests were conducted to allow accurate measurement of methanol and water usage over an extended period of time. These tests were performed with the FCT dual test station and associated LabVIEW software.

3.4.3. Electrochemical Impedance Testing

Electrochemical impedance spectroscopy (EIS) tests use voltage or current fluctuations to characterize the performance of fuel cells. In this research, voltage controlled electrochemical impedance tests were performed to determine the high frequency resistance of the fuel cells. Ionic losses can also be described with the data collected from EIS tests. During EIS testing, a sinusoidal current perturbation is applied to the fuel cell and the amplitude and phase shift of the voltage response is measured at different frequencies. This response is used to determine the fuel cell impedance. Impedance is the ratio between a time-dependent voltage and a time-dependent current. Impedance has both imaginary and real components. The Nyquist plot is a graphical representation of the fuel cell impedance data from an EIS test. In a typical Nyquist plot like the one below, the high frequency response is located on the leftmost part of the curve, and the frequency decreases as you move to the right along the curve. There are three regions in the plot that describe ohmic losses, anode activation losses, and cathode activation losses. At still lower frequencies, mass transfer losses may be observed. In this research, the EIS tests were performed to determine the ohmic losses. When the fuel cell is subjected to a high frequency signal, there is no imaginary impedance and thus the intercept with the real axis provides the real impedance, or ohmic resistance. Anode and cathode activation loops which describe activation losses were also observed during EIS testing, though these were not quantified. Mass transport losses can also be described by EIS tests, though none were observed in this study.

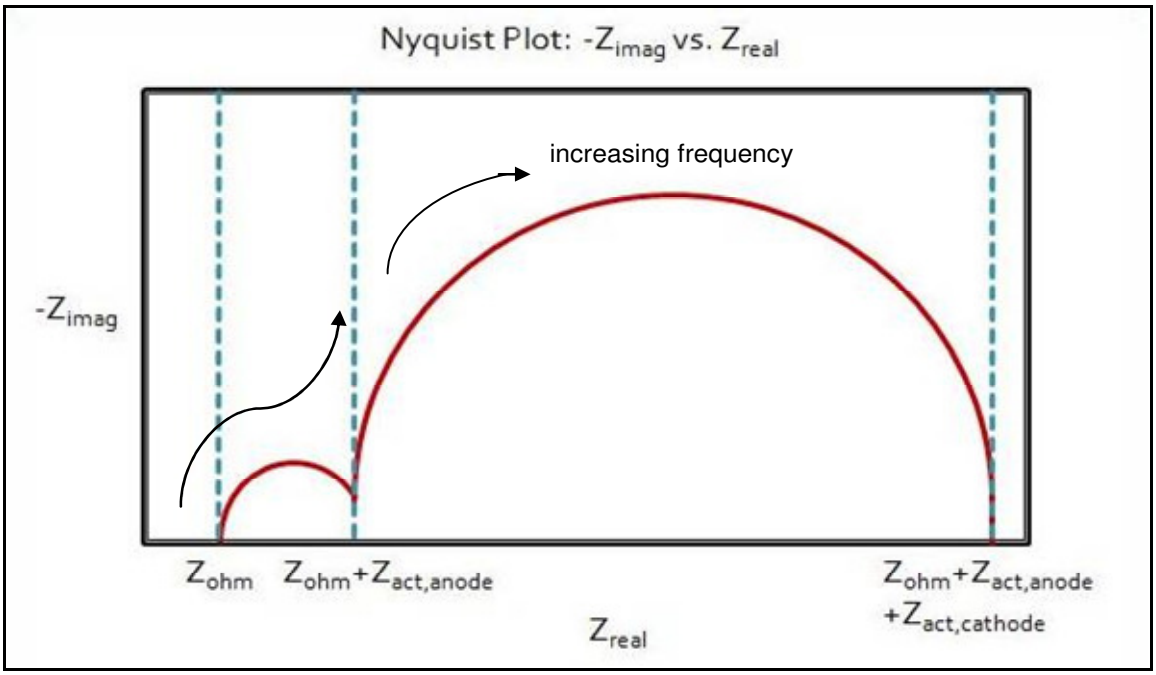

Figure 12. Typical Nyquist plot electrochemical impedance spectroscopy data of a fuel cell.

In this research, EIS tests were performed after each potentiostatic test to determine the high frequency resistance of the methanol fuel cell in each environmental condition. The EIS tests performed were current controlled tests. The FCT dual test station applied a constant control current and an AC sinusoidal perturbation with an amplitude of 0.01 A (corresponding to approximately 10% of the applied control current). A logarithmic frequency sweep from 10 kHz to 0.1 Hz was applied with the FCT dual test station, and the voltage response was measured and recorded with the FCT dual test station and associated LabVIEW software.

4. NUMERICAL MODEL

This chapter discusses the numerical model used to describe the mass transport and electrochemistry associated with the direct methanol fuel cell. The model is a one dimensional, iso-thermal, steady-state model. The model predicts the methanol and water concentration profiles in the anode and cathode GDLs and in the Nafion® membrane, and the methanol and water crossover within the Nafion® membrane. The model assumes diffusion and convection in the anode GDL, diffusion and convection in the Nafion® membrane, and multi-component diffusion and convection in the cathode GDL as described by the Maxwell-Stefan equations.

4.1. One-Dimensional Model Geometry

This model represents a single passive direct methanol fuel cell as a one dimensional object. The regions of the fuel cell that experience mass transport are the methanol fuel tank, the anode and cathode gas diffusion layers, the anode and cathode catalyst layers, and the Nafion® membrane. Figure 13 below shows the geometric representation of the methanol fuel cell. The model consists of a set of one dimensional nonlinear ordinary differential equations coupled by boundary conditions. While the model could be solved by a variety of techniques, a commercial multi-physics modeling program (COMSOL) was used in this study. The commercial software provided the benefit of direct equation specification, a variety of solvers, and flexible output formats. In addition, the development of a one dimensional model in the commercial code facilitates the development of multi-dimensional code should that be desirable in the future. The methanol fuel tank is assumed to be well-mixed and is represented by a single point designated FT which corresponds to boundary B1. The anode GDL is represented by the line segment designated A_{GDL} and corresponds to sub-domain D1. The anode catalyst layer is represented by the single point designated A_{CL} and corresponds to boundary B2 (an internal boundary). The Nafion® membrane is represented by the line segment designated Mem and corresponds to sub-domain D2.

The cathode catalyst layer is represented by the single point designated C_{CL} and corresponds to boundary B3 (an internal boundary). The cathode GDL is represented by the line segment designated C_{GDL} and corresponds to sub-domain D3. The environment is represented by the single point designated Env and corresponds to boundary B4.

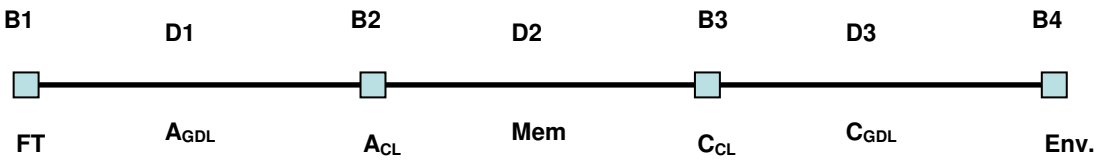

Figure 13. Diagram of 1-D model geometry.

This geometry was defined in the COMSOL Multiphysics Modeling and Simulation model [33]. The lengths of each domain are listed in the following table.

Table 2. Geometry Parameters

Region	Length
Anode GDL	0.20 mm
Nafion® Membrane	0.12 mm
Cathode GDL	0.20 mm

A mesh was created using the selective mesh option available in COMSOL. Both the anode and cathode GDL regions were divided into 20 elements. The membrane region was divided into 12 elements. Also notice that nodes fall on each of the boundaries. This mesh format was chosen to improve computational speed while still providing enough data points to accurately describe nature of the mass transport within the fuel cell. Simulations completed with twice as many elements provided approximately the same results. A comparison of these two results from the two meshed geometries is found in the appendix. The meshed regions of the 1-D geometry are illustrated in Figure 14.

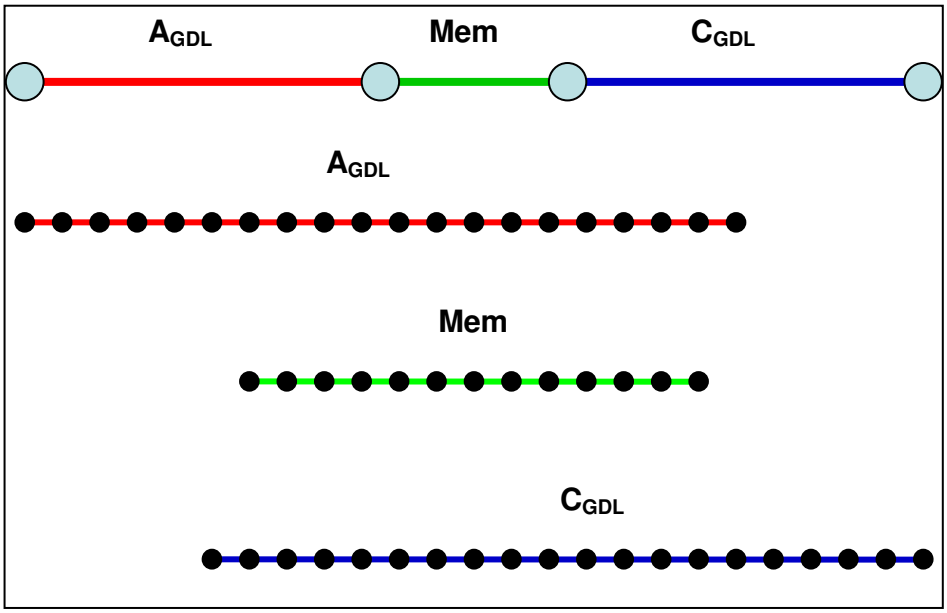

Figure 14. COMSOL geometry and mesh comparison.

4.2. One-Dimensional Mass Transport Model

This section describes in detail the assumptions, equations, boundary conditions, and parameters used to create a one dimensional numerical model of a direct methanol fuel cell. This model describes the mass transport of various species involved in the direct methanol fuel cell including water, methanol, and oxygen.

4.2.1. Model Assumptions

The following assumptions are used to simplify the numerical model.

- The cathode catalyst layer is single point.
- The anode catalyst layer is a single point.
- The temperature is constant throughout the fuel cell (iso-thermal).
- The gas diffusion layers experience equal compression across the entire surface.
- All species transport occurs in one dimension.
- The fuel cell is operating in steady state conditions for the period of interest.
- The concentration of the methanol in the fuel tank does not change for the period of interest.
- The fuel tank is a well mixed tank.
- Transport of CO_2 through the anode GDL and storage tank is neglected.

- Methanol and water in the anode GDL and Nafion® membrane exist as incompressible liquids.
- Water, oxygen, and nitrogen in the cathode GDL exist as ideal gases.

The fuel cell reaction itself is exothermic and releases thermal energy through a heat interaction with the environment. However, due to the high thermal conductivities of the methanol fuel solution, the gas diffusion layers, the current collectors, and other associated hardware, as well as a large external surface area for the test hardware, the thermal conductance of the heat transfer path is high. Therefore, the temperature throughout the fuel cell is assumed to be constant, and heat transfer aspects of the fuel cell are neglected.

Within a direct methanol fuel cell a methanol oxidation reaction occurs at the anode and an oxygen reduction reaction occurs at the cathode. These reactions occur on the surface of the catalyst particles which are embedded within the catalyst layers. Because the catalyst layers are relatively thin compared to the gas diffusion layers and the Nafion® membrane, the catalyst layer thickness is neglected. The catalyst layers are assumed to exist as single points at which the oxidation-reduction reactions occur. The fuel tank is also treated as a single point with a given methanol concentration since it is assumed to be well mixed.

The gas diffusion layers are compressed between the membrane electrode assembly and the current collector plates. In this study, the current collector plates are perforated with small holes in a staggered pattern. The regions of the gas diffusion layer that are compressed by the current collector are under higher pressure than the regions that are exposed by the holes. Thus the areas under the current collector also experience less electrical contact resistance. However, the areas exposed by the holes provide a more direct path for the corresponding reactants to reach the reaction sites. While these aspects of the fuel cell are often addressed in two or three dimensional models, they are neglected here because it is assumed that the compression is constant across the entire gas diffusion layer, and the entire gas diffusion layer has equal access to the reactants.

The oxidation reaction that occurs at the anode also produces carbon dioxide. Some of the carbon dioxide can be dissolved back into the solution, while some of it exists in the gaseous phase and produces bubbles. These bubbles can cover portions of

the catalyst layer or fill pores in the gas diffusion layer blocking reaction sites. In order to keep the model simple, the transport of carbon dioxide through the anode GDL, the presence of carbon dioxide bubbles, and the storage of carbon dioxide in the fuel tank are neglected.

4.2.2. Conservation Equations

Conservation of mass. The steady state conservation of mass equation (continuity equation) states that there is no change in the mass within a control volume over time, which requires that the divergence of the mass flux is zero. Conservation of mass under steady flow conditions is expressed as:

$$\nabla \cdot \left(\rho \vec{v}^{*} \right) = 0 \tag{4.1}$$

In the above equation, ρ is the density of the mixture and $\vec{v}^{*}$ is the mass average velocity vector of the mixture.

Conservation of species. Species in the system are conserved according to the conservation of species equation. Within regions where the flow is steady and there are no chemical reactions this equation is gien by:

$$\nabla \cdot \left(- D_i \nabla c_i + c_i \vec{v} \right) = 0 \tag{4.2}$$

In the preceding equation, D_i is the diffusion coefficient of species i, c_i is the molar concentration of species i, and $\vec{v}$ is the molar average velocity vector. The equation states that the divergence of the sum of the diffusive flux and the convective flux is equal to zero. In the following sub-sections, the species equation is developed in more detail for each of the applicable regions: anode gas diffusion layer, Nafion® membrane, and cathode gas diffusion layer. The species equation is not applied to reacting regions in this model as they are represented by single points in space.

Anode Gas Diffusion Layer. The conservation of species equation is applied to both methanol and water in the anode gas diffusion layer. The species conservation equations are modified to account for the effects of the GDL porosity and tortuosity in the porous regions,

$$\nabla \cdot \left(- D_{CH_3OH} \varepsilon^{\tau} \nabla c_{CH_3OH} + c_{CH_3OH} \vec{\mathrm{v}} \right) = 0 \tag{4.3}$$

$$\nabla \cdot \left(- D_{H_2O} \varepsilon^{\tau} \nabla c_{H_2O} + c_{H_2O} \vec{\mathrm{v}} \right) = 0 \tag{4.4}$$

where ε and τ are the porosity and tortuosity of the GDL respectively. The use of the porosity and tortuosity to correct the diffusivity for solutions in porous structures was proposed by Bruggemann and discussed by O'Hayre et al. [34] and Cunningham et al. [35]. An in-depth discussion of various methods of adjusting diffusivities for applications involving flow in porous structures can be found in the text by Wesselingh [36]. The diffusivities used here are the binary diffusivities for a methanol and water solution. The binary diffusivity for methanol in water is the same as the binary diffusivity for water in methanol. Several different values for this binary diffusivity are used in the literature [21,37,38,39]. A binary diffusivity of 2.8×10^{-9} m^2/s was used by Jeng et al. [21] and Scott et al. [37] and is also used in this paper.

Integration of equation 4.1 in conjunction with the one dimensional assumption yields a constant mass flux

$$\rho \mathrm{v}^{*}_{\mathrm{GDL,a}} = m_{CH_3OH} + m_{H_2O} \tag{4.5}$$

where ρ is the density, $\mathrm{v}^{*}_{GDL,a}$ is the mass average velocity of the mixture in the anode GDL, m_{CH_3OH} is the mass flux of methanol, and m_{H_2O} is the mass flux of water. This can also be expressed in terms of molar flux

$$\mathrm{cv}_{\mathrm{GDL,a}} = n_{CH_3OH} + n_{H_2O} \tag{4.6}$$

where c is the mixture concentration, $v_{GDL,a}$ is the molar average velocity of the mixture in the anode GDL, and n_{CH_3OH} and n_{H_2O} are the molar flux of methanol and the molar flux of water respectively. Equation 4.6 can be solved for the molar average velocity.

$$v_{GDL,a} = \frac{n_{CH_3OH} + n_{H_2O}}{c} \tag{4.7}$$

This velocity can then be used in conjunction with 1D versions of equations 4.3 and 4.4 to determine the concentration field in the anode GDL.

$$\frac{d}{dx}\left(- D_{CH_3OH} \varepsilon^{\tau} \frac{dc_{CH_3OH}}{dx} + c_{CH_3OH} v_{GDL,a} \right) = 0 \tag{4.8}$$

$$\frac{d}{dx}\left(- D_{H_2O} \varepsilon^{\tau} \frac{dc_{H_2O}}{dx} + c_{H_2O} v_{GDL,a} \right) = 0 \tag{4.9}$$

Nafion® Membrane. The conservation of species equation 4.2 is applied to both the methanol and water species that are dissolved in the solid Nafion® membrane. Both the methanol and the water species conservation equations assume methanol and water are transported in Nafion® by both diffusion and convection.

$$\nabla \cdot \left(- D^{eff}_{CH_3OH-N} \nabla c_{CH_3OH} + c_{CH_3OH} \vec{v} \right) = 0 \tag{4.10}$$

$$\nabla \cdot \left(- D^{eff}_{H_2O-N} \nabla c_{H_2O} + c_{H_2O} \vec{v} \right) = 0 \tag{4.11}$$

In the above equations, $D^{eff}_{CH_3OH-N}$ is the effective diffusion coefficient of methanol in Nafion®, $D^{eff}_{H_2O-N}$ is the effective diffusion coefficient of water in Nafion®, c_{CH_3OH} is the concentration of methanol in Nafion®, c_{H_2O} is the concentration of water in Nafion®, and $\vec{v}$ is the velocity vector of the liquid water and methanol solution in the Nafion® membrane. It is important to note that both the concentration of methanol and the

concentration of water within the Nafion® membrane region refer to the number of moles of methanol or water respectively per cubic meter of dry Nafion®. The model presented here assumes that the Nafion® membrane does not swell as it absorbs methanol and water, and thus the volume of the Nafion® membrane remains constant. Because the concentration of the methanol is low for the water/methanol mixture used in the direct methanol fuel cell, the bulk flux through the Nafion® membrane is approximately the flux of the water only. The bulk velocity then becomes approximately the velocity of the water:

$$\mathrm{v}_{H_2O} = \frac{n_{H_2O}}{c_{H_2O}} \tag{4.12}$$

This velocity can then be used in conjunction with one dimensional assumptions and equations 4.10 and 4.11 to get:

$$\frac{d}{dx}\left(- D^{eff}_{CH_3OH-N} \frac{dc_{CH_3OH}}{dx} + c_{CH_3OH}\mathrm{v}_{H_2O} \right) = 0 \tag{4.13}$$

$$\frac{d}{dx}\left(- D^{eff}_{H_2O-N} \frac{dc_{H_2O}}{dx} + c_{H_2O}\mathrm{v}_{H_2O} \right) = 0 \tag{4.14}$$

According to the work of Wang et al. [40] the effective diffusion coefficient of methanol in Nafion® is given by the following,

$$D^{eff}_{CH_3OH-N} = \varepsilon^{\tau} D_{CH_3OH-N} \tag{4.15}$$

where ε is the porosity of the Nafion® membrane which has a value of 0.3, τ is the tortuosity of the Nafion® membrane which has a value of 1.8, and D_{CH_3OH-N} is the diffusivity of methanol in Nafion®. Wang et al. used the following equation to describe the diffusivity of methanol in Nafion® as a function of temperature.

$$D_{CH_3OH-N} = 10\text{^}(-5.4163 - 999.778/T), \quad \text{m}^2/\text{s} \tag{4.16}$$

However, the diffusivity used by Wang et al. as described in equation 4.16 applies to methanol with a concentration gradient expressed in moles of methanol per volume of methanol and water solution. This work describes the concentration of methanol in the Nafion® membrane in terms of moles of methanol per volume of Nafion®. Equation 4.16 was adjusted to account for the definition of methanol concentration within the membrane used in this work by multiplying it by the equivalent weight of Nafion® and the density of water and by dividing it by the molar mass of water, the water content at the interface between the anode diffusion layer and Nafion® membrane (discussed in the boundary conditions section), and the density of dry Nafion®.

$$D_{CH_3OH-N} = \left(\frac{EW\rho_{H_2O}}{M_{H_2O}\lambda_{H_2O}^{D2/B2}\rho_d} \right) 10\text{^}(-5.4163 - 999.778/T), \quad \text{m}^2/\text{s} \tag{4.17}$$

Additionally, calculation of the effective diffusion coefficient of methanol in Nafion® based on an experiment conducted in this study proved the effective diffusivity proposed by Wang et al. to be too large. A diffusivity correction factor of 0.466 was multiplied by the effective diffusivity. The final equation for effective diffusion coefficient of methanol in Nafion® is given by the following.

$$D_{CH_3OH-N}^{eff} = 0.466\varepsilon^{\tau} \left(\frac{EW\rho_{H_2O}}{M_{H_2O}\lambda_{H_2O}^{D2/B2}\rho_d} \right) 10\text{^}(-5.4163 - 999.778/T), \quad \text{m}^2/\text{s} \tag{4.18}$$

The water species equation assumes that water is transported through the Nafion® membrane by both diffusion and convection. Integrating equation 4.14 for a one dimensional flow gives the following water flux equation.

$$n_{H_2O} = -D_{H_2O-N}^{eff} \frac{dc_{H_2O}}{dx} + c_{H_2O} \text{v}_{H_2O} \tag{4.19}$$

Diffusive transport is described by the first term in equation 4.19 where the diffusivity of water in Nafion® depends on the temperature and water content of the Nafion®. The diffusivity is described by the following equation

$$D_{H_2O-N}^{eff} = \exp\left[2416\left(\frac{1}{303}-\frac{1}{T}\right)\right] \times\left(2.563-0.33\lambda_{H_2O}+0.0264\lambda_{H_2O}{}^2-0.000671\lambda_{H_2O}{}^3\right)10^{-10} \tag{4.20}$$

where λ_{H_2O} is the local water content in the Nafion® membrane [34]. Equation 4.20 applies when water content is greater than 4. The units for water diffusivity in Nafion® are m^2/s. Water content is defined as the number of molecules of water in Nafion® per sulfonic acid site. Water content is related to concentration by the following equation.

$$\lambda_{H_2O} = c_{H_2O}\frac{EW}{\rho_d} \tag{4.21}$$

According to Lu et al. [15] the non-diffusive component of water transport (i.e. the second term in equation 4.19) is attributable electro-osmosis and hydraulic permeation. Modifying equation 4.19 to describe these contributions explicitly yields,

$$n_{H_2O} = -D_{H_2O-N}^{eff}\frac{dc_{H_2O}}{dx}+n_d\frac{i}{F}-\frac{k_p\rho}{\mu M_{H_2O}}\frac{dP}{dx} \tag{4.22}$$

where n_d is the electro-osmotic drag coefficient, k_p is the hydraulic permeability of the Nafion® membrane, μ is the viscosity of water, ρ is the water-Nafion® solution density, and M_{H_2O} is the molar mass of water. The second term on the right side of the equation describes the water flux due to electro-osmosis which depends on the electrical current. The third term on the right side of the equation describes the water flux due to hydraulic permeation which is driven by a pressure gradient according to Darcy's Law.

Following the assumption that water flux is driven only by diffusion and convection, and assuming that convection includes both electro-osmosis and hydraulic permeation, the convection term in equation 4.19 can be set equal to the sum of the electro-osmosis and hydraulic permeation terms of equation 4.22. Solving for the water velocity then gives the following equation.

$$\mathrm{v}_{H_2O} = \frac{n_d i}{c_{H_2O} F} - \frac{k_p \rho}{c_{H_2O} \mu M_{H_2O}} \frac{dP}{dx} \tag{4.23}$$

Substituting the water velocity from equation 4.23 into equation 4.19 provides the following form of the water flux equation which is used in this model.

$$n_{H_2O} = -D^{eff}_{H_2O-N} \frac{dc_{H_2O}}{dx} + c_{H_2O}\left(\frac{n_d i}{c_{H_2O} F} - \frac{k_p \rho}{c_{H_2O} \mu M_{H_2O}} \frac{dP}{dx} \right) \tag{4.24}$$

The pressure inside the Nafion® membrane is assumed to vary linearly with respect to position. Therefore, the pressure gradient $\frac{dP}{dx}$ is a function of the pressure difference across the membrane and the membrane thickness. The work of Lu et al. describes the pressure gradient as the following [15]

$$\frac{dP}{dx} = \frac{P_c - P_a}{d_M} \tag{4.25}$$

where P_c is the pressure at the Nafion® cathode surface, P_a is the pressure at the Nafion® anode surface, and d_M is the Nafion® membrane thickness. Consistent with Lu's work, it is assumed that no external pressure is applied to the anode fuel or cathode gas stream. Thus the anode side of the membrane is at atmospheric pressure (P_0). The cathode gas diffusion layer is assumed to act like a capillary tube, and the cathode pressure is assumed to be equal to the liquid water pressure in the tube. The surface tension of the water causes a liquid water and air interface to form in the tube [41]. The pressure

difference between the liquid water and the air in the capillary tube is the capillary pressure (P_{cap}). According to the work of Lu et al., the equation for the capillary pressure in the cathode gas diffusion layer is

$$P_{cap} = P_g - P_l = 2\sigma \frac{\cos(\theta_c)}{r_c} \tag{4.26}$$

where σ is the surface tension of water, θ_c is the contact angle between the solid-liquid and liquid-gas interfaces, and r_c is the GDL pore radius. However, this equation does not account for the relationship between capillary pressure and diffusion layer saturation. Therefore, data from an empirical model presented in the work of Sole et al. [42] is used to correlate the capillary pressure to the cathode diffusion layer saturation instead of using Equation 4.26 for capillary pressure. Figure 15 shows the correlation between capillary pressure and diffusion layer saturation.

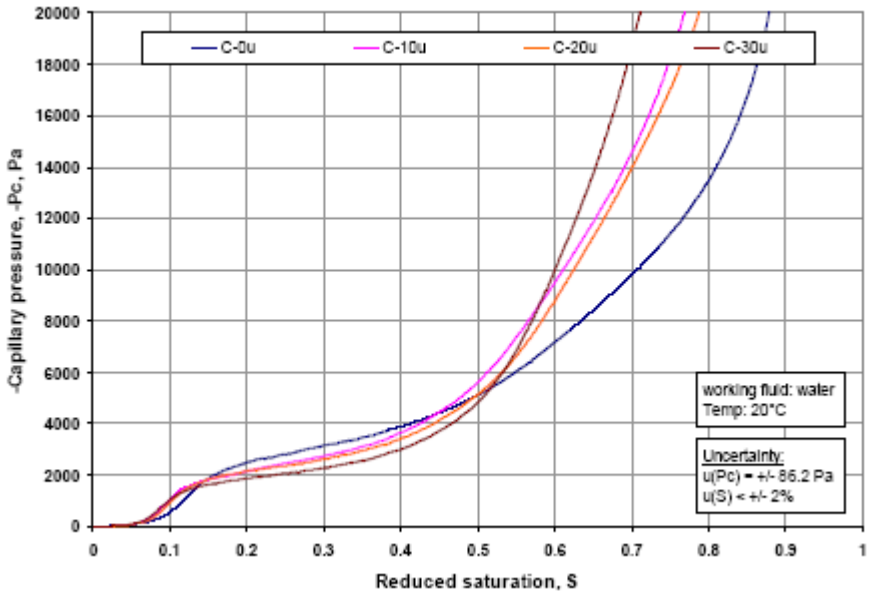

Figure 15. Empirical correlation between capillary pressure and saturation in uncompressed carbon cloth diffusion layers, created by Joshua David Sole [42].

With the capillary pressure determined (as a function of saturation) from Figure 15 and assuming the cathode gas is at atmospheric pressure, the liquid pressure at the cathode is given by the following equation.

$$P_c = P_0 - P_{cap} \tag{4.27}$$

Expressing the anode pressure as the sum of the anode gauge pressure ($P_{a,ga}$) and the atmospheric pressure yields:

$$P_a = P_{a,ga} - P_0 \tag{4.28}$$

Substituting equation 4.28 and equation 4.29 into equation 4.25 yields

$$\frac{dP}{dx} = -\left(\frac{P_{cap} + P_{a,ga}}{d_M} \right) \tag{4.29}$$

This pressure gradient can then be used in conjunction with equation 4.24 to describe the molar flux of the water in the Nafion® membrane:

$$N_{H_2O} = -D^{eff}_{H_2O-N} \nabla c_{H_2O} + c_{H_2O} \left(\frac{n_d i}{c_{H_2O} F} + \frac{k_p \rho (P_{cap} + P_{a,ga})}{c_{H_2O} \mu M_{H_2O} d_M} \right) \tag{4.30}$$

Cathode Gas Diffusion Layer. Three species are assumed present in the cathode gas diffusion layer. These are oxygen, water vapor, and nitrogen. It is assumed that no liquid water is present in the cathode gas diffusion layer. The three gaseous species present in the GDL are assumed to move by diffusion and convection only. The Maxwell-Stefan diffusion equations are used to model the diffusive transport of the three gaseous species. A complete mass transport equation (including diffusion and convection) takes the form of [43]

$$\frac{\partial \rho \omega_i}{\partial t} + \nabla \cdot \left(\rho \omega_i \vec{v}_g^{\,*} - \rho \omega_i \sum_{j=1}^{n} \mathbb{D}_{ij} \left(\nabla X_j + \left(X_j - \omega_j \right) \frac{\nabla P}{P} \right) - D_i^T \frac{\nabla T}{T} \right) = R_i \tag{4.31}$$

where ρ is the gas mixture density, ω_i is the mass fraction of species *i*, $\vec{v}_g^{\,*}$ is the mass average velocity vector of the gas mixture, $\mathbb{D}_{ij}$ is the *ij* component of the multicomponent Fick diffusivity, X_j is the molar fraction of species *j*, *P* is the pressure of the gas mixture, D_i^T is the generalized thermal diffusion coefficient, and R_i is the reaction rate. By applying the steady state assumption the time derivative term can be dropped, and by assuming that no reactions occur within the cathode GDL the reaction rate term can be dropped. Also, in this model we assume that the temperature is constant throughout the fuel cell, thus making the temperature gradient term zero. Assuming that the gas pressure within the cathode GDL is constant makes the pressure gradient term zero. After applying these assumptions, the resulting conservation of species equation for the cathode gas diffusion layer becomes the following,

$$\nabla \cdot \left(\omega_i \rho \vec{v}_g^{\,*} - \rho \omega_i \sum_{j=1}^{N} \mathbb{D}_{ij} \nabla X_j \right) = 0 \tag{4.32}$$

For two or three species, as is the case in this model, the multicomponent Fick diffusivities are calculated from the multicomponent Maxwell-Stefan diffusivities as is described in more detail in the referenced texts [43,44,45,46]. Only the basic components of a ternary system are presented in this paper. Additional terms are calculated via cyclic permutation of the species indices (e.g., 1's become 2's, 2's become 3's, and 3's become 1's) as suggested in the referenced text [42]. Also note that, similarly to the diffusivities in the anode GDL, the cathode diffusivities are corrected for porosity and tortuosity [34,35] as follows.

$$\mathbb{D}_{11} = \frac{\dfrac{(\omega_2+\omega_3)^2}{X_1\tilde{D}_{23}^{eff}} + \dfrac{\omega_2^{\,2}}{X_2\tilde{D}_{13}^{eff}} + \dfrac{\omega_3^{\,2}}{X_3\tilde{D}_{12}^{eff}}}{\dfrac{X_1}{\tilde{D}_{12}^{eff}\tilde{D}_{13}^{eff}} + \dfrac{X_2}{\tilde{D}_{12}^{eff}\tilde{D}_{23}^{eff}} + \dfrac{X_3}{\tilde{D}_{23}^{eff}\tilde{D}_{13}^{eff}}} \tag{4.33}$$

$$\mathbb{D}_{12} = \frac{\dfrac{\omega_1(\omega_2+\omega_3)}{X_1\tilde{D}_{23}^{eff}} + \dfrac{\omega_2(\omega_1+\omega_3)}{X_2\tilde{D}_{13}^{eff}} - \dfrac{\omega_3^{\,2}}{X_3\tilde{D}_{12}^{eff}}}{\dfrac{X_1}{\tilde{D}_{12}^{eff}\tilde{D}_{13}^{eff}} + \dfrac{X_2}{\tilde{D}_{12}^{eff}\tilde{D}_{23}^{eff}} + \dfrac{X_3}{\tilde{D}_{23}^{eff}\tilde{D}_{13}^{eff}}} \tag{4.34}$$

$$\tilde{D}_{ij}^{eff} = \varepsilon^{\tau}\tilde{D}_{ij} \tag{4.35}$$

where $\tilde{D}_{ij}^{eff}$ is the *ij* component of the corrected Maxwell-Stefan diffusivity. It has been shown that for multicomponent diffusion in gases at low density that the multicomponent Maxwell-Stefan diffusivities, $\tilde{D}_{ij}$, can be replaced with the binary diffusivities, D_{ij}, for each species [43]. Equation 4.35 can then modified to produce the following equation for the corrected Maxwell-Stefan diffusivity.

$$\tilde{D}_{ij}^{eff} = \varepsilon^{\tau}D_{ij} \tag{4.36}$$

The binary diffusivity for a component of a mixture is a function of the mixture pressure, temperature, and of the component properties [47].

$$D_{ij} = \frac{a}{P}\left(\frac{T}{\sqrt{T_{cr,i}T_{cr,j}}}\right)^{b}\left(P_{cr,i}P_{cr,j}\right)^{1/3}\left(T_{cr,i}T_{cr,j}\right)^{5/12}\left(\frac{1}{M_i}+\frac{1}{M_j}\right)^{1/2} \tag{4.37}$$

In the preceding equation, *a* and *b* are dimensionless constants determined experimentally, $T_{cr,i}$ and $T_{cr,j}$ are the critical temperatures of, $P_{cr,i}$ and $P_{cr,j}$ are the critical pressures, and M_i and M_j are the molar masses of species *i* and species *j* respectively.

For the one dimensional case considered here, equation 4.32 becomes:

$$\frac{d}{dx}\left(\omega_i \rho \mathrm{v}_{\mathrm{g}}^{*} - \rho\omega_i \sum_{j=1}^{N} \mathbb{D}_{ij} \frac{dX_j}{dx}\right) = 0 \tag{4.38}$$

where $\mathbb{D}_{ij}$ is found using the approach presented in equations 4.33 -4.36 with the diffusivity found from equation 4.37.

4.2.3. Boundary Equations

In each domain of the model, differential equations are used to describe the conservation of the respective species within that domain. Boundary conditions are required for each species conservation equation. These boundary conditions are one of two types: concentration (Dirichlet) or flux (Neumann) conditions. Boundary conditions are described here for each of the three sub-domains as illustrated in Figure 13.

Anode Diffusion Layer. At the surface between the methanol fuel tank and the anode diffusion layer, the methanol solution is assumed to be held at a constant concentration. Therefore, both the methanol and water concentrations are known, providing the first two concentration boundary conditions. At the interface between the anode diffusion layer and the Nafion® membrane (boundary B2 which corresponds to the anode catalyst layer), both the flux of methanol and the flux of water are known. The flux of methanol arriving at this boundary (by diffusion and convection) is equal to the sum of the flux through the Nafion® membrane and the amount of methanol consumed by the electrochemical reaction as described in equation 4.39.

$$N_{CH_3OH}^{D1/B2} = \left[-D_{CH_3OH} \varepsilon^{b} \frac{dc_{CH_3OH}}{dx} + c_{CH_3OH} \mathrm{v} \right]^{D1/B2} = N_{CH_3OH}^{D2/B2} + \frac{i}{6F} \tag{4.39}$$

The flux of water arriving at the anode diffusion layer and Nafion® membrane boundary is equal to the sum of the flux of water through the Nafion® membrane plus the water consumed by the electrochemical reaction.

$$N_{H_2O}^{D1/B2} = \left[-D_{H_2O}\varepsilon^{\tau}\frac{dc_{H_2O}}{dx} + c_{H_2O}\mathrm{v} \right]^{D1/B2} = N_{H_2O}^{D2/B2} + \frac{i}{6F} \tag{4.40}$$

Equations 4.39 and 4.40 couple fluxes of methanol and water respectively between sub-domains. In addition, the concentrations in the two sub-domains are coupled as described in the next section.

Nafion® Membrane. Two separate second order differential equations are used to describe the mass transport of methanol and water through the Nafion® membrane. Therefore, two boundary conditions are required for each of the two differential equations, or four boundary conditions total for the membrane region. Water at the boundary of the anode diffusion layer and the Nafion® membrane is assumed to exist in the liquid phase, and the Nafion® at this interface is assumed to be fully saturated. The water content (λ_{H_2O}) of Nafion® is the ratio of the number of water molecules to the number of charged sulfonic acid ($SO_3^- H^+$) sites. The water content, which ranges from 0 for fully dehydrated to 22 for fully saturated [34], is assumed to be equal to 22 at this interface. The methanol adsorbed into the Nafion® membrane is assumed to supplement water, thereby increasing the total (water and methanol) content of the Nafion® (λ_T). Also, the work of Ren et al. [48] found that the concentration of methanol within the ion-cluster pores of the membrane is essentially the same as the external methanol concentration, which in this case is the concentration of methanol within the anode diffusion layer. The mole fraction of water within the ion-cluster pores of the membrane is assumed to be the same as the mole fraction of water within the water/methanol mixture in the anode diffusion layer. These assumptions form the basis of the following derivations.

The water content (λ_{H_2O}) and the methanol content (λ_{CH_3OH}) within the Nafion® membrane are described with respect to the total content in the membrane in Equations 4.41 and 4.42 respectively,

$$\lambda_{H_2O} = X_{H_2O}\lambda_T \tag{4.41}$$

$$\lambda_{CH_3OH} = X_{CH_3OH}\lambda_T \tag{4.42}$$

where X_{H_2O} and X_{CH_3OH} are the mole fractions of water within the membrane and methanol within the membrane respectively. Combining equations 4.41 and 4.42 and solving for the methanol content in the Nafion® membrane (sub-domain D2) at the interface between the anode diffusion layer and the membrane (boundary B2) gives Equation 4.43,

$$\lambda_{CH_3OH}^{D2/B2} = \frac{X_{CH_3OH}^{D2/B2}}{X_{H_2O}^{D2/B2}} \lambda_{H_2O}^{D2/B2} \tag{4.43}$$

where water content ($\lambda_{H_2O}^{D2/B2}$) at the interface is equal to 22 (fully hydrated membrane).

At the interface between the membrane and anode diffusion layer, the ratio of these mole fractions in the membrane is assumed to be equal to the ratio of the concentrations of methanol and water within the anode diffusion layer. The equation for methanol content in the membrane at this interface then becomes:

$$\lambda_{CH_3OH}^{D2/B2} = \frac{c_{CH_3OH}^{D1/B2}}{c_{H_2O}^{D1/B2}} \lambda_{H_2O}^{D2/B2} \tag{4.44}$$

where the water content is known and the concentrations of both methanol and water within the anode GDL are determined from the species conservation equation 4.14. However, using the concentration of the methanol in the anode diffusion layer to

determine the methanol content in the membrane neglects any changes that may occur in the concentration of methanol within the anode catalyst layer. As current is produced within the catalyst layer, methanol is consumed and the concentration changes can be very significant. And because the methanol crossover rate is strongly dependent on the methanol concentration at the interface between the membrane and catalyst layer, this aspect cannot be neglected.

A semi-empirical approach is employed to determine the methanol concentration at this interface. First, the volumetric current density is described using Butler-Volmer kinetics with the assumption of high activation overpotential.

$$j = j_0 \frac{c_{CH_3OH}}{c^0_{CH_3OH}} e^{-\alpha n F \eta_a / RT} \tag{4.45}$$

In this equation, η_a is the anode overpotential which corresponds to the open circuit voltage minus the cathode activation loss and the ohmic loss, each of which is dependent on the overall cell current density and the cell operating conditions. The equation for the anode overpotential is the following,

$$\eta_a = V_{OC} - \eta_c(i, c_{O2}, T, \Theta) - iASR(T, \Theta) \tag{4.46}$$

where V_{OC} is the open circuit voltage, η_c is the cathode overpotential, and ASR is the area specific resistance. Combining equations 4.45 and 4.46 yields,

$$j = c_{CH_3OH} B(i, c_{O2}, T, \Theta) \tag{4.47}$$

where B is a function of the cell operating conditions. As a first approximation, only the current density dependence is considered such that,

$$j = c_{CH_3OH} \beta(i) \tag{4.48}$$

where β is considered the anode reaction rate coefficient. The transport of methanol through the catalyst layer can be described by an ordinary differential equation written in terms of the methanol concentration,

$$\nabla \cdot \left(- D_{CH_3OH-CL}^{eff} \nabla c_{CH_3OH} \right) = S \tag{4.49}$$

where $D_{CH_3OH-CL}^{eff}$ is the effective diffusion coefficient of methanol in the catalyst layer and S is the sink or source of methanol. The effective diffusion coefficient of methanol in the anode catalyst layer as presented by Rice et al. [49] is given as,

$$D_{CH_3OH,cl}^{eff} = \varepsilon_{cl}^{\tau_{cl}} 10\text{^}\left(\text{-5.4163-}\frac{999.778}{T} \right) \tag{4.50}$$

where ε_{cl} is the porosity of the catalyst layer (chosen as 0.6), and τ_{cl} is the tortuosity of the catalyst layer (chosen as 1.8). In this case, methanol is consumed and therefore S is the volumetric methanol consumption given by,

$$S = -\frac{j}{6F} = \frac{-c_{CH_3OH}\beta(i)}{6F} \tag{4.51}$$

Combining equations 4.49and 4.51 for a one dimensional application yields the following ordinary differential equation written in terms of methanol concentration.

$$D_{CH_3OH-CL}^{eff} \frac{d^2}{d^2x} c_{CH_3OH} = \frac{c_{CH_3OH}\beta(i)}{6F} \tag{4.52}$$

Equation 4.52 is subject to the following boundary conditions,

$$c_{CH_3OH}(x=0) = c_{CH_3OH}^{D1/B2} \tag{4.53}$$

$$c_{CH_3OH}(x=L) = c_{CH_3OH}^{CL/N} \tag{4.54}$$

where $c_{CH_3OH}^{D1/B2}$ is the methanol concentration at the interface between the anode diffusion layer and the anode catalyst layer, $c_{CH_3OH}^{CL/N}$ is the methanol concentration at the interface between the anode catalyst layer and the Nafion® membrane, and *L* is the length of the anode catalyst layer. Solving equation 4.52 for methanol concentration and applying the boundary condition equations 4.53 and 4.54 gives the following (complete derivations for equations 4.55 and 4.57 are given in the appendix).

$$c_{CH_3OH} = c_{CH_3OH}^{D1/B2} e^{(\sqrt{\beta})x/L} + \frac{c_{CH_3OH}^{D1/B2}\left(c_{CH_3OH}^{CL/N} \Big/ c_{CH_3OH}^{D1/B2} - e^{(\sqrt{\beta})}\right)\left(e^{(\sqrt{\beta})x/L} - e^{(\sqrt{\beta})x/L}\right)}{\left(-e^{(\sqrt{\beta})} + -e^{(\sqrt{\beta})}\right)} \tag{4.55}$$

Finally, the current density, i, is simply the integration of the volumetric current density, j, across the length of the catalyst layer, given by the following.

$$i = \int_{x=0}^{x=L} \beta c_{CH_3OH}\, dx \tag{4.56}$$

Solving equation 4.56 for the concentration of methanol at the interface between the anode catalyst layer and the membrane gives the following.

$$c_{CH_3OH}^{CL/N} = -c_{CH_3OH}^{D1/B2} \frac{\left(\left(\frac{i\sqrt{\beta}}{\alpha c_{CH_3OH}^{D1/B2} L} + 1 - e^{(\sqrt{\beta})}\right)\left(-e^{(\sqrt{\beta})} + -e^{(\sqrt{\beta})}\right) - e^{(\sqrt{\beta})}\left(e^{(\sqrt{\beta})} + e^{(\sqrt{\beta})}\right) + 2e^{(\sqrt{\beta})}\right)}{\left(e^{(\sqrt{\beta})} + e^{(\sqrt{\beta})} - 2\right)} \tag{4.57}$$

The methanol concentrations at the anode GDL/CL interface and the CL/membrane interface are related by equation 4.57, provided that the current density, *i*, and the functional form of *β(i)* are known. In this work, the current density is known for each experiment and *β(i)* takes the form of a simple liner expression with the slope and

intercept chosen to minimize the absolute error over all nine 12-hour potentiostatic experiments. If the simple linear form of $\beta(i)$ cannot be used to fit the experimental data, more complicated forms or forms that include cathode reactant concentration, temperature and relative humidity explicitly can be employed.

Substituting $c_{CH_3OH}^{CL/N}$ for $c_{CH_3OH}^{D1/B2}$ in equation 4.44 gives the following equation for the methanol content in the membrane at the interface between the anode diffusion layer and the membrane.

$$\lambda_{CH_3OH}^{D2/B2} = \frac{c_{CH_3OH}^{CL/N}}{c_{H_2O}^{D1/B2}} \lambda_{H_2O}^{D2/B2} \tag{4.58}$$

Both the concentrations of methanol and of water in the membrane (sub-domain D2) at the interface between the anode GDL and the Nafion® membrane (boundary B2) can now be determined using the following equations:

$$c_{CH_3OH}^{D2/B2} = \frac{\lambda_{CH_3OH}^{D2/B2} \rho_d}{EW} \tag{4.59}$$

$$c_{H_2O}^{D2/B2} = \frac{\lambda_{H_2O}^{D2/B2} \rho_d}{EW} \tag{4.60}$$

where EW is the equivalent weight of Nafion® and ρ_d is the density of dry Nafion®.

Two additional boundary conditions are required within the membrane (sub-domain D2) at the interface between the Nafion® membrane and the cathode GDL (boundary B3). First, the entire amount of methanol that reaches the interface is assumed to be oxidized in a reaction that produces carbon dioxide and water. Therefore, the concentration of methanol at this interface is assumed to be zero, and the following boundary condition is applied.

$$c_{CH3OH,D2}^{B3} = 0 \tag{4.61}$$

While this is a common assumption for methanol concentration at the cathode membrane and GDL interface, in actuality there is a concentration drop across the cathode catalyst layer similar to the concentration drop found across the anode catalyst layer. Although it was not applied here, an equation similar to equation 4.57 could be derived at and applied to the cathode catalyst layer to account for the methanol concentration drop.

Second, a concentration boundary condition is applied to the water at the interface between the Nafion® membrane and the cathode GDL (boundary B3). The general formula for water content in a Nafion® membrane is given by,

$$\lambda_{H_2O} = 0.0043 + 17.81a_w - 39.85a_w^{\,2} + 36.0a_w^{\,3} \quad \text{for } 0 < a_w \le 1 \tag{4.62}$$

where a_w is the water vapor activity (essentially relative humidity) [34] of the surrounding air. However, the interface between the Nafion® membrane and the cathode GDL (boundary B3) is exposed to humid air through the open GDL pores and is exposed to liquid water through the saturated GDL pores. By assuming that the membrane is locally saturated (water content of 22) at areas exposed to liquid water, equation 4.62 can be modified to describe the water content of the Nafion® membrane at the interface between the membrane and cathode GDL (boundary B3) as follows,

$$\lambda_{H_2O}^{D2/B3} = 22s + \left(0.0043 + 17.81a_w - 39.85a_w^{\,2} + 36.0a_w^{\,3}\right)(1-s) \quad \text{for } 0 < a_w \le 1 \tag{4.63}$$

where s is the liquid water saturation of the cathode GDL, and the water vapor activity is given by,

$$a_w = \frac{P_v}{P_{sat}} \tag{4.64}$$

where P_v is the partial pressure of water vapor in the cathode GDL at the interface and P_{sat} is the saturation water vapor pressure at the operating temperature [34]. The partial pressure of the water vapor in the cathode GDL is given by,

$$P_v = \frac{c_{H_2O}}{c_{H_2O} + c_{O_2} + c_{N_2}} P_0 \tag{4.65}$$

where the concentrations of the respective gases are determined by solving the mass species conservation equations in the cathode GDL and P_0 is the atmospheric pressure (the pressure of the gas within the GDL).

With the water content in the membrane at the interface determined from equation 4.63, the water concentration in the membrane at the interface (boundary B3) is determined using equation 4.66.

$$c_{H_2O}^{D2/B3} = \frac{\lambda_{H_2O}^{D2/B3} \rho_d}{EW} \tag{4.66}$$

Cathode Gas Diffusion Layer. Three second order differential equations are used to describe the mass transport of water, oxygen, and nitrogen within the cathode gas diffusion layer (GDL). Therefore, two separate boundary conditions are required to solve the differential equations associated with each of the three species, or a total of six boundary conditions are required. At the cathode catalyst layer, a reduction half reaction occurs that consumes the oxygen arriving from the cathode GDL. A methanol oxidation reaction also occurs that consumes the methanol that crossed over through the Nafion® membrane and produces carbon dioxide and water. No reactions occur at the boundary between the cathode GDL and the atmosphere and the gas mixture at this boundary is assumed to exist at the same molar concentration ratio as the surrounding air which is known.

At the boundary between the Nafion® membrane and the cathode GDL, the flux of water entering the cathode GDL (by diffusion and convection) is equal to the flux of water leaving the Nafion® membrane plus the amount of water produced by the cathode reduction reaction and by the methanol oxidation reaction (oxidation at the cathode of methanol that crossed over through the membrane). However, species within pores that are saturated with liquid water are assumed to be immobile. Therefore, saturation of the

cathode GDL effectively reduces the area of the GDL though which the gas can flow. Equations 4.67 and 4.68 adjust for the saturation of the GDL. The following is the boundary condition (boundary B3) for the flux of water.

$$n_{H_2O}^{D3/B3} = \left[-\rho\omega_{H_2O} \sum_{j=H_2O,N_2,O_2} \mathbb{D}_{H_2O,j} \frac{dX_j}{dx} + \omega_{H_2O}\rho v_g^* \right]^{D3/B3} = \frac{\left(n_{H_2O}^{D2/B3} + \frac{i}{2F} + 2n_{CH_3OH}^{D2/B3} \right)}{(1-s)} \quad (4.67)$$

The oxygen that leaves the cathode GDL at the interface (boundary B3) is consumed by the cathode reduction reaction and the methanol oxidation reaction. The flux of oxygen leaving the cathode GDL (by diffusion and convection) at the interface between the Nafion® membrane and the cathode GDL (boundary B3) is given by,

$$n_{O_2}^{D3/B3} = \left[-\rho\omega_{O_2} \sum_{j=H_2O,N_2,O_2} \mathbb{D}_{O_2,j} \frac{dX_j}{dx} + \omega_{O_2}\rho v_g^* \right]^{D3/B3} = \frac{\left(\frac{-i_{cell}}{4F} - \frac{3}{2} n_{CH_3OH}^{D2/B3} \right)}{(1-s)} \quad (4.68)$$

The nitrogen within the cathode GDL is inert and is not produced or consumed in any reactions associated with the fuel cell. Therefore, there is no mass transfer of nitrogen within the cathode GDL, and the flux of nitrogen at the boundary between the Nafion® membrane and the cathode GDL (boundary B3) is zero.

$$n_{N_2}^{D3/B3} = \left[-\rho\omega_{N_2} \sum_{j=H_2O,N_2,O_2} \mathbb{D}_{N_2,j} \frac{dX_j}{dx} + \omega_{N_2}\rho v_g^* \right]^{D3/B3} = 0 \quad (4.69)$$

Solving equation 4.69 for the cathode gas velocity gives equation 4.70

$$v_g^{*D3/B3} = \left[\sum_{j=H_2O,N_2,O_2} \mathbb{D}_{N_2,j} \frac{dX_j}{dx} \right]^{D3/B3} \quad (4.70)$$

where $\mathrm{v}_g^{*D3/B3}$ is the mass averaged velocity at the boundary between the membrane and the cathode diffusion layer. The equation for the cathode gas velocity can now be used in conjunction with equation 4.32.

At the boundary between the cathode GDL and the atmosphere (boundary B4), the mole fractions of all three species, water, oxygen, and nitrogen, in the cathode GDL can be determined from given the relative humidity and temperature of the air using equations 4.71 - 4.73.

$$c_{H_2O}^{D3/B4} = \frac{\Theta_{env} P_{sat,env}}{RT} \tag{4.71}$$

$$c_{O_2}^{D3/B4} = \frac{0.21\left(P_0 - P_{sat,env}\Theta_{env}\right)}{RT} \tag{4.72}$$

$$c_{N_2}^{D3/B4} = \frac{0.79\left(P_0 - P_{sat,env}\Theta_{env}\right)}{RT} \tag{4.73}$$

where Θ_{env} is the relative humidity of water in environmental air, $P_{sat,env}$ is the saturation pressure of water vapor in the environmental air, and P_0 is atmospheric pressure.

5. RESULTS AND DISCUSSION

This chapter will present and discuss the experimental and numerical results from this study. The effects of relative humidity and temperature on the cell performance will be analyzed. This will include discussion of potentiostatic, electrochemical impedance spectrum, and polarization tests. The mass transport results from the numerical model will then be compared to experimental methanol and water usage results. Finally, the influence of the environment on fuel cell performance and fuel utilization will be discussed.

5.1. Relative Humidity and Temperature Test Results

Experimental results for this section will be divided into three sections discussing the effects of relative humidity and temperature on the potentiostatic tests, electrochemical impedance test, and polarization tests, respectively. All temperatures and relative humidities reported in the following sections are nominal (set point) temperature and relative humidity values and not the actual measured values. The differences between the nominal and the actual values for the 12-hour potentiostatic tests are summarized in Table 3.

Table 3. Nominal and Actual Temperatures and Relative Humidities for 12-hour Potentiostatic Tests.

			Actual Temp.			Actual RH		
Test	Nominal Temp. (C)	Nominal Relative Humidity (%)	Mean (C)	Range (+/- C)	Standard Deviation (C)	Mean (C)	Range (+/- C)	Standard Deviation (C)
22	50	10	49.2	5.13	1.51	10.1	3.20	0.592
23	50	50	50.8	3.46	1.10	51.1	9.15	3.04
24	50	90	52.1	6.75	2.21	87.7	15.7	6.41
25	37.5	10	35.2	3.12	1.87	10.0	1.75	0.326
26	37.5	50	37.5	2.55	1.49	51.7	14.1	4.25
27	37.5	90	37.7	3.46	1.86	90.2	15.3	1.86
28	25	10	26.4	0.578	0.271	10.6	7.75	1.57
29	25	50	26.2	0.349	0.241	52.4	11.9	6.86
30	25	90	26.7	0.944	0.446	90.4	5.20	1.44

5.1.1. Potentiostatic Data

Nine potentiostatic tests were performed at a cell voltage of 0.3 volts and for a test duration of 12 hours. These tests were conducted for 12 hours to allow the fuel cells to reach a steady operating condition and to allow a measurable amount of fuel to be consumed. Figure 16 below shows the average current densities of each test and the associated relative humidities and temperatures.

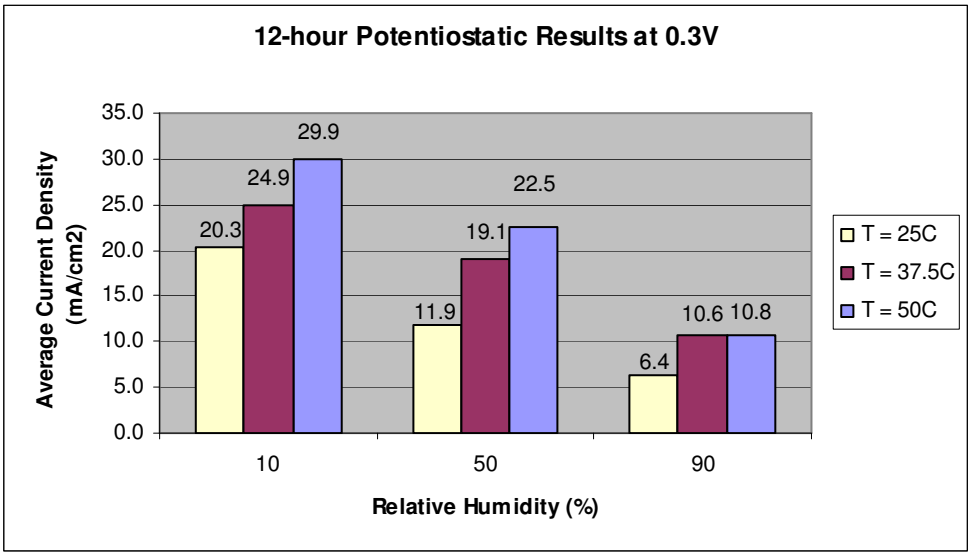

Figure 16. Average current densities from 12-hour potentiostatic tests. Cell voltage is 0.3 volts.

The most noticeable trend trends are that average current densities increase with increasing temperature and decrease with increasing relative humidity. For any given three tests performed at a given relative humidity, the test performed at the highest temperature (50ºC) produced the highest average current density and the test performed at the lowest temperature (25ºC) produced the lowest average current density. For example, of the three tests performed at 10% relative humidity, the test performed at 50ºC produced the highest average current density of 29.9 mA/cm^2, while the test performed at 25ºC produced the lowest average current density of 20.3 mA/cm^2.

The fact that current density increased with increasing temperature was expected. Increasing temperature increases the current density by increasing the exchange current density, increasing the ionic conductivity of the Nafion® membrane, and decreasing mass transport losses by decreasing the diffusivities of the gaseous species with in the cathode GDL. Increasing the relative humidity of the surroundings also improves the ionic conductivity of the membrane by increasing the water content. However, increasing the relative humidity of the surroundings also decreases the rate of evaporation of water from the cathode gas diffusion layer and increases the likelihood of flooding. The fact that increasing the relative humidity actually decreased the current production suggests that flooding did occur and was more prevalent at higher relative humidities. The presence of visible liquid water on the cathode diffusion layer surface was also noted after all tests performed at both 50% and 90% relative humidity.

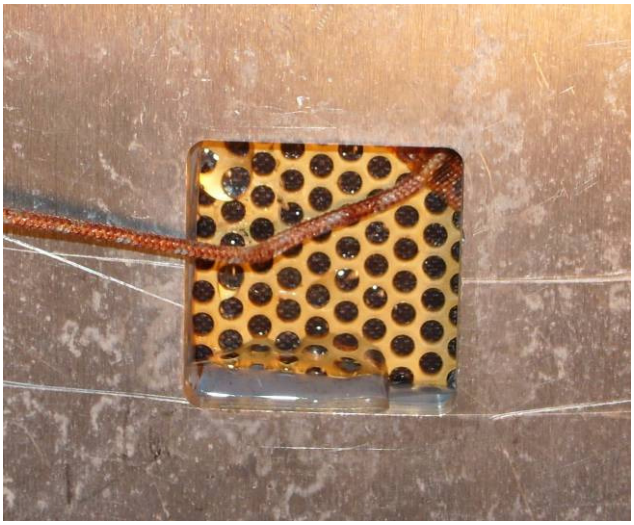

Figure 17. Cathode flooding after 12-hour potentiostatic test performed at 50ºC and 90% relative humidity.

For each temperature and relative humidity combination, three 30 minute potentiostatic tests, three electrostatic impedance tests, and three polarization tests were performed in addition to the 12 hour potentiostatic test. Figure 18 below shows a comparison of potentiostatic tests performed at three different cell voltages. The potentiostatic tests shown in Figure 18*a* were performed at a cell voltage of 0.3V and the results are very similar to those from the 12 hour potentiostatic. The potentiostatic tests

shown in Figure 18*b* were performed at a cell voltage of 0.2V. As expected, the tests depicted in Figure 18*b* produced higher current densities than the respective tests depicted in Figure 18*a* because they were conducted at a lower cell voltage. However, decreasing the cell voltage from 0.2 volts to 0.1 volts in some cases actually led to a decrease in current production. While this could possibly be attributed to flooding, this can only be postulated at this time. Because the 12-hour potentiostatic tests were only conducted at 0.3V, conducting additional 12-hour potentiostatic tests at 0.1V while measuring the fuel usage for the duration of the test would provide enough information to predict the theoretical saturation levels for the cathode gas diffusion levels using the numerical model presented in this paper. However, further tests capable of measuring the level of saturation within the cathode gas diffusion layer would have to be conducted to validate the model and determine if flooding was the actual cause of these decreases in current densities.

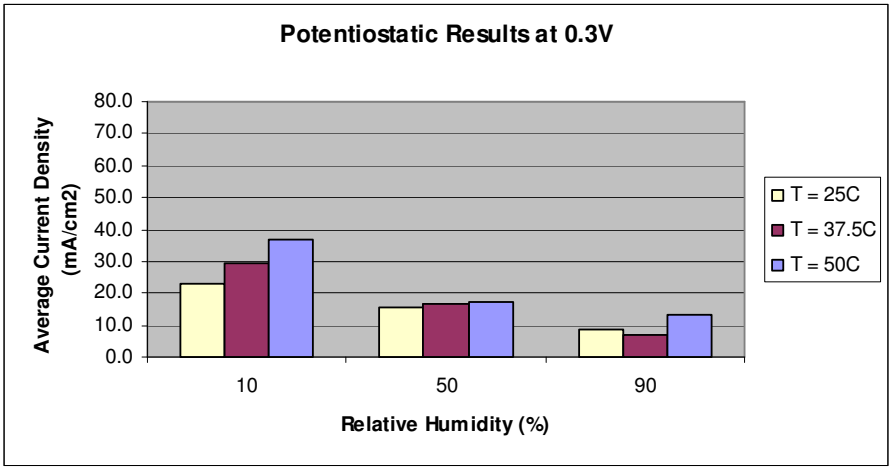

a)

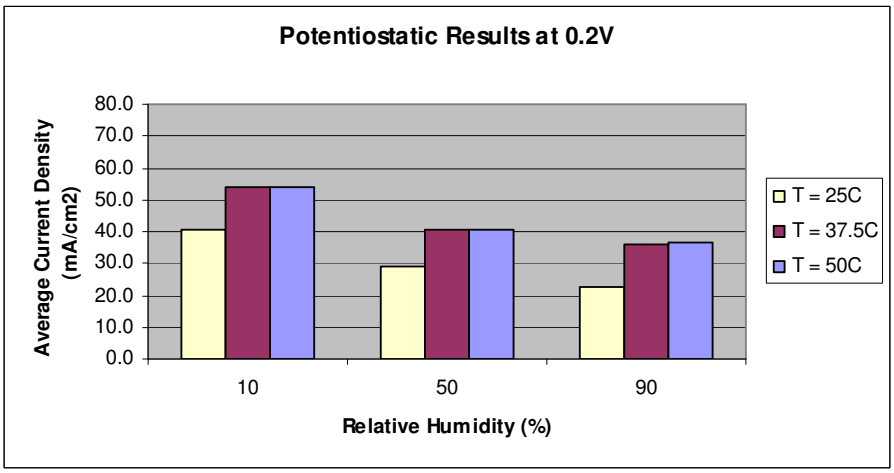

b)

c)

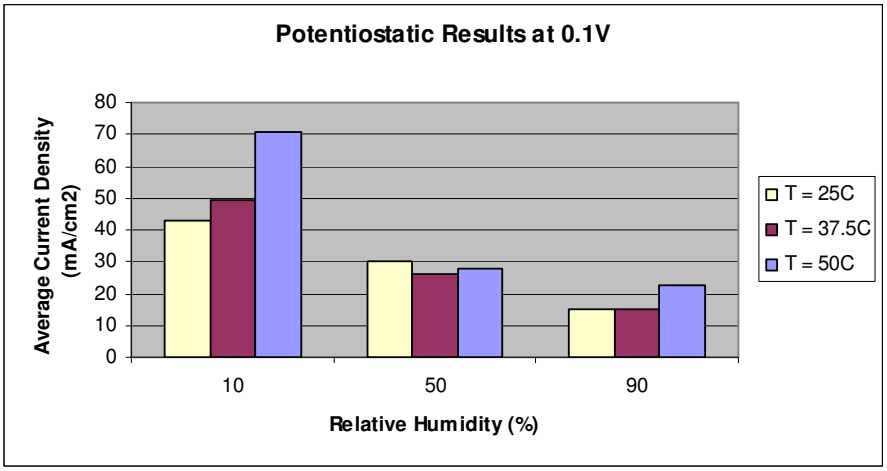

Figure 18. Potentiostatic test results. Cell voltages of (*a*) 0.3V, (*b*) 0.2V, and (*c*) 0.1V.

5.1.2. Electrochemical Impedance Spectroscopy Data

Electrochemical impedance spectroscopy tests are commonly used to distinguish between the different losses occurring within a fuel cell. Following each 30 minute potentiostatic test performed (at 0.1 V, 0.2 V, or 0.3 V), an EIS test was performed at a current corresponding to the cell voltage of the previous potentiostatic test. During EIS tests, a sinusoidal current perturbation is applied to the fuel cell and the resultant voltage response is recorded. The test is applied over a large range of frequencies, and both the real and imaginary impedances of the fuel cell are determined at each frequency interval from the measured impedance magnitude and phase shift of the voltage response. EIS testing is discussed in more detail in the experimental section of the paper.

A sinusoidal current perturbation was applied with an amplitude of 0.01A and the frequency was varied from 10 kHz to 0.1 Hz for each EIS test performed during this study. The imaginary impedance was plotted against the real impedance for each frequency interval to produce a Nyquist plot. The high frequency resistance of the fuel cell system corresponds to the real impedance at the point where the imaginary impedance is zero. The high frequency resistances determined from each EIS test are summarized in Table 4 below.

Table 4. High frequency resistance values from EIS tests performed at (a) 0.3 V, (b) 0.2 V, and (c) 0.1V. Units are in ohm-cm^2.

***a*) HFR for 0.3V tests (ohm-cm^2)**

	Relative Humidity (%)		
Temperature (C)	10	50	90
25.0	4.05	7.46	7.04
37.5	3.18	2.42	5.71
50.0	3.85	4.36	4.47

***b*) HFR for 0.2V tests (ohm-cm^2)**

	Relative Humidity (%)		
Temperature (C)	10	50	90
25.0	4.12	6.66	5.64
37.5	3.28	2.43	6.06
50.0	3.73	4.93	4.63

***c*) HRF for 0.1V tests (ohm-cm^2)**

	Relative Humidity (%)		
Temperature (C)	10	50	90
25.0	4.03	7.62	6.71
37.5	3.12	2.48	5.68
50.0	3.82	4.42	4.45

The high frequency resistances of the DMFC determined from the EIS tests range from 2.42 ohm-cm^2 to 7.62 ohm-cm^2. No clear trends in the high frequency resistances are visible. If the high frequency resistances decreased as the relative humidity increased, it could be postulated that the increase in relative humidity improved the hydration of the membrane thus increasing the ionic conductance and reducing the ionic resistance. However, the fact that there is no clear decrease in HFR as the relative humidity increases may suggest that the Nafion® membrane experienced the same level of hydration during all tests. The average high frequency resistance for all tests performed was 4.68 ohm-cm^2.

Though there are no clear trends in the high frequency resistances, the range of values measured can be compared to the high frequency resistances of other DMFCs published in literature. Liu et al. [50] performed EIS tests on DMFCs incorporating various anode diffusion media. Methanol and air were supplied through dual pass flow channels during testing. The resulting high frequency resistances ranged from 0.183 ohm-cm^2 to 0.218 ohm-cm^2. Chen et al. [51] performed EIS tests on a passive DMFC

that utilized a porous metal foam cathode current collector. These tests were performed at a cell voltage of 0.3 V with a four molar methanol solution, at a room temperature of 22.4ºC, and a relative humidity of 75%. The resulting high frequency resistances for these tests ranged from approximately 0.4 ohm-cm^2 to 0.8 ohm-cm^2. When comparing the high frequency resistances from testing conducting in this study to those published in literature, it is found that the high frequency resistances from this study are approximately one order of magnitude larger than those published in literature. The low results for ohmic resistance reported in other studies coupled with the lack of clear trends with hydration (as observed in this work) could suggest that cells in this work experience a large resistance mechanism (e.g. contact resistance) that is not affected by membrane hydration. Because current density decreases linearly with ohmic losses, the ohmic losses resulting from the large high frequency resistances in this study can potentially account for up to a 10x reduction in current density in comparison to those published in literature.

The portion of the Nyquist plot found to the right of the imaginary impedance intersection with the real impedance axis can often describe anode activation losses, cathode activation losses, and mass transport losses. Figure 19 and Figure 20 show the Nyquist plots for tests producing the lowest HFR (2.42 Ω-cm^2) and the highest HFR (7.62 Ω-cm^2) respectively.

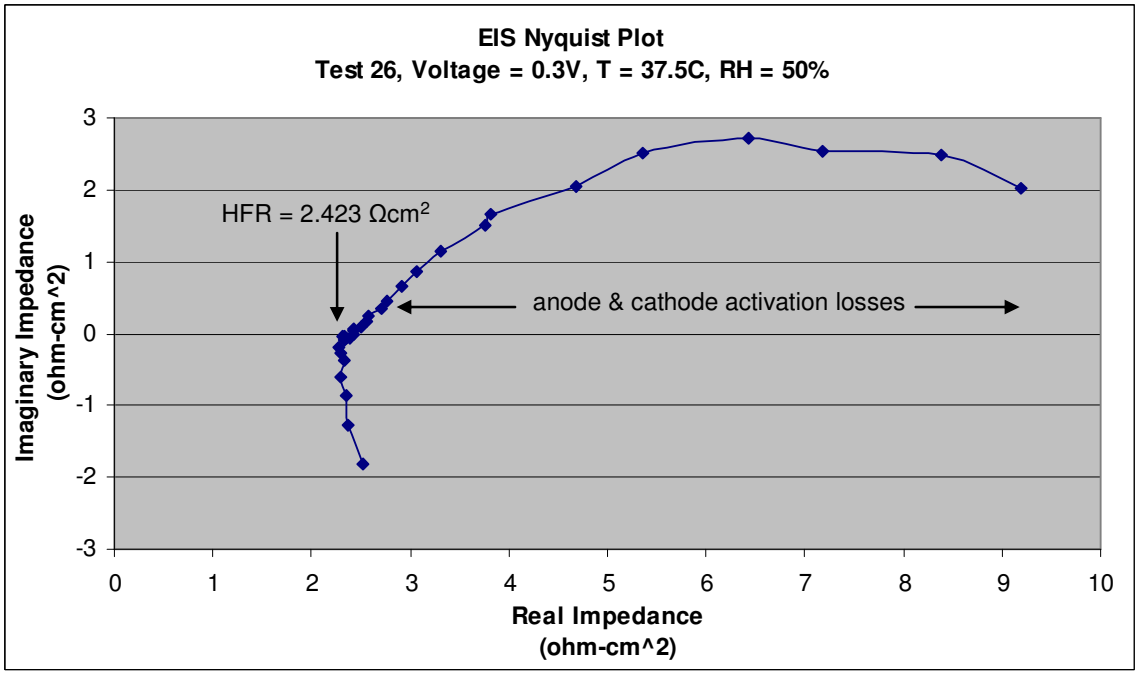

Figure 19. EIS Nyquist plot for Test 26 performed 0.3V, 37.5°C, and 50% relative humidity.

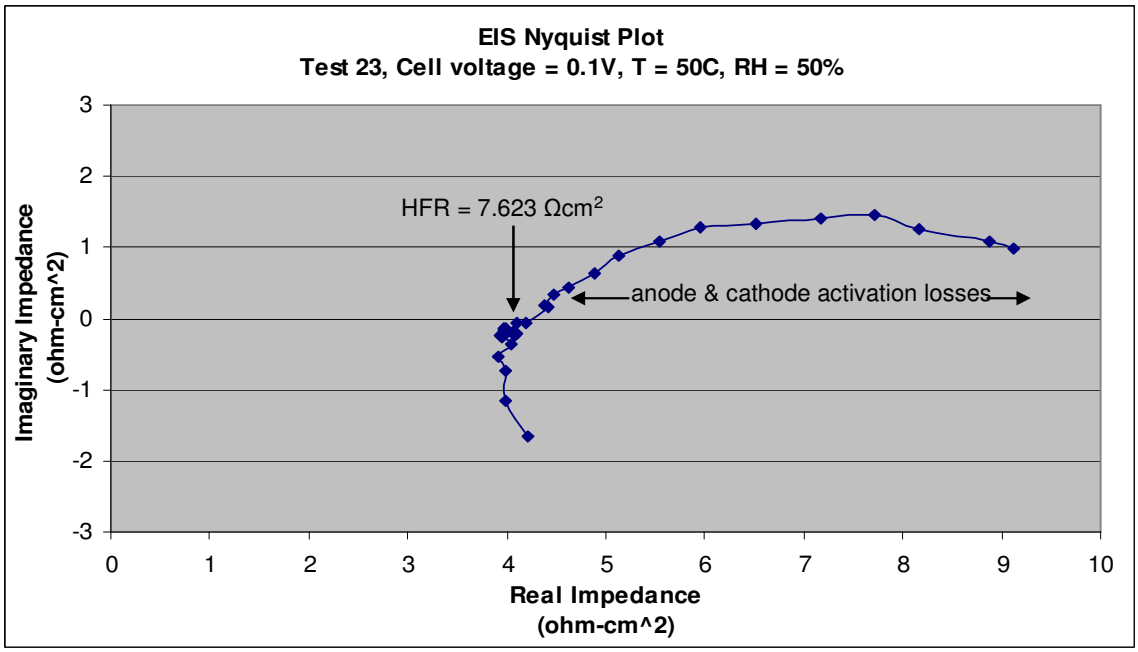

Figure 20. EIS Nyquist plot for Test 23 performed 0.1V, 50°C, and 50% relative humidity.

The Faradaic resistance is a measure of a fuel cells resistance to an electrochemical reaction. The value of the Faradaic resistance can be calculated by subtracting the HFR from the value of real impedance at the point within the anode and cathode activation loss region where the imaginary impedance is zero. For more information of the Faradaic resistance of a fuel cell see the referenced text [34]. Though the imaginary impedance on both plots does not return to zero within the measured region, it can be assumed that the sum of the HFR and the Faradaic resistance must be at least greater than 9 Ω-cm^2. This suggests that the anode and cathode activation loss are on the same order of magnitude as the ohmic losses. These activation losses will be inspected in further detail in the polarization test section.

5.1.3. Polarization Data

Polarization tests were also performed following each 30 minute potentiostatic test. These tests were voltage sweep tests that began at the open circuit voltage. Every 15 seconds, the cell voltage was reduced by a 0.02V decrement until a cell voltage of 0.1 volts was achieved. Then the cell voltage was increased every 15 seconds in 0.02V increments until the voltage returned to the open circuit voltage. The maximum power density for each test was calculated. These maximum power densities are plotted against their respective relative humidities and temperatures in Figure 21, Figure 22, and Figure 23.

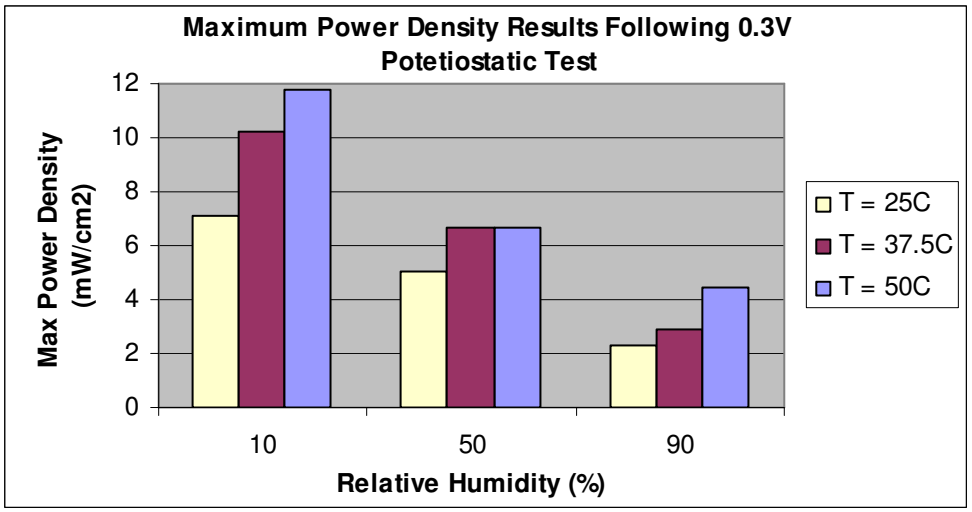

Figure 21. Maximum power density results for polarization tests following the 0.3V potentiostatic tests.

Figure 21 shows that for all polarization tests performed following the 0.3V potentiostatic tests, the maximum power density increases at a given relative humidity as temperature increases, and that the maximum power density decreases at a given temperature as relative humidity increases.

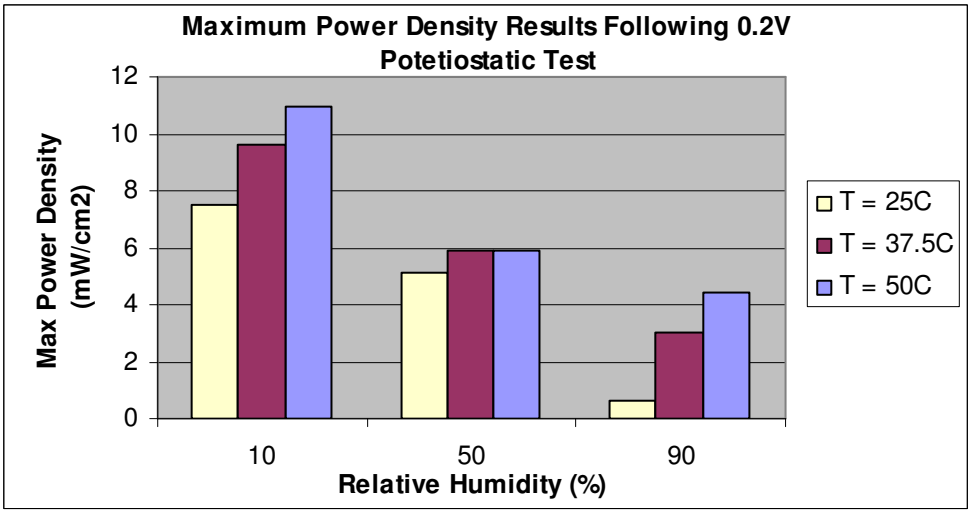

Figure 22. Maximum power density results for polarization tests following the 0.2V potentiostatic tests.

Figure 22 shows that for all polarization tests performed following the 0.2V potentiostatic tests, the maximum power density increases at a given relative humidity as temperature

increases, and that the maximum power density decreases at a given temperature as relative humidity increases. The maximum power densities found in Figure 22 are very similar to those found Figure 21.

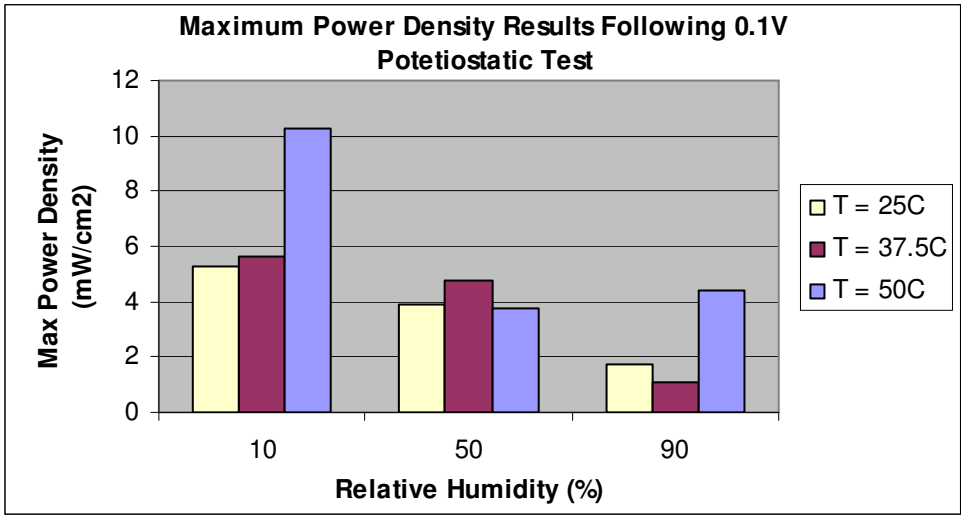

Figure 23. Maximum power density results for polarization tests following the 0.1V potentiostatic tests.

Figure 23 shows the maximum power densities for the polarization tests performed following the 0.1V potentiostatic tests. Unlike trends found in Figure 21 and Figure 22, the performance does not necessarily decrease at a given relative humidity as temperature decreases. In fact, for tests ran at 50% relative humidity, the maximum power density occurred at 37.5ºC rather than 50ºC. Also, the maximum power density does not necessarily decrease at a given temperature as relative humidity increases. For example, for tests ran at 50ºC, the maximum power density was higher at 90% relative humidity than it was at 50% relative humidity. The fact that the trends found in Figure 21 and Figure 22 do not necessarily apply to Figure 23 suggest that a factor is negatively affecting the polarization tests conducted after the 0.1V potentiostatic tests that was not present in polarization tests conducted after the 0.2V and 0.3V potentiostatic tests. The fact that the average current densities for six of nine of the potentiostatic tests performed at 0.1V were lower than the average current densities for the corresponding potentiostatic tests performed at 0.2V suggests that an increase in flooding may have been the factor

that negatively affected the performance. However, as previously discussed, additional testing is required to confirm this hypothesis.

The highest maximum power density measured in this study, 11.8 mW/cm^2, was obtained at a temperature of 50ºC and a relative humidity of 10%. While this is much lower than power densities of forced convection fuel cells which are typically on the order of 60 mW/cm^2 at 40ºC, this power density is comparable to published peak power densities for other air breathing direct methanol fuel cells (30 mW/cm^2 [52] at an ambient temperature of 50ºC with 3 wt% methanol and 17.4 mW/cm^2 [53] for a DMFC stack operating at an ambient temperature of 20ºC and a relative humidity of 21ºC with 3 molar methanol). The work of Chen et al. [52] concluded that the flooding at the cathode was the main weakness of their air-breathing DMFC. That conclusion also supports the theory that flooding is the leading cause of the decreases in current production seen in this study.

The shape of the polarization curves can also provide insight into the behavior of the fuel cell. Activation losses dominate the low current region of the polarization curve. Because the activation overpotential increases logarithmetically with cell current density, there is very little change in activation overpotential in the higher current regions of the polarization curve. These regions instead tend to be dominated by ohmic losses and mass transport losses. The ohmic losses can be calculated from the high frequency resistances determined from the EIS testing. Mass transport losses are harder to quantify. Mass transport losses may not be clearly visible in the polarization curves presented here because other losses, such as the ohmic losses, are overwhelming.

Figure 24, Figure 25, and Figure 26 below show polarization test plots, obtained following the 0.3V potentiostatic tests, at 25ºC, 37.5ºC, and 50ºC respectively. For each curve, there is a sharp initial decrease in cell voltage while the current density remains low. This drop in cell voltage is characteristic of activation losses. Following this initial decrease in cell voltage, there is an apparent linear decrease in cell voltage with respect to increasing current density, which is characteristic of ohmic losses. There is no visible sudden decrease in cell voltage in the high current density region of the polarization curves which might suggest that the limiting current density for this fuel cell was not reached. On the other hand, mass transport losses due to flooding are suggested by the

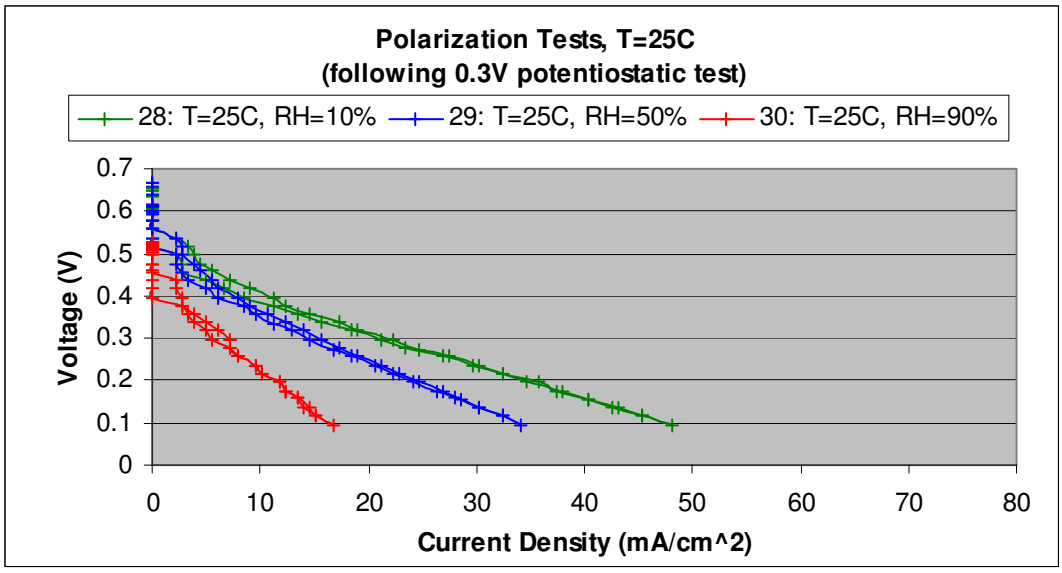

Figure 24. Polarization tests performed 25°C following 0.3V potentiostatic tests.

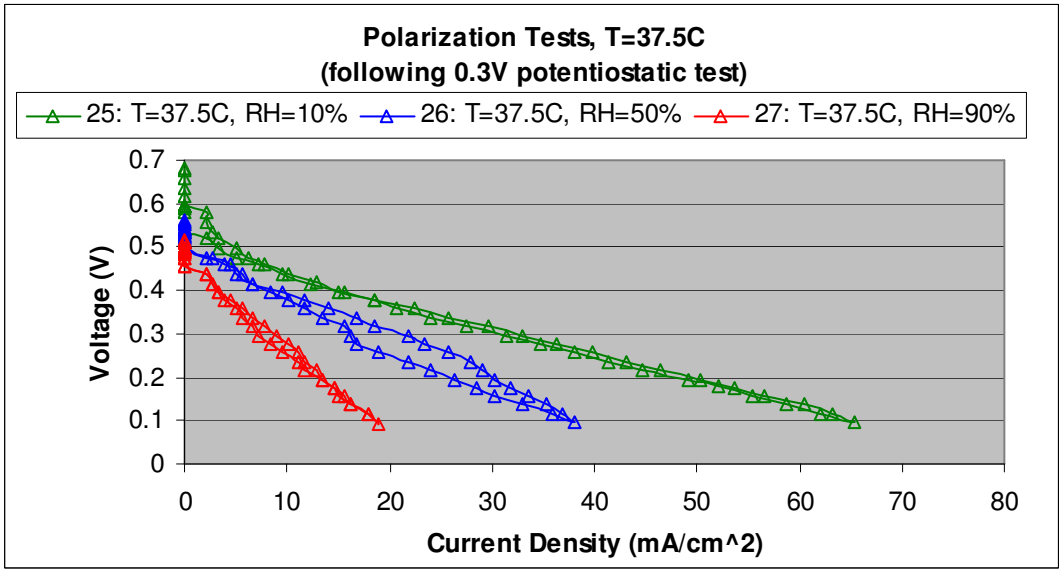

Figure 25. Polarization tests performed 37.5°C following 0.3V potentiostatic tests.

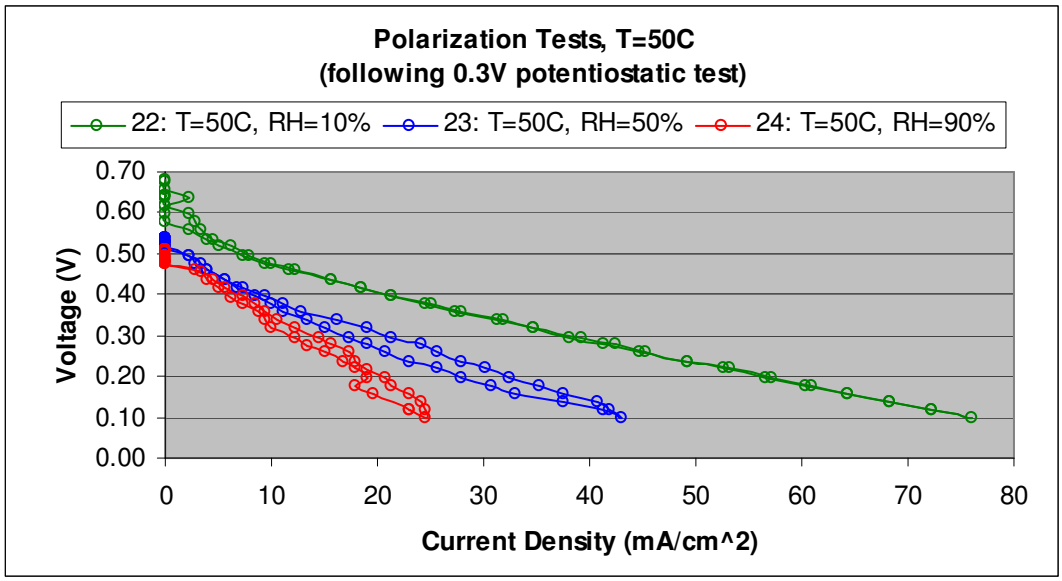

Figure 26. Polarization tests performed 50ºC following 0.3V potentiostatic tests.

observation of liquid water at the cathode in tests performed at 50% and 90% relative humidity, and the observation that current density decreased with increasing relative humidity.

In the data presented in Figure 24 - Figure 26 , the increasing relative humidity appears to be associated with a steeper slope in the ohmic region. However, no such trend was found for the resistances in the high frequency impedance. This suggests that complete flooding of specific regions (e.g. at the bottom of the cell) could be the cause. Flooding of the cathode GDL would prevent oxygen from accessing the cathode reaction sites, preventing cathode reactions from occurring at flooded areas of the cathode. This would essentially reduce the cathode active area, which would lead to a linear decrease in performance in proportion to the inactivated area. This performance decline would be larger in environments that are conducive to flooding, such as high relative humidity environments. Therefore, complete flooding of selected areas is most likely responsible for the degradation of polarization performance with increasing relative humidity observed in tests performed at 50% and 90% relative humidity.

In the absence of complete flooding of selected areas, the losses associated with the polarization tests can be drawn from the polarization data. The sum of the fuel cell voltage losses is found by subtracting the cell voltage from the open circuit voltage.

Given the high frequency resistance of a fuel cell, the ohmic losses can be subtracted from the total voltage loss to get the sum of the activation and mass transport losses for a polarization test. The ohmic overpotential is equal to the product of the high frequency resistance of the fuel cell and the cell current. Figure 27 shows the calculated activation and mass transport overpotential and the ohmic overpotential for the polarization test conducted at 50ºC and 10% relative humidity.

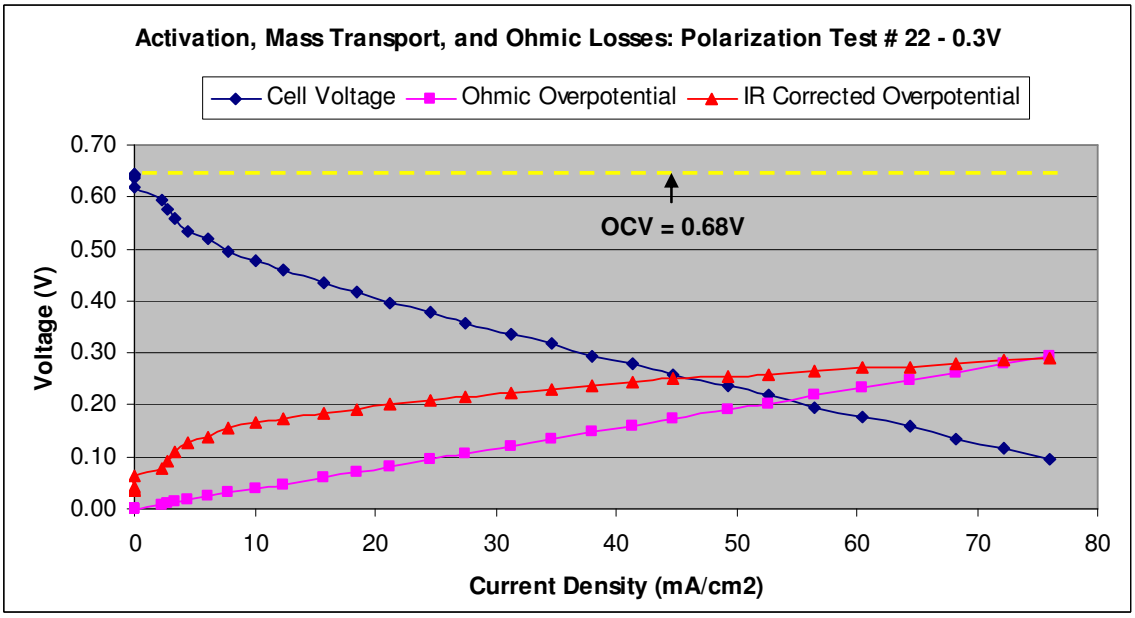

Figure 27. Activation and mass transport losses and ohmic losses for polarization test # 22. Performed at 50ºC and 10% relative humidity.

The largest losses to the DMFC during this particular polarization test are losses not associated with the cell resistance. These losses, termed "IR Corrected" overpotentials, are assumed to be predominately activation losses in the low relative humidity tests such as the test depicted in Figure 27. These losses increased sharply in the low current density region, as is characteristic of activation losses. Activation losses typically increase less rapidly in the high current density regions. The ohmic losses increase linearly with current density over the entire range of current densities. At a current density of 76 mA/cm^2, the ohmic overpotential was approximately the same magnitude as the activation overpotential. Mass transport losses typically increase at an increasing rate with current density, and this behavior was not observed. Further, the selective flooding

associated with visible droplets was not observed for this test. These observations suggest that mass transport losses were small for this test.

The polarization losses of test 22 depicted in Figure 27 can be compared to those of test 24 depicted in Figure 28. The IR-Corrected overpotential for test 24 was larger than the ohmic overpotential. The IR-Corrected overpotential also increased at a faster rate as current density increased suggesting mass transport losses are contributing to the overpotential. This suggests that flooding is even more of a problem than the high ohmic resistance for this test which was conducted at 90% relative humidity. Also, open circuit voltage was lower in this test than in test 22 which was conducted at 10% relative humidity. This could be due to the increased significance of methanol crossover which occurs when current production is low.

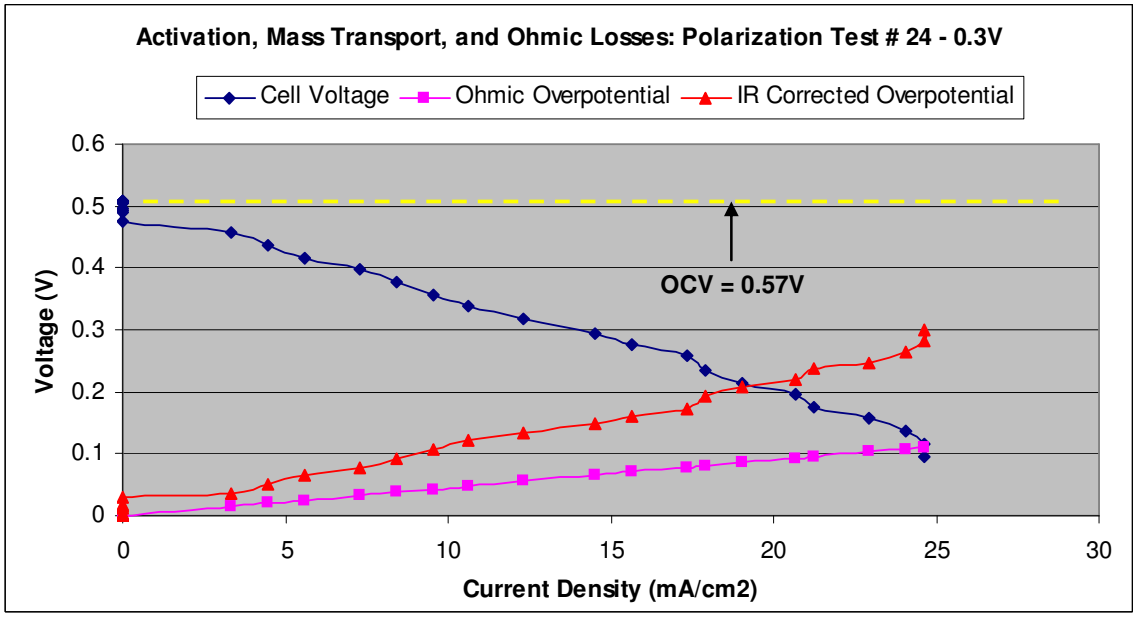

Figure 28. Activation and mass transport losses and ohmic losses for polarization test # 24. Performed at 50°C and 90% relative humidity.

5.1.4. Methanol and Water Consumption Utilization

The total amount of dilute methanol consumed during each 12 hour potentiostatic test was measured. Given the methanol concentration at the beginning and end of each test and the total mass of dilute methanol consumed, the mass of methanol and the mass

of water that were removed from the fuel cell methanol tank during the test were calculated. By integrating the current density for a given 12 hour potentiostatic test, the amount of methanol reacted at the anode was calculated. The difference in the total mass of methanol removed from the fuel tank and the mass of methanol reacted at the anode is the mass of methanol lost to methanol crossover. These steps can be repeated to calculate to mass of water reacted at the anode and the mass of water lost to water crossover. The figures below describe the mass breakdown of water removed from the fuel cell during the 12-hour tests.

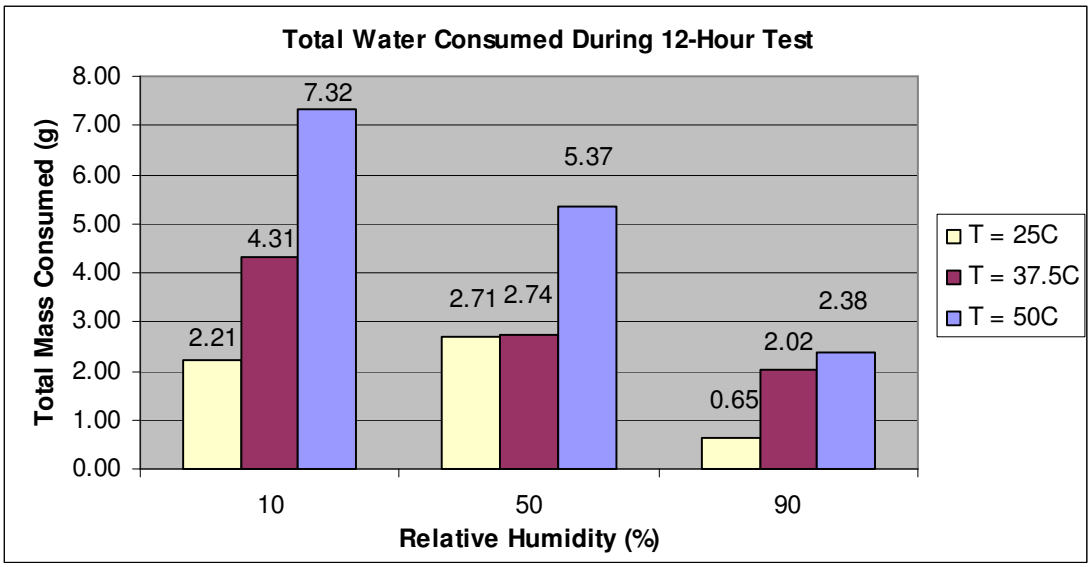

Figure 29. Total water consumed during 12-hour potentiostatic test.

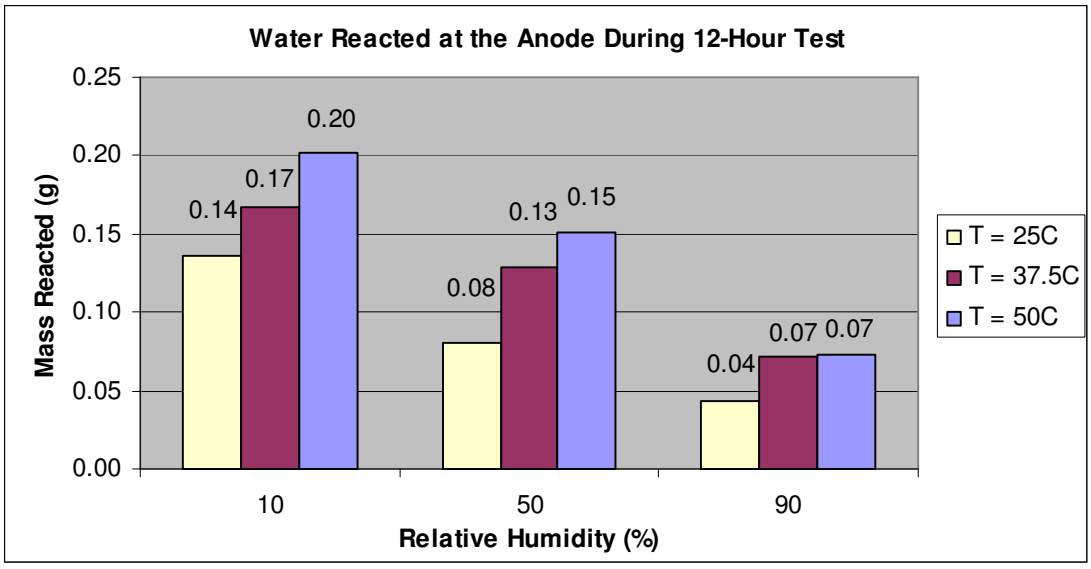

Figure 30. Total water reacted at the anode during 12-hour potentiostatic test. Note: scale is 1/16x the scale for the total water consumption.

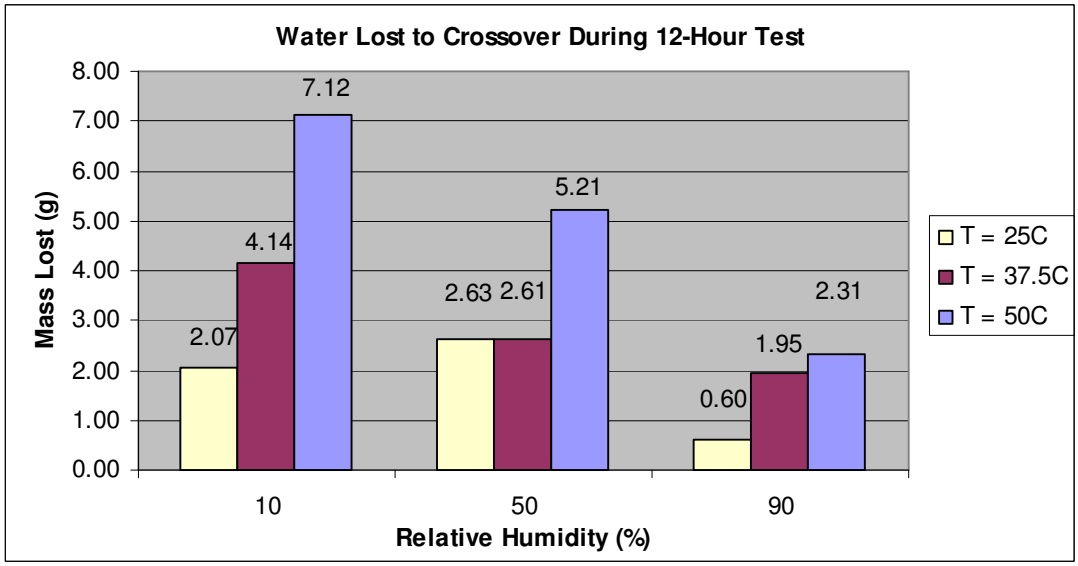

Figure 31. Total water lost to crossover during 12-hour potentiostatic test.

The mass of water consumed is closely related to both the operating temperature and the relative humidity. For each relative humidity set point, the mass of water consumed during the test increased with increasing temperature. The mass of water reacted at the anode increased with increasing temperature because the reaction rate of methanol fuel cells increases with increasing temperature. However, approximately 95% of the water consumed during each test was lost to water crossover and not reacted at the

anode. Water lost to crossover must ultimately be removed from the system by evaporation to the environment or by drainage of liquid water. For tests conducted at 10% relative humidity, the mass of water lost to water crossover increased with increasing temperature. This trend also applies to tests conducted at 90% relative humidity. However, this did not hold true for tests conducted at 50% relative humidity. Slightly more water was lost to crossover during the test conducted 25ºC (test 29) than during the test conducted at 37.5ºC (test 26). Further analysis of test 29 suggests that it may be an anomaly that is best treated as an outlier.

The relative humidity also played a large factor in the rate of water removal from the fuel cell. For tests performed at 37.5ºC the rate of water removal from the fuel cell decreased with increasing relative humidity, as expected. In low relative humidity environments water evaporates at a faster rate than at high relative humidity environments. As water is evaporated and removed from the diffusion layer, more water diffuses from the fuel tank across the membrane. This was also the case for tests performed at 50ºC. However, for the tests performed at 25ºC, the mass of water removed due to crossover was larger at 50% relative humidity (test 29) than at 10% (test 28). Again, the mass of water lost to crossover during test 29 was larger than expected. The magnitude of the mass of water lost to crossover during this test did not fit either the trends observed while changing the relative humidity or the trends observed while changing the temperature. This test was likely an anomaly that experienced an unusually high water crossover rate. With the exception of test 29, the mass of water lost to crossover during the 12-hour tests increased with increasing temperature and decreased with increasing relative humidity.

The methanol consumption by the fuel cell exhibited different trends than the water consumption. While temperature affected the rate of methanol consumption by the fuel cell similarly to the rate of water consumption, the relative humidity affected the rate of methanol consumption differently than the rate of water consumption. Figure 32 to Figure 34 describe the mass breakdown of methanol consumed by the fuel cell during the 12-hour tests.

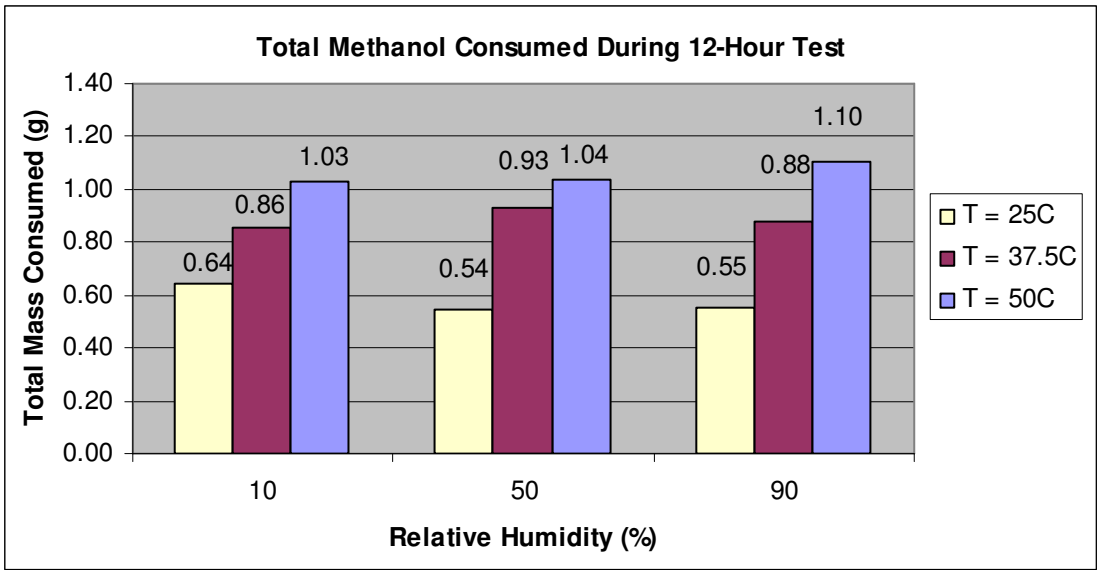

Figure 32. Total methanol consumed during 12-hour potentiostatic test.

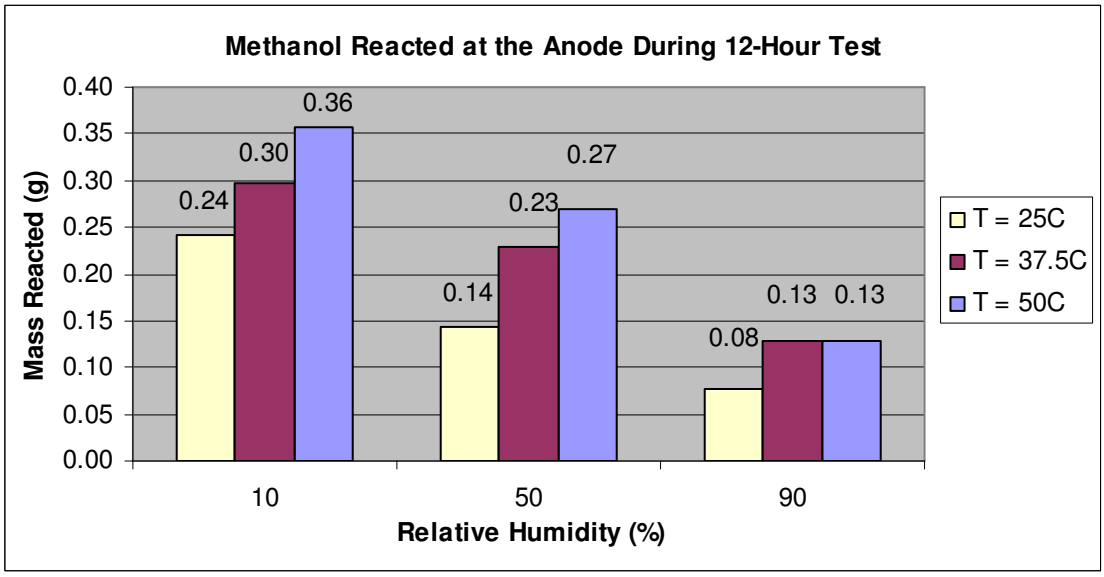

Figure 33. Total methanol reacted at the anode during 12-hour potentiostatic test. Note: scale is reduced in comparison to total methanol consumption figure.

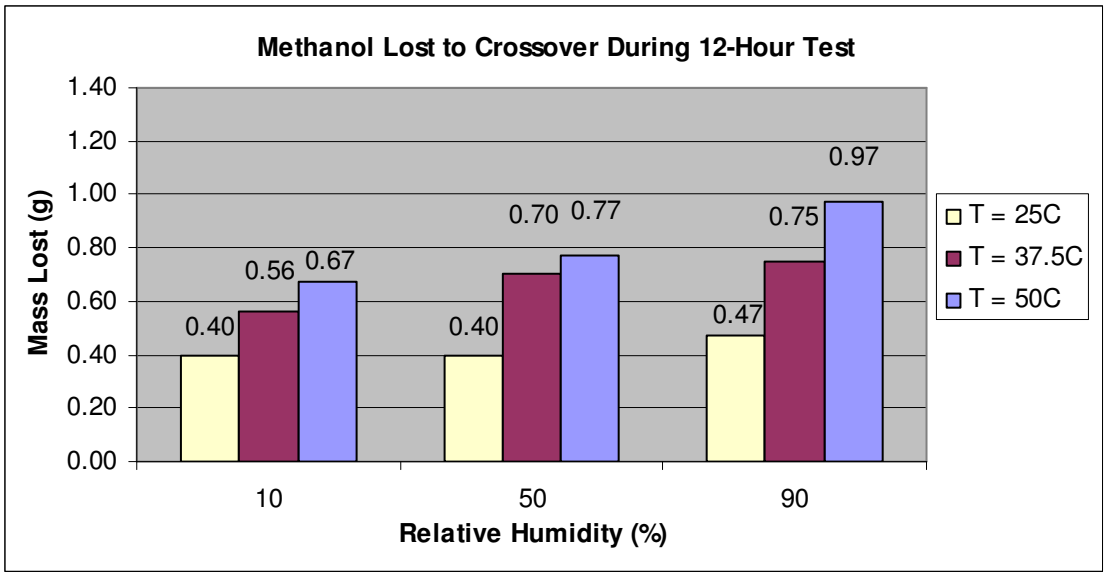

Figure 34. Total methanol lost to crossover during 12-hour potentiostatic test.

Figure 32 shows the total mass of methanol consumed during each of the nine 12-hour potentiostatic tests. It is obvious from the figure that increasing temperature increases the mass of methanol consumed during testing. The figure also shows that relative humidity has little to no effect on the total mass of methanol consumed during testing. However, analysis of Figure 33 and Figure 34 reveals that temperature and relative humidity do affect both the amount of methanol reacted at the anode and the amount of methanol lost to methanol crossover.

Figure 33 looks very similar to Figure 30 because the mass of methanol reacted at the anode is stoichiometrically related to the mass of water reacted at the anode. Specifically, for every one mole of methanol reacted at the anode, one mole of water is reacted. Both figures directly reflect the current production levels of the fuel cell during the 12-hour test. As the relative humidity was increased, the current production decreased, and thus the mass of methanol reacted decreased. However, the fact that the overall amount of methanol consumed changed very little with increasing relative humidity means that, while the mass of methanol reacting was decreasing, the mass of methanol lost to crossover was increasing. This behavior can be clearly seen in Figure 34. For any given temperature, as the relative humidity was increased, the mass of methanol lost due to methanol crossover increased.

The most probable reason that the levels of methanol crossover increased with increasing relative humidity is that increasing the relative humidity decreased the current production and consequently less methanol was being removed from the anode catalyst layer due to the anode oxidation reaction. This increased the amount of methanol within the anode catalyst layer available for diffusion through the Nafion® membrane. This phenomena is very common for methanol fuel cells, and designing DMFC systems to operate the cells at high current densities is one technique used to reduce methanol crossover. The increase in methanol crossover at low current density suggests that diffusion is the dominant mode of methanol transport through the membrane. If convection (with water crossover) had been the dominant mode of methanol transport through the membrane, then methanol crossover would have decreased with increasing relative humidity, opposite to the trend observed here.

Temperature also affected the rate of methanol crossover. As shown in Figure 34, for any given relative humidity, the rate of methanol crossover increased with increasing temperature. The fact that increasing temperature also increases the rate of current production and thus the rate of methanol consumed in the anode reaction suggests that less methanol should be available for crossover as temperature increases. However, the opposite trend was observed. There are two probable reasons that methanol crossover increases with temperature. The first is that increasing the temperature increases the diffusivity of methanol in both the anode diffusion layer and in the Nafion® membrane, which in turn increases the rate of diffusion. The second is that increasing temperature increases the rate of methanol evaporation at the cathode. The model proposed in this paper operates under the assumption that all of the methanol that reaches the cathode catalyst layer is immediately oxidized and there is no methanol mass transport through the cathode diffusion layer. However, the transient multiphase and multicomponent model developed by Rice et al. [49] suggests that more methanol actually leaves the cathode via evaporation than is oxidized at cathode catalyst layer. Though the assumption that all of the methanol that reaches the cathode catalyst layer reacts is very common, it is also based on the assumption that the levels of methanol that reach the cathode catalyst layer are small enough that the reactions can occur quickly. If the levels of methanol crossover are high then this may not be the case. Also, the methanol

oxidation reaction requires the presence of oxygen. However, areas of the catalyst layer that are flooded may contain little to no oxygen. This suggests that methanol that reaches areas of the cathode catalyst layer that are flooded may not immediately react. Instead, it is possible some of this methanol enters the diffusion layer and evaporates into the atmosphere. If this was the case then increasing the temperature would have increased the rate of methanol evaporation and thus increased the rate of methanol removal from the fuel cell. However, though a significant portion of the methanol may leave the fuel cell via evaporation, the concentration at the cathode is still approximately equal to zero because evaporation occurs very quickly. Therefore, the zero concentration assumption is still applicable for modeling purposes.

Another interesting observation can be made by comparing the graphs in Figure 35. The graphs compare the percentages of methanol lost due to crossover to the percentages of methanol reacted at the anode for each 12-hour test. The three graphs shown are very similar, suggesting that operating temperature has very little affect on the relationship between the percent of methanol lost to crossover and the percent of methanol reacted. This suggests that although increasing temperature increases the mass of methanol consumed in the anode reaction, the mass of methanol that is lost due to crossover increases proportionately. However, changing relative humidity is shown to change the percentages of methanol lost to crossover and the methanol reacted. As the relative humidity increases, more methanol is lost to crossover and less methanol is consumed in the anode reaction.

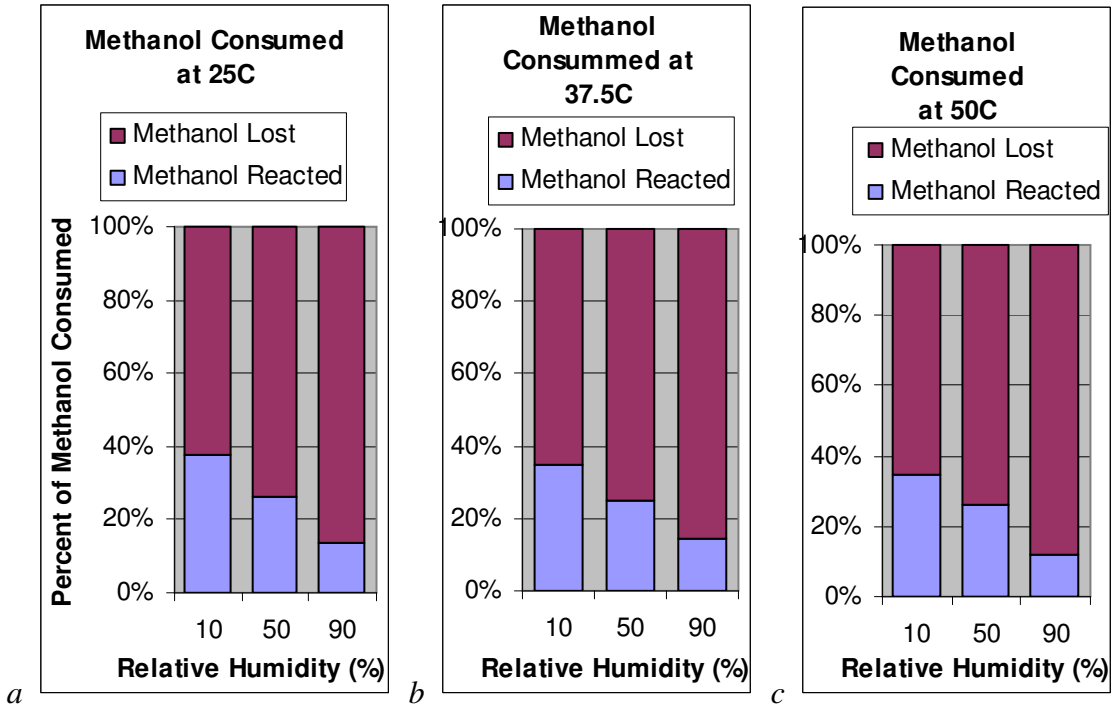

Figure 35. Comparison of percentages of methanol lost due to methanol crossover and the percentages of methanol consumed in the anode reaction during the 12-hour tests at (a) 25ºC, (b) 37.5ºC, and (c) 50ºC.

Three additional tests were conducted on the DMFC. These tests were conducted to provide insight into the nature of the crossover of water and methanol in the fuel cell in the absence of current production. The fuel cell remained at its open circuit voltage which was monitored throughout the duration of these tests. These tests were conducted at two temperature and relative humidity combinations and the results are compared to those of similar tests conducted while producing current. During test Diff1, the fuel cell was filled with the methanol water solution and placed in the environmental chamber as usual. The mass of the methanol water solution was measured before and after the test. The concentration was monitored for the duration of the 12-hour test, and the open circuit voltage was monitored as well. The test was conducted at 25ºC and 50% relative humidity. Test Diff2 was performed in the same manner but was conducted at 50ºC and 50% relative humidity. Test Diff3 was performed slightly differently. A hyperdermic needle was inserted into the fueling port of the DFMC in order to allow air to pass to or from the fuel tank to ensure that the anode compartment pressure was equal to the

ambient pressure. Table 5 summarizes the results from these tests. The methanol and water consumption results from tests 23 and 29 are also listed for comparison.

Table 5. Summary of methanol and water consumption in tests conducted with no current. Tests 23 and 29 are listed for comparison.

		Water						Methanol		
Test	Temp	RH	Consumed	Reacted	Lost	Electro-osmotic Drag	Diffusion and Hydraulic Permeation	Consumed	Reacted	Lost
29	25	50	2.71	0.080	2.63	1.20	1.43	0.543	0.143	0.400
Diff1	25	50	0.636	0	0.636	0	0.636	0.651	0	0.651
23	50	50	5.36	0.151	5.21	2.26	2.94	1.03	0.269	0.768
Diff2	50	50	1.70	0	1.70	0	1.70	1.07	0	1.07
Diff3	50	50	2.40	0	2.40	0	2.40	1.15	0	1.15

In Table 5, the consumed columns designate the total amount of water or methanol that was removed from the anode fuel tank during the 12-hour tests. The reacted columns designate the amount of water or methanol that was consumed in the anode reaction. The lost columns designate the amount of water or methanol that crossed over the membrane. The "electro-osmotic drag" and the "diffusion and hydraulic permeation" columns designate the amount of water that was predicted by the model to have crossed over the membrane due electro-osmotic drag or due to diffusion and hydraulic permeation respectively.

Although tests Diff2 and Diff3 were conducted under the same external conditions, the amount of water and methanol that was lost during each test differs. For the duration of test Diff3, the anode compartment pressure was equal to the environmental pressure because a hypodermic needle served as an open air passage between the two. However, the needle was not present during test Diff2. Instead, the anode compartment was completely sealed. As methanol and water were removed from the anode fuel tank, a void space developed that most likely acted as a vacuum in the anode compartment. This would have reduced the rate of water and methanol crossover relative to those values in test Diff3, as observed. Test Diff1 was also conducted without a anode compartment pressure vent and thus most likely experienced a small pressure drop in the anode compartment.

The anode compartments were also sealed during all of the 12-hour potentiostatic tests that were conducted at 0.3V. This makes it likely that carbon dioxide released from the anode oxidation reaction accumulated and increased the pressure in the anode compartment until the carbon dioxide relief valve was cracked. This would have increased the amount of water and methanol that crossed over the membrane due to hydraulic permeation. Comparing test 29 with test Diff1 shows that the amount of water that crossed over the membrane due to hydraulic permeation and diffusion in test 29 is approximately twice the amount that crossed over in test Diff1. This also suggests that the anode compartment during test 29 was under higher pressure than the anode compartment of test Diff1.

The amount of methanol that crossed the membrane in the three tests that ran without current production (Diff1 to Diff3) was greater than the respective tests conducted with current production, regardless of the pressure differences in the anode compartments. This suggests that the primary method of methanol transport through the membrane was diffusion and not convection for these tests. This is because, although there was more water crossover in tests with current production due to electro-osmotic drag and an increased pressure in the anode compartment, the amount of methanol that crossed over during these tests was less than the amount of methanol crossing over in the respective tests without current production. If convection were the primary method of mass transport, then the rate of methanol crossover would increase as the rate of water crossover increased, which was not the case. This also suggests that methanol diffusion decreases with increasing current production. This trend supports the hypothesis previously presented that suggests that current production consumes methanol in the catalyst layer thus lowering the methanol concentration in the Nafion® membrane at the interface between the anode diffusion layer and membrane, thereby decreasing the concentration gradient in the membrane and ultimately decreasing the rate methanol of diffusion.

5.2. Model Results

The numerical model was used to understand the mass transport phenomena occurring within the fuel cell during each of the nine 12-hour potentiostatic tests conducted. The average fuel cell temperature, current density, ambient temperature, ambient relative humidity, and methanol concentration in the fuel tank were all calculated from the experimental results and were used as independent variables for the model. These values are shown in Table 6. The gauge pressure in the anode fuel tank, the level of water saturation in the cathode gas diffusion layer, and the anode reaction rate coefficient were the final independent variables, though none of these was measured during testing.

Table 6. Averages of experimental data used as input for numerical model.

Test #	22	23	24	25	26	27
Avg. Temperature (C)	49.1	50.6	51.9	35.1	37.5	37.8
Avg. Relative Humidity	10.1	51.2	87.8	10.0	51.8	90.2
Avg. Concentration (w/w%)	5.00	4.77	4.26	4.76	4.5	4.70
Avg. Current Density (mA/cm^2)	29.9	22.5	10.8	24.8	19.1	10.6
Test #	28	29	30	Diff1	Diff2	Diff3
Avg. Temperature (C)	26.4	26.0	26.7	26.4	50.4	50.9
Avg. Relative Humidity	10.8	50.0	90.4	32.5	49.8	49.8
Avg. Concentration (w/w%)	5.43	5.10	5.58	4.22	3.89	3.86
Avg. Current Density (mA/cm^2)	20.2	11.9	6.39	0.00	0.00	0.00

In order to predict the gauge pressure in the anode fuel tank during testing, a 12-hour test (test Diff3) was conducted at a temperature of 50ºC, a relative humidity of 50%, and with no electrical current. Because the fuel cell produced no current during the test, all of the methanol and water consumed during the test were due to crossover. This test was performed with a needle inserted into the anode fuel port to ensure that the pressure within the anode fuel tank remained at atmospheric pressure throughout the entire test. The methanol and water consumption during this test were then calculated. Simulations were then run with the numerical model. The anode gauge pressure was set to zero and the cathode saturation was varied. The results from this simulation are summarized in Table 7.

Table 7. Summary of simulation results for test Diff3.

		Methanol			Water		
Saturation	Cathode Capillary Pressure (Pa)	Predicted Consumption (g)	Actual Consumption (g)	% Error	Predicted Consumption (g)	Actual Consumption (g)	% Error
0.500	-5000	1.14	1.15	-1.25	4.74	2.40	97.3
0.512	-5500	1.13	1.15	-2.21	4.27	2.40	77.9
0.525	-6000	1.11	1.15	-3.19	3.79	2.40	58.1
0.537	-6500	1.10	1.15	-4.17	3.31	2.40	37.9
0.550	-7000	1.09	1.15	-5.17	2.82	2.40	17.3
0.562	-7500	1.08	1.15	-6.19	2.31	2.40	-3.76
0.575	-8000	1.07	1.15	-7.23	1.79	2.40	-25.4
0.587	-8500	1.06	1.15	-8.28	1.26	2.40	-47.7
0.600	-9000	1.04	1.15	-9.36	0.704	2.40	-70.6

Row associated with the smallest percent error for water consumption is highlighted.

Increasing the simulation saturation increased the capillary pressure in the cathode GDL and thus increased the back diffusion due hydraulic permeation. Changing the saturation has a strong effect on the water consumption for that reason. However, changing the saturation had only a minimal effect on the methanol consumption. This suggests that the primary mechanism of methanol transport in this test was diffusion and not convection. In other words, changes in the flux of water have only minimal effects on the flux of methanol. This agrees with the observations made during the experimental testing. A saturation value of 0.5625 predicted the water consumption during test Diff3 most accurately, corresponding to a -3.760% error for water consumption and a -6.190% error for methanol consumption.

Simulations of the 12-hour potentiostatic test conducted at 50ºC and 50% relative humidity (test 23) were conducted while varying both the saturation and the anode gauge pressure. Test 23 was chosen because it had the same nominal temperature and nominal relative humidity as test Diff3. However, the potentiostatic test was conducted at 0.3V thus allowing the fuel cell to produce current. This test was also conducted without a needle in the anode fuel port. Therefore, pressure could build up within the anode fuel tank until the carbon dioxide pressure relief valve cracked and relieved the pressure. While the anode gauge pressure in test 23 should be different than the gauge pressure of test Diff3, the saturation of test 23 should be equal to or greater than the saturation of test Diff3 because in test 23 a higher rate of water crossover flux was present in addition to

water that was produced by the cathode reaction. The simulation results for test 23 are summarized in Table 8. For a saturation of 0.5625 (the saturation predicted for test Diff3), the model predicted that the anode gauge pressure was between 0.4 and 0.5 psi. Though the cracking pressure for the carbon dioxide pressure relief valve was rated at 0.3 psi, tests showed that the valve was capable of holding up to 0.6 psi before cracking. Therefore, an anode gauge pressure of 0.5 psi was used in the model for all of the nine 12-hour potentiostatic tests. This procedure was employed because the anode pressure was not measured during the tests. In future work, the anode should be vented or the pressure monitored.

Table 8. Summary of simulation results for test 23.

			Methanol			Water		
Anode Gauge Pressure (psi)	Saturation	Cathode Capillary Pressure (Pa)	Predicted Consumption (g)	Actual Consumption (g)	% Error	Predicted Consumption (g)	Actual Consumption (g)	% Error
0.000	0.525	-6000	1.023	1.037	-1.34	5.207	5.365	-2.94
0.200	0.537	-6500	1.023	1.037	-1.29	5.431	5.365	1.23
0.400	0.562	-7000	1.021	1.037	-1.48	5.214	5.365	-2.81
0.500	0.562	-7500	1.023	1.037	-1.35	5.531	5.365	3.09
0.600	0.575	-8000	1.022	1.037	-1.44	5.419	5.365	1.02
0.800	0.575	-6000	1.022	1.037	-1.44	5.419	5.365	1.02

Anode gauge pressure was varied. Row associated with the smallest percent error for water consumption is highlighted.

Test Diff2 was conducted at the same temperature and relative humidity as test Diff3 but water and methanol consumptions were less in test Diff2. The only difference between the tests was that test Diff2 did not have a needle inserted into it to ensure that the anode compartment was at the same pressure as the environment. This suggests that the pressure in the anode compartment was not equal to the environmental pressure, but rather was less than the environmental pressure because methanol and water were being removed from a sealed compartment. The same applies to test Diff1. The process used to determine the anode compartment pressure for test 23 was repeated for tests Diff1 and Diff2. Because there was no current applied during these tests, the anode compartments should have had a small negative pressure due to the methanol and water that left the sealed anode compartment. Test Diff2 was conducted approximately the same relative

humidity and temperature as test Diff3. Therefore, it was assumed that the saturation of the cathode GDL in test Diff2 was approximately equal to 0.5625 (the saturation found in test Diff3). The model predicted the pressure within the anode compartment for test Diff2 to be -0.2 psi. This anode compartment pressure was also assumed for test Diff1.

With a chosen anode gauge pressure of 0.5 psi, the cathode GDL saturation and the anode reaction rate coefficient were the only two remaining independent variables. Because the saturation was not measured during each test, a range of probable saturation values were used for each simulation. A range of anode reaction rate coefficient values were also used. For each simulation, the model was then used to calculate concentration and mass flux profiles for water, methanol, and oxygen in the different applicable regions of the fuel cell. Given the mass flux of methanol and water out of the fuel tank and the duration of the tests, the theoretical total masses of methanol and water removed from the fuel cell during the 12-hour tests were calculated. The saturation and anode reaction rate coefficient combination that provided water and methanol consumption levels closest to those measured experimentally was selected as the representative combination for that respective test. The predicted saturation, methanol consumption, water consumption, and cathode GDL relative humidity values for each test are listed in Table 9.

Table 9. Predicted saturation, methanol consumption, water consumption, and cathode GDL relative humidity values.

					Methanol			Water			
Test #	Anode Gauge Pressure (psi)[1]	Saturation[2]	Cathode Capillary Pressure (Pa)	Anode Reaction Rate Coefficient[3]	Predicted Consumption (g)	Actual Consumption (g)	% Error	Predicted Consumption (g)	Actual Consumption (g)	% Error	Predicted RH in Cathode GDL
22	0.500	0.588	-8.50E+03	2.84E+03	1.10	1.03	6.15	7.26	7.33	-0.909	58.8
23	0.500	0.563	-7.50E+03	2.25E+03	1.02	1.04	-1.36	5.53	5.37	3.10	86.6
24	0.500	0.513	-5.50E+03	1.03E+03	1.17	1.10	6.55	2.34	2.39	-1.78	105
25	0.500	0.588	-8.50E+03	2.36E+03	0.891	0.859	3.68	4.61	4.31	6.87	44.2
26	0.500	0.600	-9.00E+03	1.82E+03	0.883	0.929	-4.98	2.71	2.74	-1.08	74.6
27	0.500	0.500	-5.00E+03	9.58E+02	0.829	0.878	-5.56	2.05	2.02	1.35	105
28	0.500	0.600	-9.00E+03	1.83E+03	0.628	0.641	-2.04	2.39	2.21	8.00	31.0
29	0.500	0.563	-7.50E+03	1.07E+03	0.581	0.543	7.03	2.50	2.71	-7.97	68.6
30	0.500	0.538	-6.50E+03	5.12E+02	0.581	0.550	5.66	0.663	0.645	2.77	97.7
Diff1	-0.200	0.500	-5.00E+03	NA	0.891	0.651	37.0	0.399	0.636	-37.3	57.3
Diff3	-0.200	0.563	-7.50E+03	NA	1.06	1.07	-1.15	1.46	1.71	-14.7	63.9
Diff4	0.000	0.563	-7.50E+03	NA	1.08	1.15	-6.19	2.31	2.40	-3.76	68.6

[1]Anode gauge pressures determined by procedure on pages 94-96. [2]Saturations determined by adjusting saturation to minimize the water consumption error. [3]Anode reaction rate coefficients determined by adjusting coefficient to minimize methanol consumption error.

The small percent error between the predicted consumption values and the actual consumption values shows the model agrees well with experimental data for the selected parameters. The predicted relative humidity in the cathode gas diffusion layer also increases with increasing ambient relative humidity as expected. However, the saturation and anode reaction rate coefficient chosen to put the model predications into agreement with the experimental data must be analyzed to ensure they are well founded .

The saturation values predicted by the model range from 0.5 to 0.6, meaning that the model predicts that approximately half of the pores in the cathode GDL were saturated with water and thus would allow no gaseous species to pass. Analysis of the experimental data suggested that the level of flooding of the cathode GDL increased as the ambient relative humidity increased, which suggests that the saturation of the GDL should also increase with increasing relative humidity. The saturation values that were predicted by the model for each test are shown in Figure 36.

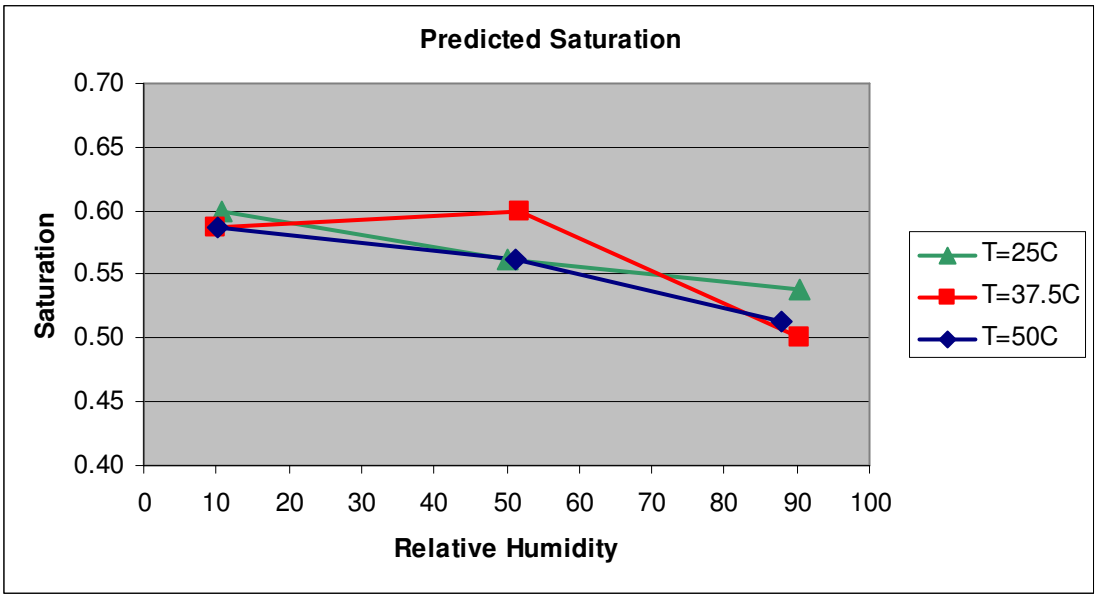

Figure 36. Saturation value predicted by the model for different temperatures and relative humidities.

According to the model, the saturation values for the cathode GDL actually tend to decrease as the relative humidity increases. However, this is not what was suggested by the experimental data. This can most likely be attributed to the model assumption that

liquid water in saturated pores is immobile. This means that water cannot be removed from the cathode GDL in the liquid phase, which in reality is not the case. In actuality, liquid water was removed from the cathode GDL in the liquid phase because drops of water that formed on and fell from the cathode GDL surface were observed. The model does not account for this transport and instead assumed that all of the water was transported in the gaseous phase through non-saturated pores. Therefore, the model most likely under-predicted the saturation levels in order increase the pore area available for vapor transport. Another disadvantage of the vapor-only transport model is that in two cases the model could only achieve sufficient vapor flow by predicting vapor content in excess of saturation as shown by the predicted cathode relative humidity values greater than 100 in. A two phase model would have accounted for mass transport of water in both the liquid and gas phases and would have more accurately predicted the cathode GDL saturation.

The anode reaction rate constant was assumed to be a function of current since the cell current affects the overpotentials associated with the cathode and the ohmic elements of the cell and thus influences the remaining overpotential available for driving the anode reaction. Using linear regression, the anode reaction rate constants used to match the experimental data in Table 9 were fit to a liner form,

$$\beta = (\mathrm{m})i - \mathrm{b} \tag{5.1}$$

where m is 99.01 cm^2-$mole^{-1}$ and b is -93.3 A-$mole^{-1}$. The R-squared value for the fit was 0.995 suggesting that the two parameters provided a good fit to the nine experimental points. The reaction rate coefficient increases with current, indicating that the anode volumetric current production becomes more sensitive to concentration as the cell current rises (because less overpotential is available to drive the anode reaction).

The model was capable of predicting the methanol concentration profiles within the anode diffusion layer and within the Nafion membrane in addition to predicting the species flux profiles in each region. The concentration and flux profiles produced by the numerical model for test number 26 (37.5ºC and 50% relative humidity) are shown in the figures below. Figure 37 shows the predicted methanol concentrations in the anode

diffusion layer and in the Nafion® membrane. Notice the concentration at the origin corresponds to the average concentration of methanol, inside the methanol fuel tank, measured during the 12-hour potentiostatic test. The discontinuity in concentration that occurs at approximately 200 microns corresponds to the reduction in concentration within the anode catalyst layer (assumed to be very thin) due to the anode reaction and due to the step change in water content between the GDL and the membrane. The concentration in the membrane reaches zero at the interface with the cathode catalyst layer at approximately 325 microns.

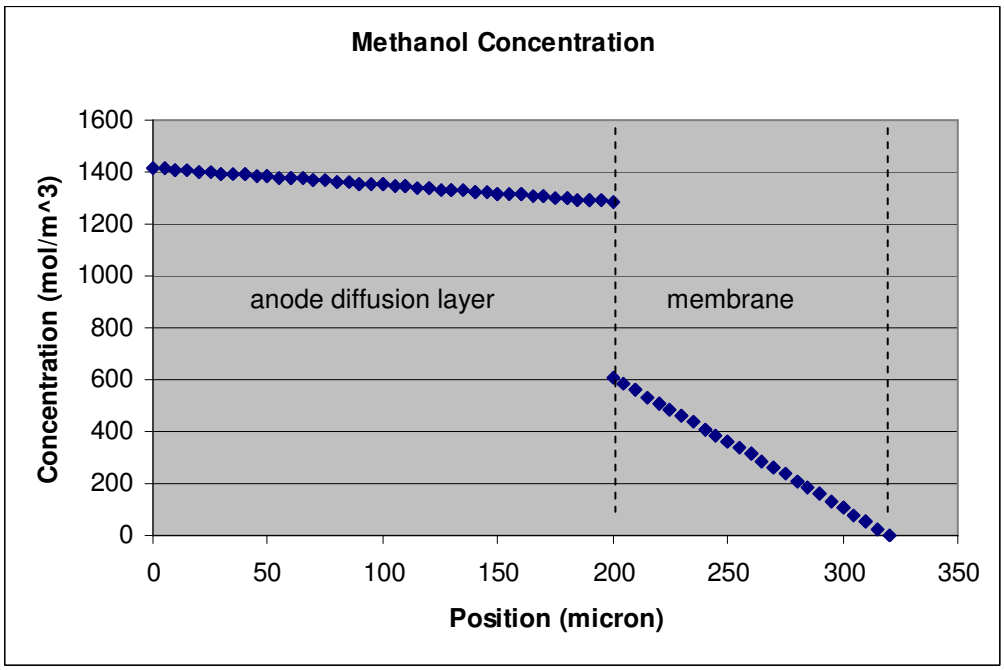

Figure 37. Predicted methanol concentration profile in the anode diffusion layer and in the Nafion membrane.

The predicted methanol flux values within the anode diffusion layer and the membrane are shown in Figure 38. The flux discontinuity at approximately 200 microns is caused by the consumption of methanol in the anode reaction. All methanol that reaches the cathode catalyst layer is assumed to undergo an immediate oxidation reaction. Therefore, there is no methanol flux beyond the interface between the membrane and the cathode catalyst layer. Both the diffusive and convective flux profiles are shown. The diffusive flux appears to be approximately five times larger than the convective flux in

both regions. This supports the assertion previously made when analyzing the experimental data that the dominant form of mass transfer through the membrane was diffusion and not convection. Also, the methanol diffusive and convective fluxes change with respect to location. This is especially noticeable within the membrane. Although the bulk flow in the membrane varies very little within the membrane, the convective flux is larger in the left region of the membrane than in the right region because the methanol concentration is larger in the left region. As the convective flux decreases, the diffusive flux increases because the concentration gradient increases.

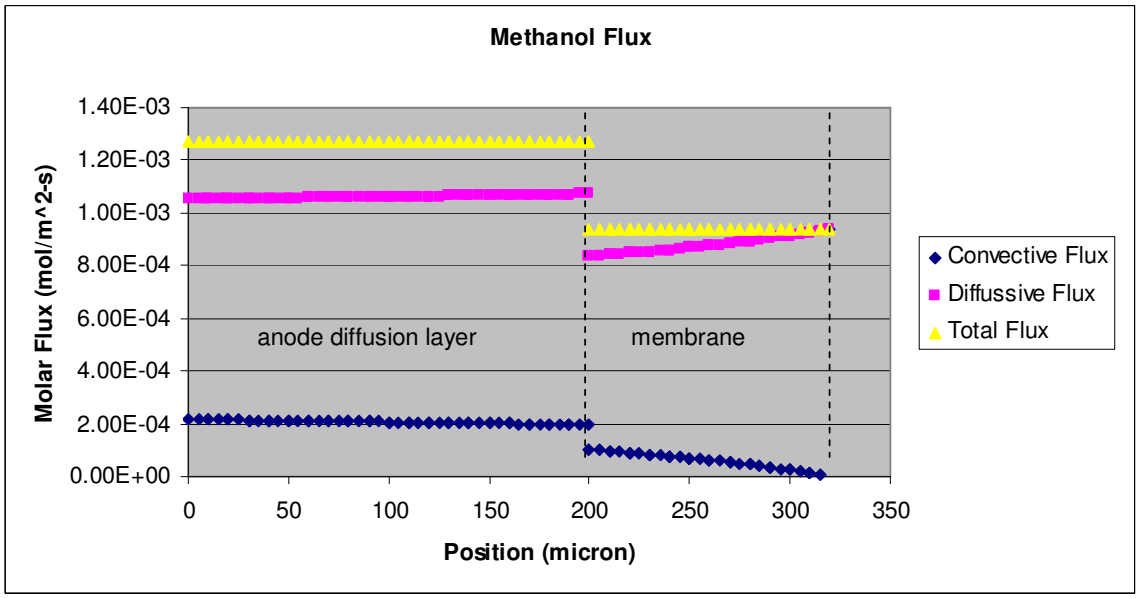

Figure 38. Predicted methanol flux in the anode GDL and the PEM.

The concentration profile of water is shown in Figure 39, and the water flux profile is shown in Figure 40. Unlike methanol, the concentration of water increases in the anode diffusion layer from left to right. As shown in Figure 40, water is actually diffusing from the interface diffusion layer between the diffusion layer and the membrane back across the diffusion layer towards the fuel tank. However, the net flux is still to the right towards the membrane because the convective flux is so large. The large convective flux can be attributed to hydraulic permeation which drives the water towards the membrane. After some water is reacted in the anode, the water moves from left to right across the membrane due to diffusion. The convective flux in the membrane is

actually negative because the hydraulic pressure at the interface between the membrane and the cathode GDL is actually higher than the pressure at the membrane/anode diffusion layer interface due to the capillary pressure in the cathode GDL.

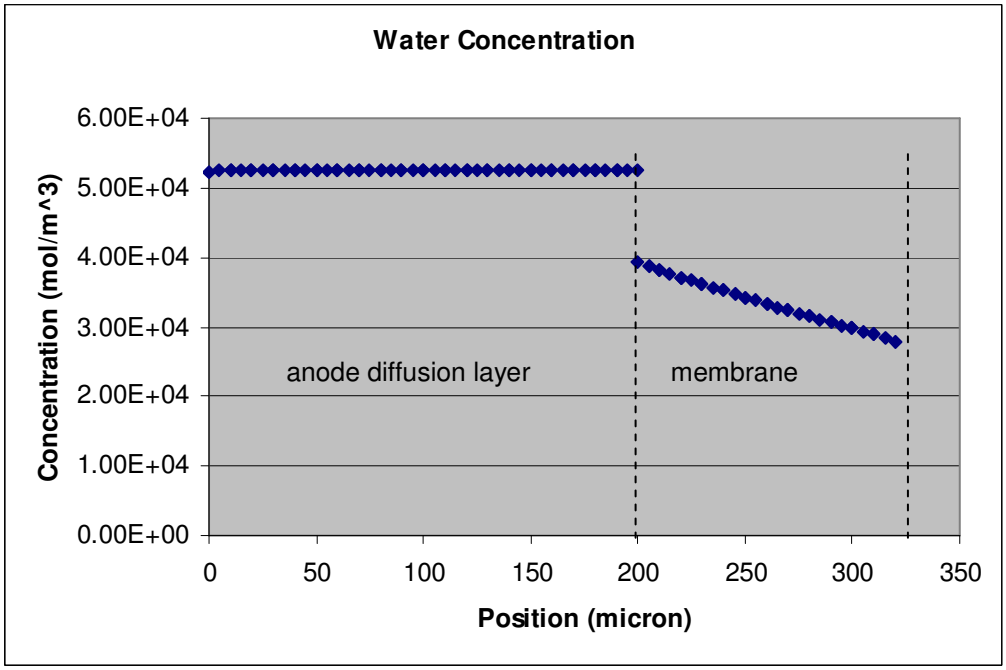

Figure 39. Predicted water concentration profile in the anode diffusion layer and in the Nafion membrane.

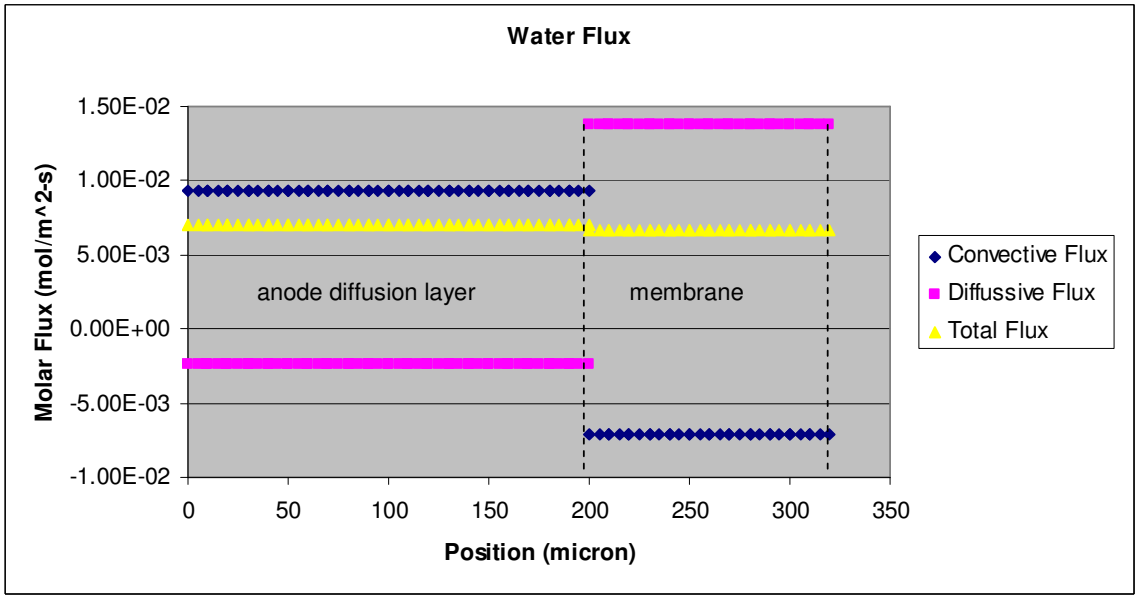

Figure 40. Predicted water flux in the anode GDL and the PEM.

The model also predicted the fluxes for all species in each of the regions. Table 10 shows the predicted total flux, diffusive flux, and convective flux values for methanol, water, and oxygen. Because the convective and diffusive flux changes with respect to location, the average was taken within each region.

Table 10. Predicted molar fluxes (mol/m^2-s) for methanol, water, and oxygen.

	Anode Diffusion Layer		
	Total Flux	Convective Flux	Diffusive Flux
Methanol	1.27E-03	2.07E-04	1.06E-03
Water	1.28E-03	3.65E-03	-2.38E-03

	Nafion Membrane		
	Total Flux	Convective Flux	Diffusive Flux
Methanol	9.38E-04	8.47E-05	8.79E-04
Water	6.69E-03	-7.08E-03	1.38E-02

	Cathode Gas Diffusion Layer		
	Total Flux	Convective Flux	Diffusive Flux
Water	9.52E-03	1.07E-04	9.41E-03
Oxygen	-4.96E-04	1.12E-03	-1.61E-03

Within the anode diffusion layer, diffusion is the primary mode of mass transport for methanol while convection is the primary mode of mass transport for water. The water diffusive flux in the anode diffusion layer is actually negative because the concentration of water in the fuel tank is slightly lower than the concentration of water at the diffusion layer and membrane boundary. The convection in the anode diffusion layer is caused by hydraulic permeation. In the membrane, diffusion is the primary mode of transport for both methanol and water. The convective flux of water is actually negative due to the capillary pressure at the membrane and cathode GDL interface. In the cathode GDL, diffusion is the primary mode of transport for both water and oxygen. The oxygen diffuses from the environment to the cathode where it is consumed in the cathode reaction. Although the total flux of the oxygen is negative, the convective flux of water is positive because the overall bulk velocity of the gasses in the GDL is positive.

In summary, the experiments conducted showed that the performance of a direct methanol fuel cells is affected by both the ambient temperature and ambient relative humidity. The current production capabilities of the DMFC increase with temperature

due to improved reaction kinetics. However, the performance tends to decrease with increasing relative humidity. This phenomena has been attributed to selective flooding of the cathode gas diffusion layer which denies the catalyst layer sufficient access to oxygen. The methanol and water consumption levels were also shown to increase with temperature. This was both due to increased levels of methanol and water reacted at the anode and to increased membrane diffusivity. Increasing the relative humidity decreased the water consumption because it decreased the rate of water evaporation and because it decreased the current production and the associated electrosomotic drag. However, increasing the relative humidity had little effect on the overall methanol consumption. While the rates of methanol reacted decreased, the rates of methanol that crossed over the membrane increased. This was attributed to a larger concentration gradient in the membrane, resulting from reduced levels of methanol being reacted in the anode catalyst layer. The numerical model supported the assertions made about the mass transport of both methanol and water within the fuel cell. The model provided insight into the modes of transport within the fuel cell, and provided concentration and flux profiles.

6. CONCLUSIONS AND RECOMMENDATIONS

This study has characterized the performance of a passive air breathing direct methanol fuel cell for a range of relative humidities and temperatures. While there is large amount of performance data available in the literature for methanol fuel cells, the majority of the data is for forced convection fuel cells. Very little performance data is available for passive direct methanol fuel cells, and test results that have been reported do not cover a sufficiently wide range of operating temperatures and relative humidities. In this work, potentiostatic tests, electrochemical impedance spectroscopy tests, and polarization tests were used to describe the effects of varying temperature and relative humidity on the performance of the passive DMFC. Furthermore, a one dimensional model was developed to provide insight into the modes of transport within the fuel cell.

6.1. Relative Humidity and Temperature Conclusions

Both relative humidity and temperature had strong effects on the overall performance of the direct methanol fuel cell. Increasing the temperature was shown to improve the current production capabilities of the fuel cell, although increasing temperature also increased the rates of methanol and water crossover. Increasing relative humidity proved to decrease the current production capabilities of the fuel cell, while increasing the rate of methanol crossover, and decreasing the rate of water crossover.

Increasing the temperature improved the performance of the fuel cell by increasing the reaction kinetics within the fuel cell. The highest peak power density achieved in this study was 11.8 mW/cm^2 while operating with an ambient temperature and relative humidity of 50ºC and 10% respectively. Increasing the temperature also improved the performance of the fuel cell by decreasing the amount of methanol lost to crossover. This phenomena was attributed to a decreased methanol concentration at the interface between the anode catalyst layer and the Nafion® membrane due to increased levels of methanol reacted within the catalyst layer. If the temperature of the fuel cell could be raised by passively insulating the system while preserving reactant flow or by

using thermal energy from some other system, then increasing the temperature of the DMFC could be a viable means to increase cell performance.

Increasing the relative humidity had negative effects on the fuel cell in nearly all aspects. The current production of the fuel cell decreased with increasing relative humidity. This was attributed to flooding of the cathode GDL which limited the flow of oxygen to the cathode catalyst layer. Flooding was visible while testing at both 50% and 90% relative humidity. This suggests that passive methods of reducing or preventing flooding must be applied before passive DMFC operation will be feasible in humid environments. The methanol crossover rates increased with increasing relative humidity. This was attributed to reduced levels of methanol reaction within the anode catalyst layer associated with reduced levels of current caused by flooding. The fuel cell produced the highest current densities while operating at a relative humidity of 10%. The only negative effect of operating the fuel cell at low relative humiditiy was that the water crossover rate increased due to increased evaporation.

6.2. Model Conclusions

A one dimensional steady state mass transport model was developed to provide insight into the methods of water and methanol transport within the fuel cell. The numerical model provided methanol and water concentration and flux profiles and predicted cathode saturation levels. The model suggested that the primary mode of methanol transport within the fuel cell was diffusion. The model also suggested that methanol crossover could be reduced by increasing the current density as observed in the experimental testing. The model suggested that water transport due to diffusion in the Nafion® membrane was just as prevalent as water transport due to electro-osmotic drag. The model did not, however, predict increased levels of water saturation within the cathode diffusion layer as the relative humidity increased. This was attributed to the fact that this model was a single phase model that could not account for liquid water transport. The numerical model successfully provided insight into the means of water and methanol transport within the cell and confirmed assertions made from the experimental data about the fuel cell behavior. Both the experimental data and the model predictions suggested that the primary method of methanol transport in both the anode diffusion layer and

Nafion® membrane was diffusion. They also both suggested that methanol crossover in the membrane decreased as the cell current density increased due to methanol reacted in the anode which in turn lowered the concentration of methanol at the catalyst layer/membrane interface thus reducing the methanol concentration gradient and the rate of diffusion in the membrane. Both the experimental data and the model predictions also suggested the methanol and water consumption increase with increasing temperature due to increasing diffusivities. Lastly, they both suggested that water consumption rates increased as the relative humidity decreased, both due to increased water reacted at the anode and due to increased rates of evaporation at the cathode.

6.3. Recommendations and Future Research

The experimental data contained within this work show that the passive direct methanol fuel cell performs better under low relative humidities and high temperatures. The tests and model also suggest that flooding was the primary cause of decreased current production. This implies that it would be ideal to operate DMFCs at low relative humidities. However, tests were only conducted at three different relative humidities. While 10% relative humidity proved to be better than 50% or 90%, no tests were run between 10% and 50%. Additional testing within this range may show that there is a certain relative humidity below which flooding does not occur and above which flooding is prevalent and hinders performance. It would also be useful to repeat these tests while varying the methanol concentration. Increasing the methanol concentration tends to increase the current production capabilities of the fuel cell, although it also increases the rate of methanol crossover. Running tests while varying the methanol concentration may suggest an optimal concentration.

In general, this fuel cell performed similarly to other fuel cells reported in literature. However, the high frequency resistance of the fuel cell was relatively high during all testing. It is possible that this was due to a high contact resistance between the fuel cell and the current collectors. Redesigning the fuel cell test hardware to improve the compression of the diffusion layers may help lower the cell resistance and improve overall performance. Other aspects of the fuel cell hardware design such as the diffusion

layer material or the current collector design could be addressed. By employing a cathode diffusion layer with increased Teflon content one could feasibly reduce the levels of cathode flooding.

The numerical model did successfully predict methanol and water consumption levels and provided concentration and flux profiles. However, the model predicted that the cathode saturation levels would decrease with increasing ambient relative humidity, which was not the case during the experimental testing. This could be because the model assumed that liquid water present in the gas diffusion layer was immobile. The results of this assumption was that the model had to decrease the saturation in the cathode GDL in order to increase the number of unsaturated pores to allow gaseous water to flow through these pores when in reality the water was leaving the GDL in the liquid phase through saturated pores. This could be addressed by converting the model to at two phase model within the cathode diffusion layer. The decrease in saturation with increasing relative humidity could also have been a result of using a constant value for the electro-osmotic drag coefficient as opposed to an equation that accounts for temperature, which could be easily remedied.

The model also showed that there was a relationship between cell current and the anode reaction rate coefficient. The cell current is currently related to the anode reaction rate coefficient though a liner regression fit. However, it would be more accurate to actually model the catalyst layer as a domain in space within which methanol and water diffuse and the anode reaction takes place. This would allow the model to more accurately predict the methanol concentration drop within the anode catalyst layer. Additionally, this method for representing the methanol concentration drop within anode catalyst layer could also be applied to the cathode catalyst layer where methanol is being consumed.

Lastly, the model was employed in COMSOL in order to ease the progression from a one dimensional model to a two or three dimensional model. In the case that these models would be desirable, the model could be evolved. Additionally, an electrochemical analysis and a thermodynamic analysis could be added to the model. This electrochemical analysis would be desirable in order to use the model to predict the electrochemical response to varying environmental and fuel cell parameters such as

temperature, relative humidity, membrane thickness, and GDL porosity. The thermodynamic analysis would be desirable to determine the self-heating nature of the fuel cell which could be especially useful in stack design. The model could also be expanded to consider both the electrochemical and mass transport effects of carbon dioxide production within both the anode and cathode catalyst layers.

6.4. Closing Remarks

The direct methanol fuel cell is a feasible source of small scale portable power. However, the fuel cells must be capable of producing reliable power in various operating environments. This work showed that temperature and relative humidity have strong effects on the power production capabilities of the passive air breathing direct methanol fuel cell. The fuel cell produced the most power when operating at a low relative humidity of 10% and a high temperature of 50ºC. The experimental results suggested that flooding was a major problem reducing fuel cell performance when operating at 50% and 90% relative humidities. The experimental data suggested that flooding had little effect on the overall methanol consumption. However, the model suggested that while flooding decreased the amount of methanol reacted at the anode by reducing the overall current density, the flooding increased the rate of methanol crossover. Therefore, from both a fuel efficiency perspective and from a power production perspective, it is very important to prevent flooding of the cathode. Future work could include testing new ways of preventing flooding in higher humidity environments, as flooding appears to be one of the largest barriers to passive direct methanol fuel cells today.

WORKS CITED

[1] Smart Fuel Cell Company. <http://www.sfc.com/en/>

[2] Casio Worldwide. <http://world.casio.com/info/2002/fuelcell.html>

[3] Defense Update. <http://defense-update.com/products/f/fuel-cells.htm>

[4] DaeHo Ko, MinJeong Lee, Won-Hyouk Jang, Ulrike Krewer. "Non-isothermal dynamic modeling and optimization of a direct methanol fuel cell." J. Power Sources. (2008).

[5] Mauritz, Kenneth A., Moore, Robert B., 2004, "State of Understanding of Nafion," Chem. Rev., 104, pp. 4535-4585.

[6] Gregory Jewett, Zhen Guo, Amir Faghri. "Water and air management systems for a passive direct methanol fuel cell." J. Power Sources. (2007).

[7] Thomas A. Zawodzinski, Jr., Charles Derouin, Susan Radzinski, Ruth J. Sherman, Van T. Smith, Thomas E. Springer, Shimshon Gottesfeld. "Water uptake by and transport through Nafion® 117 membranes."

[8] Yoshitsugau Sone, Per Ekdunge, Daniel Simonssan. "Proton conductivity of Nafion® 117 as measured by a four-electrode AC impedance method." J. Electrochem. Soc. (1996).

[9] Sukkee Um, Chao-Yang Wang. "Computational study of water transport in proton exchange membrane fuel cells." J. Power Sources. (2006).

[10] Jean-Marc Le Canut, Rami M. Abouatallah, David A. Harrington. "Detection of membrane drying, fuel cell flooding, and anode catalyst poisoning on PEMFC stacks by electrochemical impedance spectroscopy." J. Electrochem. Soc. (2006).

[11] Wang, Chao-Yang, 2004, "Fundamental models for fuel cell engineering." Chem. Rev., 104, pp. 4727-4766.

[12] Hyunchul Ju, Chao-Yang Wang, Simon Cleghorn, Uwe Beuscher. "Nonisothermal modeling of polymer electrolyte fuel cells I. Experimental validation." J. Electrochem. Soc. (2005).

[13] Tibor Fabian, Jonathan D. Posner, Ryan O'Hayre, Suk-Won Cha, John K. Eaton, Fritz B. Prinz, Juan G. Santiago. "The role of ambient conditions on the performance of a planar, air-breathink hydrogen PEM fuel cell."

[14] Seong Uk Jeong, Eun Ae Cho, Hyoung-Jhun Kim, Tae-Hoon Lim, In-Hwan Oh, Sung Hyun Kim. "Effects of cathode open area and relative humidity on the performance of air-breathing polymer electrolyte membrane fuel cells." J. Power Sources. (2006).

[15] G. Q. Lu, F. Q. Liu, Chao-Yang Wang. "Water transport through Nafion® 112 membrane in DMFCs." Electrochemical and Solid-State Letters. (2005).

[16] E. Peled, A. Blum, A. Aharon, M. Philosoph, Y. Lavi. "Novel approach to recycling water and reducing water loss in DMFCs." Electrochemical and Solid-State Letters. (2003).

[17] Peled, E., Duvdevani, T., Melman, A., 1998, "A Novel Proton-Conducting Membrane," Electrochem. Solid-State Lett., 1, pp 210-211.

[18] Chen, C.Y., Yang, P., 2003, "Performance of an Air-breathing Direct Methanol Fuel Cell," Journal of Power Sources, 123, pp. 37-42.

[19] Weber, Adam Z., Newman, John, 2004, "Modeling Transport in Polymer-Electrolyte Fuel Cells", Chem. Rev. , 104, pp. 4679-4726.

[20] Scott, K., Argyropoulos, P., Sundmacher, K., 1999, "A model for the liquid feed direct methanol fuel cell," Journal of Electroanalytical Chemistry, 477, pp. 97-110.

[21] Jeng, K.T., Chen, C.W., 2002, "Modeling and simulation of a direct methanol fuel cell anode," Journal of Power Sources, 112, pp. 357-375.

[22] Baxter, S.F., Battaglia, V.S., White, R.E., 1999, "Methanol Fuel Cell Model: Anode," Journal of the Electrochemical Society, 146 (2), pp. 437-447.

[23] Sundmacher, K., Schultz, T., Zhou, S., Scott, K., Ginkel, M., Gilles, E.D., 2001, "Dynamics of the direct methanol fuel cell (DMFC): experiments and model-based analysis," Chemical Engineering Science, 56, pp. 333-341.

[24] Schlögl, R., 1966, "Membrane permeation in systems far from equilibrium," Berichte der Bunsengesellschaft fűr Physikalische Chemie, 70, pp.400-414.

[25] Meyers, Jeremy P., Newman, John, 2002, "Simulation Of The Direct Methanol Fuel Cell II. Modeling and Data Analysis of Transport and Kinetic Phenomena," Journal of the Electrochemical Society, 149 (6), pp. A718-A728.

[26] Pollard R., Newman, J., 1980, "Silicon Deposition on a Rotating Disk," Journal of the Electrochemical Society., 127 (3), p. 744-752.

[27] Schultz, Thorsten, Sundmacher, Kai, 2005, "Rigorous Dynamic Model Of A Direct Methanol Fuel Cell Based On Maxwell–Stefan Mass Transport Equations And A Flory–

Huggins Activity Model: Formulation And Experimental Validation," Journal of Power Sources, 145, pp. 435–462

[28] Murgia, G., Pisani, L., Shukla, A.K., Scott, K., 2003, "A Numerical Model of a Liquid-Feed Solid Polymer Electrolyte DMFC and Its Experimental Validation," Journal of the Electrochemical Society, 150 (9), pp. A1231-A1245.

[29] O'Hayre, Ryan, Fabian, Tibor , Litster, Shwan, Prinz, Fritz B., Santiago, Juan G., 2007, "Engineering model of a passive planar air breathing fuel cell cathode," J. Power Sources, 167, pp. 118-129.

[30] Paquin, Mathieu, Fréchette, Luc G., 2008, "Understanding cathode flooding and dry-out for water management in air breathing PEM fuel cells," J. Power Sources, 180, pp. 440-451.

[31] Frank P. Incropera, David P. DeWitt. Fundamentals of Heat and Mass Transfer. Fourth Ed. John Wiley & Sons. (1996).

[32] "Micro Fuel Cell (MFC) for Micro Air Vehicle (MAV) Power," Program SBIR, Air Force Topic Number AF06-144

[33] COMSOL Multiphysics. 3.5a

[34] O'Hayre, R., Cha, S.-W., Colella, W., and Prinz, F. B., 2006, *Fuel Cell Fundamentals*, John Wiley and Sons, Inc., New York, NY.

[35] Cunningham, R. E., and Williams, R. J. J., 1980, *Diffusion in Gases and Porous Media*, Plenum Press, New York, NY.

[36] Wesselingh, J. A., Krishna, R., 2000, *Mass Transfer in Multicomponent Mixtures,* Delft University Press, Delft, the Netherleands.

[37] K. Scott, K., Taama, W., Cruickshank, J., 1997, "Performance and modelling of a direct methanol solid polymer electrolyte fuel cell," Journal of Power Sources, 65, pp 159-171.

[38] Yang, W.W., Zhao, T.S., Xu, C., 2007, "Three-dimensional two-phase mass transport model for direct methanol fuel cells," Electrochimica Acta, 53, pp. 853–862.

[39] Yin, Ken-Ming, 2008, "A theoretical model of the membrane electrode assembly of liquid feed direct methanol fuel cell with consideration of water and methanol crossover," Journal of Power Sources, 179, pp. 700–710.

[40] Wang, Z.H., Wang, C.Y., 2003, "Mathematical Modeling of Liquid-Feed Direct Methanol Fuel Cells," Journal of the Electrochemical Society, 150 (4), pp. A508-A519.

[41] White, Frank M., 2003, *Fluid Mechanics*, 5th ed., McGraw-Hill, New York, NY.

[42] Sole, Joshua David, 2008, "Investigation Of Water Transport Parameters And Processes In The Gas Diffusion Layer Of PEM Fuel Cells," Dissertation, Virginia Polytechnic and State University.

[43] COMSOL, 2008, *Chemical Engineering Module Users Guide*, Burlington, MA.

[44] Curtiss, C. F., and Bird, R. Byron, 1999, "Multicomponent Diffusion," Ind. Eng. Chem. Res., 38, pp. 2515-2522.

[45] Cussler, E. L., 2009, *Diffusion: Mass Transfer in Fluid Systems*, 3rd ed., Cambridge University Press, Cambridge, NY.

[46] COMSOL Multiphysics, 2008, *Maxwell-Stefan Diffusion in a Fuel Cell Unit Cell: Solved with COMSOL 3.5,* Burlington, MA.

[47] Bird, R. Byron, Steware, Warren E., Lightfoot, Edwin N., 2002, *Transport Phenomena*, 2nd ed., John Wiley & Sons, Inc., Hoboken, NJ.

[48] Ren, Xiaoming, Springer, Thomas E., Zawodzinski, Thomas A., Gottesfeld, Shimshon, 2000, "Methanol Transport Through Nafion Membranes Electro-osmotic Drag Effects on Potential Step Measurements," Journal f the Electrochemical Society, 147 (2), pp. 466-474.

[49] Rice, Jeremy, Faghri, Amir, 2006, "A transient, multi-phase and multi-component model of a new passive DMFC," International Journal of Heat and Mass Transfer, 49, pp. 4804-4820.

[50] Liu, Fuqiang, Wang, Chao-Yang, 2008, "Water and methanol crossover in direct methanol fuel cells-Effect of anode diffusion media," Electrochimica Acta, 53, pp. 5517-5522.

[51] Chen, R., Zhao, T.S., 2007, "Porous current collectors for passive direct methanol fuel cells," Electrochimica Acta, 52, pp. 4317-4324.

[52] Chen, C.Y., Yang, P., 2003, "Performance of an Air-Breathing Direct Methanol Fuel Cell," Journal of Power Sources, 123, pp. 37-42.

[53] Guo, Zhen, Faghri, Amir, 2008, "Development of a 1 W passive DMFC," International Communications in Heat and Mass Transfer, 35, pp 225-239.

APPENDIX

A1. COMSOL

Table 1. Table of COMSOL geometry parameters.

	Length	Start Coordinate	End Coordinate
Fuel Tank	NA	0.0127 m	0.0127 m
Anode GDL	2.0 E-4 m	0.0127 m	0.0129 m
Anode CL	NA	0.0129 m	0.0129 m
MEA	1.2 E-4 m	0.0129 m	0.01302 m
Cathode CL	NA	0.01302 m	0.01302 m
Cathode GDL	2.0 E-4 m	0.01302 m	0.01322 m

A2. Mesh Refinement

Two meshing schemes were used in the COMSOL simulations. The two schemes were found to be in close agreement. Therefore, the first meshing scheme with the lesser number of elements was implemented in this work. Table 2 describes the original meshing scheme used, and Table 3 describes the refined meshing scheme which had twice as many elements as the original meshing scheme.

Table 2. Mesh scheme 1.

Scheme 1 (original mesh)			
Region	**Length of Region**	**Number of Elements**	**Length of Elements**
Anode GDL	0.20 mm	20	0.01 mm
Nafion® Membrane	0.12 mm	12	0.01 mm
Cathode GDL	0.20 mm	20	0.01 mm

Table 3. Mesh scheme 2.

Scheme 2 (refined mesh)			
Region	**Length of Region**	**Number of Elements**	**Length of Elements**
Anode GDL	0.20 mm	40	0.005 mm
Nafion® Membrane	0.12 mm	24	0.005 mm
Cathode GDL	0.20 mm	40	0.005 mm

The results from both meshing schemes were approximately equal. Figure 1 compares the predicted methanol concentration profile for test 26 using both the original meshing scheme and the refined meshing scheme. The concentration profiles are virtually identical.

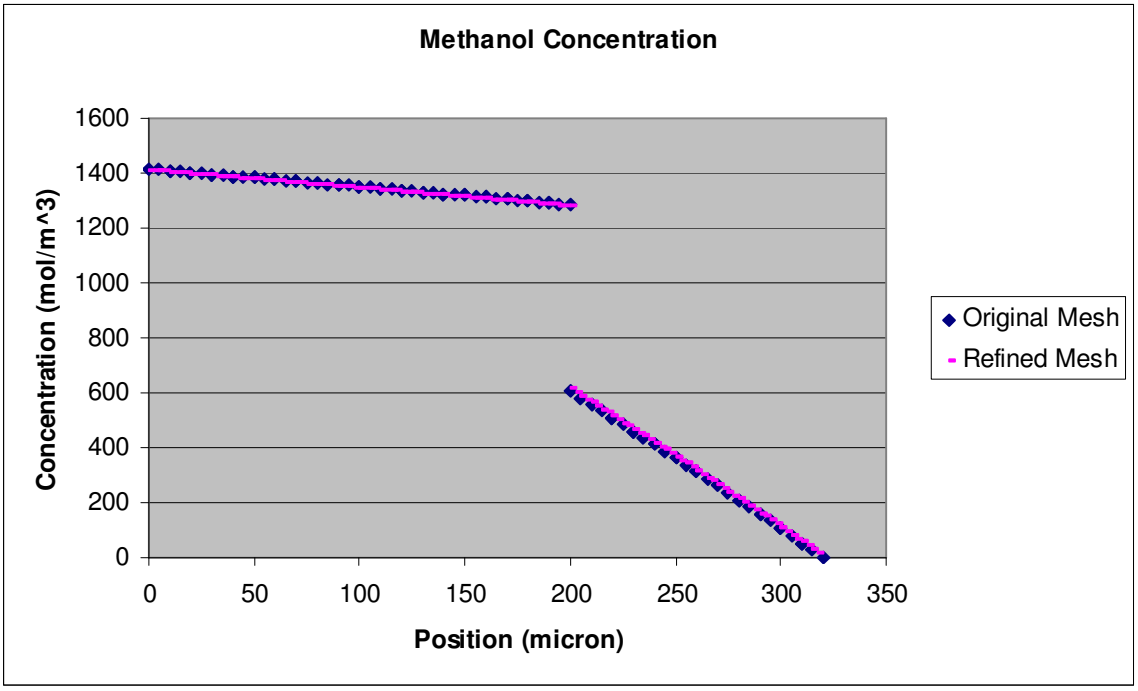

Figure 1. Meshing scheme comparison. Test 26 methanol concentration profiles.

Given that the results from both meshing schemes were approximately equal, the first meshing scheme was chosen because it provided accurate results with a minimal computational time.

A3. Material Properties

Table 4. Properties referenced in literature.

Symbol	Description	Units	Values from Literature
D_{CH_3OH-N}	Diffusivity of methanol in Nafion®	m^2/s	1.2E-10 [Yin], 4.27E-10 (T=30C) [Ren], 7.62E-10 (T=50C) [Ren], 9E-10 [Murgia], 4.9E-10 [Jeng], 1.35E-9 (T=70C) [Cruischank], 6.5E-10 [Sandhu], 4.9E-10*exp(2436(1/333-1/T)) [Scott], 10^(-5.4163-999.778/T) [Wang math model, Rice, Yaws]

D_{H_2O-N}	Diffusivity of water in Nafion®	m^2/s	2E-10 [Sandu], 7.3E-10*exp(2436(1/253-1/T)) [Scott]
$D_{CH_3OH-H_2O}$	Diffusivity of methanol in water	m^2/s	2.8E-9 [Scott, Jeng], 6.69E-9 [Yand 3d 2 phase], 1.24E-9 (eff.) [Yin], 1.1E-8 (eff.) [Murgia]
ε	GDL porosity		0.8 [Murgia], 0.7 [Yang 3d 2 phase]
b	GDL tortuosity parameter		1.5 [Murgia, Wesselingh and Krishna text]
k_ϕ	Membrane electrokinetic permeability	m^2	1.13E-19 [Sundmacher]
μ	viscosity	kg/(m-s)	3.353E-4 [Sundmacher]
k_p	Membrane hydraulic permeability	m^2	1.157E-18 [Sundmacher], 2E-18 [Yang 3d 2 phase]
θ_c	GDL contact angle	degrees	110 [Pasagullari, C Lim and CY Wang], 120 [yang 3d 2 phase]
r_c	GDL pore radius	m	1E-6 [Diviseck]
σ	Surface tension	g/s^2	62.5 [Yin, Pasaogullari], 71.7 [I&D]
n_d	Electro-osmotic drag coefficient		2.5 [Yin]

eff.: effective

A4. Reaction Rate Coefficient Derivations

Given equation **Error! Reference source not found.** which describes the concentration of methanol within the anode catalyst layer, and given the boundary conditions stated in equations **Error! Reference source not found.** and **Error! Reference source not found.**, the concentration as a function of position within the anode catalyst layer can be found.

First, equations **Error! Reference source not found.**, **Error! Reference source not found.**, and **Error! Reference source not found.** are restated as equations A.1, A.2, and A.3.

$$\frac{d^2}{d^2x}c_{CH_3OH} - \frac{\beta(i)}{D^{eff}_{CH_3OH-CL}6F}c_{CH_3OH} = 0 \tag{A.1}$$

$$c_{CH_3OH}(x=0) = c^{D1/B2}_{CH_3OH} \tag{A.2}$$

$$c_{CH_3OH}(x=L) = c^{CL/N}_{CH_3OH} \tag{A.3}$$

First, the non-dimensional variables are chosen for methanol concentration and position.

$$\hat{c}_{CH_3OH} = \frac{c_{CH_3OH}}{c_{CH_3OH}^{D1/B2}} \tag{A.4}$$

$$\hat{x} = \frac{x}{L} \tag{A.5}$$

These non-dimensional variables are then applied to equations A.1, A.2, and A.3 giving the following.

$$\frac{d^2}{d^2\hat{x}}\hat{c}_{CH_3OH} - \frac{\beta L^2}{D_{CH_3OH-CL}^{eff} 6F}\hat{c}_{CH_3OH} = 0 \tag{A.6}$$

$$\hat{c}_{CH_3OH}(\hat{x} = 0) = 1 \tag{A.7}$$

$$\hat{c}_{CH_3OH}(\hat{x} = 1) = \frac{c_{CH_3OH}^{CL/N}}{c_{CH_3OH}^{D1/B2}} \tag{A.8}$$

Equation A.6 is a second-order homogeneous differential equation with constant coefficients. The corresponding general solution is given by the following,

$$\hat{c}_{CH_3OH} = c_1 e^{\lambda_1 x} + c_2 e^{\lambda_2 x} \tag{A.9}$$

$$\lambda_1 = \sqrt{\beta} \tag{A.10}$$

$$\lambda_2 = -\sqrt{\beta} \tag{A.11}$$

where c_1 and c_2 are constants. Applying boundary conditions from equations A.7 and A.8 to equation A.9 gives the following for constants c_1 and c_2.

$$c_1 = 1 - c_2 \tag{A.12}$$

$$c_2 = \frac{\left(\frac{c_{CH_3OH}^{CL/N}}{c_{CH_3OH}^{D1/B2}} - e^{\sqrt{\beta}} \right)}{\left(-e^{\sqrt{\beta}} + e^{-\sqrt{\beta}} \right)} \tag{A.13}$$

Applying c_1 and c_2 to equation A.9 gives the following in terms of non-dimensional variables.

$$\hat{c}_{CH_3OH} = e^{(\sqrt{\beta})\hat{x}} + \frac{\left(c_{CH_3OH}^{CL/N} \Big/ c_{CH_3OH}^{D1/B2} - e^{(\sqrt{\beta})} \right)\left(e^{(\sqrt{\beta})\hat{x}} - e^{(\sqrt{\beta})\hat{x}} \right)}{\left(-e^{(\sqrt{\beta})} + -e^{(\sqrt{\beta})} \right)} \tag{A.14}$$

Applying the equations A.4 and A.5 to equation A.14 gives the following equation for methanol concentration within the anode catalyst layer.

$$c_{CH_3OH} = c_{CH_3OH}^{D1/B2} e^{(\sqrt{\beta})x/L} + \frac{c_{CH_3OH}^{D1/B2}\left(c_{CH_3OH}^{CL/N} \Big/ c_{CH_3OH}^{D1/B2} - e^{(\sqrt{\beta})} \right)\left(e^{(\sqrt{\beta})x/L} - e^{(\sqrt{\beta})x/L} \right)}{\left(-e^{(\sqrt{\beta})} + -e^{(\sqrt{\beta})} \right)} \tag{A.15}$$

Given equation A.15 for the methanol concentration in the anode catalyst layer, one can applying equations A.15 and boundary condition equations A.2 and A.3 to equation **Error! Reference source not found.** for the current production within the anode catalyst layer and solve for the methanol concentration at the catalyst layer/membrane interface giving the following.

$$c_{CH_3OH}^{CL/N} = -c_{CH_3OH}^{D1/B2} \frac{\left(\left(\frac{i\sqrt{\beta}}{\alpha c_{CH_3OH}^{D1/B2} L} + 1 - e^{(\sqrt{\beta})} \right)\left(-e^{(\sqrt{\beta})} + -e^{(\sqrt{\beta})} \right) - e^{(\sqrt{\beta})}\left(e^{(\sqrt{\beta})} + e^{(\sqrt{\beta})} \right) + 2e^{(\sqrt{\beta})} \right)}{\left(e^{(\sqrt{\beta})} + e^{(\sqrt{\beta})} - 2 \right)} \tag{A.16}$$

A5. Diffusivity Correction Factor for the Diffusion Coefficient of Methanol in Nafion®

The diffusion coefficient of methanol within the Nafion® membrane was calculated from the experimental results from test Diff3. Test Diff3 was a 12-hour open circuit voltage test performed with not current production at 50ºC and 50% relative humidity. The total methanol crossover for the test was calculated to be 1.15 grams. In order to determine the diffusion coefficient of methanol for test Diff3, all of the methanol crossover was assumed to be due to methanol diffusion through the membrane, thus is was assumed that there was no convective transport. Also, the concentration of methanol at the anode diffusion layer and membrane interface was assumed to be equal to the average concentration of methanol within the fuel tank (the methanol concentration drop within the anode diffusion layer was assumed to be small and thus neglected). The methanol that reached the cathode was assumed to oxidize immediately. Therefore it was assumed that the concentration of methanol at the interface between the membrane and the cathode GDL was zero.

The equation for methanol flux within the membrane is given by the following.

$$n_{CH_3OH} = -D^{eff}_{CH_3OH-N} \frac{dc_{CH_3OH}}{dx} \tag{A.17}$$

Modifying equation A.17 to solve for the methanol consumption in grams (u_{CH_3OH}) for a 12-hour test gives the following,

$$u_{CH_3OH} = -D^{eff}_{CH_3OH-N} M_{CH_3OH} A \times T \frac{c^{D2/B3}_{CH_3OH} - c^{D2/B2}_{CH_3OH}}{d_M} \tag{A.18}$$

where T is the length of the test in seconds and A is the cross sectional area of the cell. Rearranging to solve for the effective diffusion coefficient of methanol in the membrane gives the following.

$$D^{eff}_{CH_3OH-N} = \frac{u_{CH_3OH} d_M}{M_{CH_3OH} c^{D2/B2}_{CH_3OH} A \times T} \tag{A.19}$$

The concentration of methanol in the membrane at the membrane and anode diffusion layer interface is given by the following equations.

$$c^{D2/B2}_{CH_3OH} = \frac{\lambda^{D2/B2}_{CH_3OH} \rho_d}{EW} \tag{A.20}$$

$$\lambda^{D2/B2}_{CH_3OH} = \frac{c^{D1/B1}_{CH_3OH}}{c^{D1/B1}_{H_2O}} \lambda^{D2/B2}_{H_2O} \tag{A.21}$$

By applying the methanol consumption (1.15 g), the thickness of the membrane (1.2×10^{-4} m), the average concentration of methanol in the fuel tank during the test (3.86 grams methanol per 100 grams of methanol and water solution), the cross sectional area (5 square centimeters), and the length of the test in seconds (43200 second), the experimental effective diffusion coefficient of methanol can be found.

$$D^{eff}_{CH_3OH-N} = 2.24 \times 10^{-10} m^2 / s$$

The equation used by Wang et al. [**Error! Bookmark not defined.**] for the effective diffusion coefficient of methanol in Nafion® as modified for the concentration of methanol in terms of moles of methanol per volume of Nafion® is given by the following.

$$D^{eff}_{CH_3OH-N} = \varepsilon^{\tau} \left(\frac{EW \rho_{H_2O}}{M_{H_2O} \lambda^{D2/B2}_{H_2O} \rho_d} \right) 10\text{^}(-5.4163 - 999.778/T), \quad \text{m}^2/\text{s} \tag{A.22}$$

By applying the test conditions to equation A.22 one gets the following effective diffusion coefficient of methanol in Nafion®.

$$D_{CH_3OH-N}^{eff} = 5.07 \times 10^{-10} m^2 / s$$

Dividing the methanol diffusivity from experimental results by the equation used by methanol diffusivity derived from the equation used by Wang et al. one gets a diffusivity correction factor of 0.466.